Copyright Warning & Restrictions

The copyright law of the United States (Title 17, United States Code) governs the making of photocopies or other reproductions of copyrighted material.

Under certain conditions specified in the law, libraries and archives are authorized to furnish a photocopy or other reproduction. One of these specified conditions is that the photocopy or reproduction is not to be "used for any purpose other than private study, scholarship, or research." If a, user makes a request for, or later uses, a photocopy or reproduction for purposes in excess of "fair use" that user may be liable for copyright infringement,

This institution reserves the right to refuse to accept a copying order if, in its judgment, fulfillment of the order would involve violation of copyright law.

Please Note: The author retains the copyright while the New Jersey Institute of Technology reserves the right to distribute this thesis or dissertation

Printing note: If you do not wish to print this page, then select "Pages from: first page # to: last page #" on the print dialog screen

ABSTRACT

BIOMECHANICAL LOADING CHANGES BETWEEN SPECIES IN MILD BLAST-INDUCED TRAUMATIC BRAIN INJURY

by
Jose Juan Rodriguez

Blast-induced traumatic brain injury (bTBI) has become one of the leading injury modalities in military personnel and is considered a signature injury in veterans returning from conflicts in the Middle East. One of the main concerns in studying bTBI is translating animal experiments to clinical applications that can service veterans. Significant advances have been made using animal models in relating external shock waves to emerging neuropathophysiological and behavioral outcomes. However, it is unknown if these results are applicable to humans; and if so, can an interspecies transfer function be developed based on size, shape, and material response. This work aims to focus on relating mechanical loading (insults) between animals and humans, with the assumption that similar insults, at the tissue level, result in similar injuries. To this end, it is hypothesized that biomechanical transfer functions can be derived using a comparison of tissue level loading between live rodents, postmortem rodents, and human surrogates, based on the consideration of interspecies differences in size, material properties, and skull thickness. To accomplish this, a field validated compressed-gas driven shock tube is used to expose increasingly complex surrogates. Beginning with simple geometry surrogates, the effect of specimen size, window thickness, and material on surface loading and internal loading is investigated. Next, surrogates are developed to match the geometry of murine models and the effects of material properties on intracranial loading were elucidated. Finally, postmortem surrogates are prepared for murine and human head forms and used to investigate interspecies loading differences.

Simple geometry studies are conducted using plates of various cross-sectional areas and materials to investigate their effects on loading at three discrete incident overpressures, selected specifically based on rodent survival dose-response curves. Combined with numerical simulations, results offer insight into how surface loading varies with size and material. In three-dimensional studies, boxes were constructed and filled with previously studied brain simulants. These studies allow for the investigation of material thickness and brain simulant on both surface and internal shock loading. Results show that thicker materials offer improved protection and that 20% porcine gelatin is a potential brain simulant, based on the biomechanical performance.

Furthermore, potential brain and skin simulants are assessed by comparing intracranial pressure and skull strain between increasingly complex murine surrogates and live rats. By using geometrically similar surrogates and only altering materials, results elucidate how shock waves load biological structures on the surface and interior.

The study of postmortem surrogates allows for comparison of interspecies differences on insults. The use of similar external loading conditions allows for one-to-one comparisons between the two species. Using multiple linear regression, biomechanical transfer functions for intracranial pressure and impulse are derived based on specimen skull thickness, as well as, incident shock parameters. Based on these functions, the combination of skull thickness and incident loading parameters predict tissue independent of species. Thus, the transfer function developed in this thesis between animal models and humans, under primary blast loading conditions based on experimental data, can be used to apply animal results to humans as a good first step.

BIOMECHANICAL LOADING CHANGES BETWEEN SPECIES IN MILD BLAST-INDUCED TRAUMATIC BRAIN INJURY

by
Jose Juan Rodriguez

A Dissertation
Submitted to the Faculty of
New Jersey Institute of Technology
and Rutgers University Biomedical and Health Sciences – Newark
in Partial Fulfillment of the Requirements for the Degree of
Doctor of Philosophy in Biomedical Engineering

Department of Biomedical Engineering

August 2020

APPROVAL PAGE

BIOMECHANICAL LOADING CHANGES BETWEEN SPECIES IN MILD BLAST-INDUCED TRAUMATIC BRAIN INJURY

Jose Juan Rodriguez

Dr. Namas Chandra, Dissertation Advisor — Date
Distinguished Professor of Biomedical Engineering, NJIT

Dr. Bryan J. Pfister, Committee Member — Date
Professor and Chair of Biomedical Engineering, NJIT

Dr. Joshua R. Berlin, Committee Member — Date
Professor of Pharmacology, Physiology, and Neuroscience, Rutgers NJMS

Dr. Kevin Pang, Committee Member — Date
Professor of Pharmacology, Physiology, and Neuroscience, Rutgers NJMS

Dr. Saikat Pal, Committee Member — Date
Assitant Professor of Biomedical Engineering, NJIT

Dr. Maciej Skotak, Committee Member — Date
Research Scientist, Katmai Health Services, WRAIR

BIOGRAPHICAL SKETCH

Author: Jose Juan Rodriguez

Degree: Doctor of Philosophy

Date: August 2020

Undergraduate and Graduate Education:

- Doctor of Philosophy in Biomedical Engineering,
  New Jersey Institute of Technology, Newark, NJ,
  and Rutgers University, Biomedical and Health Sciences, Newark, NJ, 2020
- Bachlor of Science in Biomedical Engineering,
  New Jersey Institute of Technology, Newark, NJ, 2016

Major: Biomedical Engineering

Presentations and Publications:

V. Perumal, J. J. Rodriguez, M. Kannan, J. K. Perry, R. K. Gupta, N. Chandra, S.P. Karna. "Spectrophotomic Measurements of Fluorescence from Pressure Sensitive Protein Templated Gold Nanocluster Under Free and Shock Tube Set Up." *Conference Proceedings*, International Forum on Blast Injury Countermeasures (IFBIC), Tokyo, Japan 2020.

A. Ravula, J. J. Rodriguez, D. Younger, K.V. Rama Rao, N. Chandra. "Low-Level Repeated Blast TBI Results in Neurobehavioral Deficits in Animal Model." *Conference Proceedings*, Biomedical Engineering Society (BMES) Annual Meeting, Philadelphia, PA, October 2019.

J. J. Rodriguez, M. Skotak, E. Alay, N. Chandra. "The Effect of Peak Overpressure and Impulse on Reflected Pressure during Blast-Induced TBI." *Conference Proceedings*, Biomedical Engineering Society (BMES) Annual Meeting, Philadelphia, PA, October 2019.

S. Iyer, T. Fernando, J. J. Rodriguez, E. Alay, M. Skotak, N. Chandra. "'The Relationship Between the Reflected and Transmitted Pressure in a Simplified Geometry Model." *Conference Proceedings*, Biomedical Engineering Society (BMES) Annual Meeting, Philadelphia, PA, October 2019.

Z. Winfield, J. J. Rodriguez, E. Alay, M. Skotak, N. Chandra. "'The Evaluation of Biofidelic Materials for the Rat Head Model Under Shock Wave Loading" *Conference Proceedings*, Biomedical Engineering Society (BMES) Annual Meeting, Philadelphia, PA, October 2019.

J. J. Rodriguez, M. Skotak, E. Alay, N. Chandra. "The Effect of Peak Overpressure and Impulse on the Reflected Pressure: An Experimental Study Using 2D planar Geometry Model With Implications for Occupational Exposure Measurements." *Conference Proceedings*, Military Health System Research Symposium (MHSRS), Kissimmee, FL, August 2019.

J. J. Rodriguez, E. Alay, M. Skotak, J. Q. Zheng, V. Halls, N. Chandra. "The Effect of Specimen Location and Cross-sectional Area on the Distribution of Surface Pressure Under Shock Wave Loading Conditions." *Conference Proceedings*, Military Health System Research Symposium (MHSRS), Kissimmee, FL, August 2018.

This work is foremost dedicated to my family, especially Sasha, Michelle, Mildred and Jose. To my colleagues and friends that supported me throughout this time. To the animals that sacrificed their lives for my research And to the individuals and their families who donated their bodies towards my research. Thank you all.

ACKNOWLEDGMENT

I would like to first and foremost thank my advisor, Dr. Namas Chandra. I greatly appreciate the opportunities that you have provided. Beyond what you may realize you have made a profound impact on my life by allowing me to work with CIBM3. I appreciate the time and effort that you put in towards molding me into the researcher I am today. Again, I would like to thank you for your support and guidance, which was critical for the completion of my degree.

I would also like to thank the members of my dissertation committee. Dr. Maciej Skotak, thank you for all the work you put in to helping me towards the completion of my degree. You were there on the front lines of research and taught me a significant amount on how research is done. I appreciate your patience with me and working with me on the day to day operations. Maciej, I will be forever grateful for the level of honesty and advice you gave. I would not have made it this far without your assistance. Dr. Bryan Pfister, working with you was a great pleasure. Thank you for taking the time to not only give advice, put to get literally hands deep into surgeries with me. To Dr. Joshua Berlin, thanks for taking the time to work with me. Even before being on my dissertation committee your questions pushed me to think more critically. Dr. Kevin Pang, thank you for taking the time to be on my committee. I know you were hesitant at first, but I appreciate your input and assistance throughout the completion of my degree. Thank you also to Dr. Saikat Pal. You were a late addition, but I appreciate your assistance both towards the completion of me degree as well as guiding me through the teaching process.

The completion of my dissertation would not be possible without the colleagues I had at CIBM3. Thank you to Dr. Kakulavarapu Rama Rao. You helped me greatly with understanding a lot of the histochemistry and pathophysiology involved in my research. You helped me expand my knowledge beyond just mechanics and included

me in projects I would not have thought. Outside of research, I appreciate you being and ear for me, and everything you have done for me in and out of the lab.
Dr. Molly Townsend, thank you for everything. You always took the time out of your busy schedule to help me understand the mechanics and physics that affected my results. Although our time working together was short, you were a role model to me. Dr. Mahdu Murugan, thank you for your professionalism, no matter the topic, both in research and out being, you also provided thoughtful and insightful input. Thank you for the transparency and honesty with the circumstance in our lab.
Dr. Venkatesan Perumal, thank you for both your patience and teachings. Your advice about academia is greatly appreciated. Beyond research our lunches were a great release from the pressure of a PhD; I am glad that I was able to meet you before my tenure at NJIT ended. Eren Alay, thank you for everything you have done. You taught me all the things required for the day to day operations of the lab. Beyond teaching and assisting with experiments you always provided friendship. Good luck on your own PhD, I know will excel.

I would also like to acknowledge, Dr. Max Roman and Dr. Bharat Biswal. I would also like to give a special thanks to Dr. William Hunter. I would also like to thank each of you. You all taught me about research way back during my undergraduate and there is no way I would have made it this far without the direct involvement of all of you. Thank you all so much.

To all the PhD students, I appreciate the time spent working with you, and enduring difficulties of the PhD with you. Matt, Danny, Sudeepto, and Aswati you guys were role models and greatly influenced how I went through the PhD. I valued working with each of you and hope to continue our friendship after graduation. To all those still working toward graduation Abdus, Millie, Arun know that you can still come to me for any help or just an ear if needed. I always appreciate working with all of you.

I would also like to take the time to thank Supriya Iyer and Thinuri Fernado. It was my pleasure mentoring and working with you. You both were a highlight to my research day. I know the work was tiresome at some points, but I appreciate you both sticking with me and I hope I was able to teach you all somethings useful. Thank you from the bottom of my heart for the work you have done, and I am glad that I can call you friends.

To all of my friends, especially Cristian, Vishnu, Rich, Michelle, Apurva, Phil, Scott, your friendships have help keep me sane throughout this process. Thank you all so much for putting up with my, sometime too frequent, visits. Good luck to all of you I know you will be finishing right behind me. Please stay in touch, I am glad to have met everyone of you. To Leone, Towsif, Kenny, Pedram, Zaki, Bridgemohan, Ali, I am finally done boys. I can't wait to celebrate with you all and joining you as full NJIT Alumni. I would also like to show my gratitude for the friends whom I had the opportunity to work with in the admissions office at NJIT. You all gave me my first chance my freshman year so long ago. I truly believe that first opportunity set me up from all of the success I have had since then.

Last, but certainly not least, I would like to thank my family. From the simple things, like making sure I make it to school and back, to making sure I stay sane, thank you from the bottom of my heart. Despite the rocky roads that we traversed, I love all of you and would definitely not be the man I am today without you, and I will be spending the rest of my life to repay you all. Anabelle, Eva, Crystal, Dennis, Poly, thank you for giving me a home away from home and provide a place to take much needed breaks. Sasha and Michelle thank you for always being an ear. Your unconditional support and pride have been more of a motivation than you can imagine. I appreciate the both of you more than you can know. Mami and Papi, thank you both so much. I know things did not go smoothly the entire time by appreciate the innumerous things that you have done to support me. Everything I

have been able to accomplish is because of you, and I love you so much. I know I cannot say thank you enough but thank you.

To those who were not named specifically know that you are not forgotten. A PhD is not solely completed by the one who gets the title. It takes the support and help of countless individuals ranging from professors to undergraduates, and everything in between. Equally important, it requires a support structure of friends, family, and community that I am glad to have established during my tenure at NJIT. Thank everyone who helped me get to where I am today.

TABLE OF CONTENTS

TABLE OF CONTENTS
(Continued)

Chapter **Page**

TABLE OF CONTENTS
(Continued)

Chapter **Page**

LIST OF TABLES

LIST OF FIGURES

Figure **Page**

LIST OF FIGURES
(Continued)

Figure **Page**

LIST OF FIGURES
(Continued)

Figure **Page**

LIST OF FIGURES
(Continued)

Figure **Page**

LIST OF FIGURES
(Continued)

Figure **Page**

LIST OF FIGURES
(Continued)

Figure **Page**

LIST OF FIGURES
(Continued)

Figure **Page**

CHAPTER 1

INTRODUCTION

Traumatic brain injury (TBI) has received increased public attention in recent years due to its prevalence in famous athletes. Beyond athletics, TBI accounts for about 2.8 million emergency room visits and hospitalizations [1], 70-90,000 of which result in permanent neurological deficits [2, 3] and an additional 50,000 yearly losses of life [1, 2] accounting for approximately 30% of all deaths due to injuries [1]. This epidemic becomes especially prevalent in military population, where approximately 20% of the soldiers (Iraq and Afghanistan) have been diagnosed with some level of TBI [4, 5, 6]. In 2018, there were 18,949 instances across the United States armed forces, approximately 90% of which are classified as a mild injury [4]. The DoD classifies TBI as mild when the effected individual has confusion and/or disorientation that lasts for less than 24 hours, or a loss of consciousness lasting less than 30 minutes [4]. In addition, for mild TBI a computed tomography (CT) scan is not required, since the CT data is not capable of detecting injury [4] given the limitations in current technology. This makes mild TBI especially dangerous; due to lack of visible injury criteria and biomarkers, individuals can risk further injury especially after a missed diagnosis. Despite no visible injury, mild TBI in veterans has been linked to chronic conditions [7, 8] including PTSD [9, 10], depression [9], anxiety [9], and substance use [9]; with the odds of diagnosis of these conditions increasing in military personnel from 150% to 300% [9] compared to the civilian populations.

TBI can be separated into three main modalities of injury: blast, where injury is caused by an explosion; blunt, where injury is caused by physical impact with the head; and ballistic, where injury caused by penetration of the skull. Each modality, while possibly having a similar downstream biochemical, neurological,

and/or pathophysiological outcomes, has differing severities, and mechanisms that need to be identified independently. The treatment regimes in each modality need to be different since the pathology of injury differs due to varying biomechanical loading. Blast-induced traumatic brain injury (bTBI) has been gaining increased attention due to ongoing global conflicts and persistent threat of terrorism around the world [11, 12, 13]. It is an active research area covering model studies aimed at the elucidation of injury mechanisms [14, 15, 16, 17], and design of mitigation methods [18, 19, 20, 21]. This is not to say that this a new injury modality; since World War I, a connection between blasts and neurological deficits has been established [22]. Since then, among military personnel, bTBI has become one of the leading modalities of injury [23, 24]. The danger here is bTBI is predominantly mild, and within this range, shock waves can still cause diffuse brain injuries, for example, to intracranial vasculature [25, 26], without visible markers of injury. This can lead to compounding injury from even occupational low level blasts that soldiers may undergo regularly for combat readiness purposes [27]. Despite all this research, there is still a clear gap in understanding how shock waves interact with biological tissue and how this causes to brain injury. bTBI has proven to be the least understood injury modality while being the most prevalent brain injury among combat personnel; and therefore, it is increasingly important to elucidate the mechanisms of bTBI.

Part of the difficulty of studying bTBI is that injuries in the field are mixed modal. The injury modalities can be divided into four classifications: primary (injury caused by the shock wave alone); secondary (injury caused by shrapnel); tertiary (injury caused by fall or impact); and quaternary (injury caused by fire and/or gasses) [8, 28, 29]. These classifications are dependent on peak incident overpressure, which in turn, is dependent on the weight of the charge and the distance of the specimen from the epicenter of the blast [30]. When studying bTBI, researchers typically simplify and focus solely on primary blast injury assuming that specimens are at a large enough

distance for the pure shock wave to be the only biomechanical loading mechanism. This simplification also aims to focus on the damage caused solely by the shock wave; the least understood injury modality. It is also presumed, once identified, results can be superimposed with secondary, tertiary, and quaternary injury modes for more complex and realistic loading conditions.

When characterizing a shock wave, the incident blast overpressure (BOP), or side-on pressure, is widely as a metric of the severity of a shock wave. In order to measure BOP, the sensing element needs to be parallel to the direction of the shock front. The incident pressure-time profile is described as a Friedlander wave, defined by a sharp rise with a very small risetime, typically in the microsecond range, representing the shock front, followed by a nonlinear decay lasting a few milliseconds. The peak pressure of the incident pressure-time curve is the most common parameter used in bTBI studies signifying the intensity of blast [31]. The positive phase duration (time it takes overpressure to return to zero or ambient pressure) and impulse (area under the pressure time curve) are also important parameters; although they are typically ignored in the literature, it may be important to study their effects. In addition to incident overpressure, reflected overpressure (ROP) can be another important parameter when describing shock structure interactions. While incident overpressure is independent of the specimen being interacted with, the reflected overpressure is the pressure measured on the surface of the specimen impacted by the shock wave and can be anywhere from 2-8 times higher than that of the incident overpressure within the range of overpressures that cause mild injury [32]. Much larger BOP's and Mach stems can result in even higher peak ROP, but these conditions will be ignored due to the focus of this work on mild TBI. The reflected overpressure profile is dependent on the incident Mach number, rigidity of the support structure, the angle of incidence and stiffness of the impacted surface [32]. The incident Mach number is based on the ratio of shock velocity to ambient acoustic velocity and increases

nonlinearly with BOP. These arguments suggest that geometry, boundary conditions, and material properties should all influence the magnitude of net mechanical loading during insult and downstream govern the extent of the damage and injury.

Based on the current knowledge, shock waves have been postulated to have many mechanisms of insult: direct transmission, where the shock wave directly pressurizes the brain; skull flexure, where the shock wave causes the skull to deform causing stress to the surrounding tissue; thoracic surge, where the thorax is pressurized and the pressure is translated to the brain through the blood vessels; cavitation, small bubbles form and burst causing jets that damage surrounding tissue; and acceleration, where rotational and translational inertial affects cause stress to brain tissue [28, 33]. It is still unclear which mechanisms are valid, and by how much, and what roles, if any, each play during primary injury.

In order to investigate how shock waves cause injury, the use of animal models, most commonly murine, are used as a proxy to study human injury. Researchers typically use an insult to injury to outcomes experimental paradigm. With this, researchers present live specimen with an insult (biomechanical loading); in this case a shock wave, that causes pathophysiological changes i.e., injury and secondary injury cascades. The injury then causes temporally evolving behavioral changes which are studied and compared to observations in human subjects. One of the issues with this comparison is medical outcomes for humans in the field are typically self-reported. Measures, such as the Glasgow coma scale, are very subjective and are dependent on the responses of the patient and the interpretations by physicians [34], especially when diagnosing mild injury. Also, in mild injuries, humans can at best, offer imaging information and not the pathophysiological data available for animal models. As was noted earlier, imaging data may not be able to provide any information in mild TBI. Thus, direct comparison between the spatial and temporal evolution of pathophysiology in animal models with humans is all but impossible given

current technologies. Despite this hurdle, there are many studies showing similar behavioral outcomes in both veterans and animals exposed to blast [35, 36, 37, 38]. Unfortunately, despite these efforts there is no animal to human transfer function that can translate these findings in animal models to the human clinical domain [39, 40, 41]. While some medical outcomes of blast injury seem to match between species, it is unclear which metrics can predict outcomes in mild cases.

To get around these issues, another approach would be to design a research paradigm that compares similar injuries between two species. The issue with this approach is studying acute time points using human subjects is both unethical and infeasible given the current technology. The closest researchers can get to investigating human injury in a controlled environment is the use of postmortem head surrogates (PMHS), but these are unable to show the injury mechanisms that take place in living tissue and can only provide estimates of the insult. While animal models can allow for the investigation of injury metrics, such as blood brain barrier (BBB) breakdown and microglia activation, at virtually any time point and brain region; at this time, researchers do not have the same capabilities to easily quantify these metrics for humans.

This leaves comparing biomechanical loading carefully between species as the only level of the research paradigm pathway that is practical and meaningful. Thus, a fundamental question in the study of bTBI is how biomechanical loading during blast translates from animal models in the laboratory to human injury in the field. Assuming the ability to expose specimen to field relevant shock waves, it should be possible to investigate how shock loading differs between species; and therefore, how downstream injuries and outcomes are initiated by the insult. Without the need for replicating secondary cascades or other modalities of injury parameters associated with blast, insult can be further simplified and parametrically investigated. In this approach, it is presumed that an organ, (i.e., brain) of

a properly functioning live specimen, when biomechanically loaded beyond some threshold will cause pathogenesis. Pathogenesis will evolve over time, and the rate of this evolution is dependent on the severity of loading. It is also presumed that the tissue will respond similarly between species given the same loading conditions. Thus, biomechanical loading intensity at a tissue level is the primary factor that initiates pathogenesis, pathophysiology, and further into cognitive and behavioral dysfunctions. Consequently, this work targets this biomechanical loading at the tissue level.

The first step in comparing blast insult between species is identifying a method of replicating field relevant blasts in a laboratory setting. There are several different methodologies claiming to mimic the free field shock conditions necessary to study bTBI. These methods range from shock tubes [42, 43, 44, 45] to firearms [46, 47] to live field experiments [43, 48]. It is unlikely that each of these methodologies load the intended specimen in the same manner. The compressed-gas driven shock tube has been shown to accurately replicate the Friedlander wave that is characteristic of field relevant shock waves. They have been shown to match a wide variety of incident pressure profiles seen in the field [28]. Shock tubes have been used in numerous studies since their inception, to investigate shock physics [49, 50] and shock structure interactions. Relatively recently, they have also been used in biological and medical research investigating blast induced pulmonary injury with some success [51]. According to a recent survey of 70 papers, compressed driven shock tubes are the most commonly used modality for replicating field blast conditions [52]. Despite recent consensus regarding the shock tube model, there is still debate on using them to properly load a specimen [52]. Not all shock tubes can equally replicate field conditions, and many have issues with artifacts in the pressure signals caused by reflections [53], end affects [54], and blockage [31]. In order to translate insults, shock waves produced in the laboratory must be able to adequately replicate the

field measured values caused by actual explosives. Because of the discrepancies found between shock tube models between groups, there has been a call for shock models that more accurately represent insult [31, 53, 54] and for more uniformity in the representation of data in the field.

Once a specimen can be exposed to field accurate shock waves, it should then be possible to develop scaling laws or relationships between the biomechanical loading experienced by different species. These scaling laws, or more accurately transfer functions, allow for biomechanical between species to be related based on measurable parameters. Most current scaling techniques are derived from mass scaling developed by Bowen et al. [55, 56]. The primary issue with these laws is that they focus on mortality as a binary rather than the injuries of the specimen that lead to deficits short of mortality. The functions scale between species by using differences in lung volume and body mass, and while they seem adequate for pulmonary blast injury, they fail to account for the complexities of brain injury [6, 45, 57]. Body and brain mass scaling have also been proposed for functions more specific to brain injuries, but these transfer functions have also been ineffective [57, 58]. These functions ignore geometric or material differences that are present between species and that may affect specimen loading, especially under blast conditions. Mass scaling, for instance, does not account for vast differences between the percent mass of white matter between animal and human subjects that can cause changes in loading profiles [59]. Other transfer functions have taken inspiration from blunt injury models and are based on the acceleration undergone during injury [60]. Although the use of acceleration in head injury criteria (HIC) has been effective in reducing blunt injuries in automotive incidents, it fails to account for damage from the possible blast mechanisms. Blast especially within the mild range may not induce the same level of acceleration seen in blunt injuries. Furthermore HIC is based on the acceleration required to skull fracture, which does not occur in blast conditions. One key aspect, that should be

accounted for based on previous work, is the need to form a transfer function based not only on the peak BOP, but also the impulse of the BOP profile [6, 51, 61, 62].

With recent technological advances, the use of Finite Element Modeling (FEM) has become a popular method to derive transfer functions. These methods try to account for the differences in geometry and mechanical properties between species and aim to fill the gaps left by current transfer functions [57, 58]. Using FEM, Jean et al. [57] was able to show that brain mass and body mass scaling solely [42, 62, 63] does not accurately represent bTBI. In this work, it was found that the intracranial pressure did not scale with either body or brain mass, and instead found that consideration of how stress waves propagate differently based on material (skin,bone, or brain) allows for more accurate scaling [57]. Specifically this paper suggests that a more accurate scaling parameter will focus on the relative difference in acoustic impedance between brain and surrounding protective tissue. While providing some insight, many of these studies lack the validation of proper shock loading as well as validation of material properties. In the literature, these studies use a wide range of material properties to try and replicate blast insult. There are numerous studies that base the material properties solely on the ability to converge to a numerical solution rather than through data obtained from experiments to validate their models. Previous studies have shown that even on the scale of the rat, relatively small changes in material properties can have significant differences between the insult outcomes [64]. FEM excels at replicating geometrical features, but lacking a proper material model, these cannot simulate the complex boundary value problem that is at the core of shock biostructure interactions. Thus, FEM makes many assumptions that further reduce the accuracy and even the applicability of these transfer functions to real world injuries.

Without properly derived interspecies transfer functions, researchers may be exposing animals to overpressures beyond the survivable range for humans [31, 44] or

overpressures so low that clinical significance is lost. Anatomical differences between species including differences in material properties, brain and skull morphology, and orientation need to be considered moving forward with function development [31, 57, 65]. This work aims to compare tissue level loading between live rodents, postmortem rodents, and postmortem human surrogates, in order to derive a biomechanical interspecies scaling function, through the consideration of interspecies differences in size, material properties, and skull thickness.

To accomplish this goal, simple geometry surrogates were initially constructed in order to parametrically investigate how mechanical loading changes as a function of material properties, specimen size, and shell thickness. By using a combination of two-dimensional plates and three-dimensional boxes, parametric analyses were performed. These resulted in the identification of size and skull thickness as potential parameters for interspecies transfer functions. Furthermore, results show that internal structures can have significant effects on the external loading being measured. Measures of insult were defined as strain, reflected overpressure, and internal pressure within vessels.

Next, potential brain simulants were identified by comparing the response of increasingly complex murine surrogates to shock loading to that of fresh postmortem rodent brain tissue. By using skull strain and intracranial loading as insult metrics, comparisons were made that show the effects on various brain simulants under blast conditions. Chosen materials have already, in previous literature, been identified as potential brain simulants for blunt and ballistic injury, but many have not been tested under blast conditions. Results consider differences in intracranial pressure profiles (peak, risetime, duration, and impulse) to ensure the most accurate brain simulant is chosen for surrogate experiments.

Lastly, postmortem surrogates of murine and human models are used to derive an interspecies transfer function for insult metrics (peak intracranial pressure and intracranial impulse). Both specimens were exposed to three discrete incident

overpressure representing different charge weights and standoff distances. By using similar loading conditions, one-to-one comparisons are made between species, in order to identify how insult differentiates. This work aims to elucidate how various interspecies differences affect shock loading and seeks to use field accurate experiments to aid researchers with data interpretation and thus, strongly relate to the practical aspects of pressure measurements pertinent to the occupational low-level blast exposures.

In summary, blast causes TBI among soldiers and veterans, and there is a need to translate the knowledge gained from animal models to a clinical setting. To benefit soldiers and veterans, this work seeks to develop a transfer function based on data obtained through rigorous experimentation. This is currently an unfulfilled scientific knowledge gap. This thesis aims to begin to fill this gap. Assuming that similar tissue level loading leads to similar downstream injuries, it is hypothesized that *the tissue level loading between postmortem rodents and humans can be related between animals and humans through the consideration of the interspecies differences in size, material properties, and skull thickness.* In order to test this hypothesis, three specific aims were further developed:

1. Determine how size, material, and thickness affects pressure loading variation on the surface and within a specimen using simple geometry surrogates.
2. Determine how material affects pressure loading variations within brain and brain simulants.
3. Develop a transfer function to relate pressure loading variations between rat and human models of injury.

This thesis is organized as follows: In Chapter 2, specific aim 1 is addressed. In this chapter, simple geometries including flat plates and boxes were used to elucidate how size, material, and thickness affect pressure loading. Simple geometries eliminate many confounding factors and allow for investigation of the individual effects of specific parameters. Here it was concluded that thickness has significant effect on

both surface and internal loadings. Thus, these were used as specific targets in the following aims. In Chapter 3, specific aim 2 is addressed. In this chapter, increasingly complex surrogates were designed and compared to live rat specimen to determine how material affect the loading variation between brain and brain simulants. Here 20% porcine based ballistic gelatin was shown to be the best brain simulant for replicating mechanical loading seen in live rats. In Chapter 4, postmortem human surrogates (PMHS) loading is addressed. With a brain simulant selected in Chapter 3, PMHS were prepared and exposed to three discrete incident overpressures. Here intracranial pressure and impulse were compared to rat models. In Chapter 5, the second aspect of specific aim 3 was addressed. In this chapter the results of Chapter 3 and Chapter 4 were used to derive interspecies transfer functions. Due to significantly lower intracranial insult seen in PMHS as compared to rats for the same incident overpressure, size was excluded and transfer functions were derived based on specimen skull thickness and incident pressure parameters. In Chapter 6, findings are summarized, scientific contributions are outlined, and future directions, emanating from this dissertation's results, are proposed.

CHAPTER 2

PARAMETERIZATION OF SHOCK LOADING USING SIMPLE GEOMETRIES

2.1 Background and Significance

When characterizing a shock wave, the incident (or side on) blast overpressure (BOP) is widely used as a predictor of the injury [31]. The incident overpressure waveform can be described using the Friedlander equation, characterized by a shock front with a sharp rise time (in the microsecond range) followed by a nonlinear decay (in the millisecond range). The peak pressure of the overpressure-time curve is the most common parameter used in bTBI studies signifying the intensity of blast exposure. The positive phase duration and impulse are also important parameters, despite being often ignored in bTBI literature [66]. In addition to incident overpressure, reflected overpressure (ROP) can be considered as an important parameter when describing shock structure interactions. The ROP is the pressure imposed by the shock wave on the surface of an object and can be anywhere from 2 to 8 times higher than that of the incident BOP in the range of mild bTBI [32]. It should be noted that much larger BOP's and Mach stems can cause even higher peaks but will be ignored for the purposes of this work focuses on mild TBI. The reflected overpressure profile is dependent on the incident Mach number (wave velocity), rigidity of the support structure, the angle of incidence and stiffness of the impacted surface [32], suggesting that geometry, boundary conditions, and material properties should all have an effect on the magnitude of net mechanical loading during shock. Thus, this aim intends to use the ROP profile as an insult metric to examine how changes to experimental design can affect specimen loading.

The compressed gas-driven shock tube is currently the device of choice to replicate field blast conditions. Shock tubes have been used to mimic and study blast

phenomena since their inception in 1899 [49, 50] and have increased in popularity due to the repeatability and control of shock waves in a laboratory setting. With a recent survey [52] stating about 90% of primary bTBI studies use compressed gas-driven shock tubes, these shock tubes were chosen for this work. Careful optimization of shock tube operating variables facilitates the generation of tailored shock waves where the peak incident overpressure remains constant, and impulse value can be varied through lengthening of wave duration. A similar level of control has yet to be published in the open literature. These advances included in this work, are used to address the fundamental question of how the incident loading conditions translate into the corresponding insult metrics (ROP). Though the role of duration in a shock profile, and hence indirectly the impulse, has been studied by Bowen et al., these studies have been primarily restricted to relatively high overpressure lung injuries and not mild bTBI [56, 67].

In order to investigate the relationship between specimen loading and varying experimental conditions, a series of models with simplified 2D geometry was used. It should be noted that the effect of depth (along the shock direction) was not studied here. These square plates were instrumented with pressure sensors mounted flush with the front surface facing the impinging shock wave to measure ROP. The ROP is a measure of the loading on the surface of an impacted specimen. ROP is at it's maximum when the surface in question is perpendicular to the direction of the shock front. Models with simple geometries allow for a greater understanding of shock structure interactions by eliminating many of the confounding factors that arise from complex shapes and complex material properties found in biological structures. The results indicate that the reflected pressure profiles significantly differ with the plate dimensions, and the duration of the incident shock wave. This work sheds new light on the understanding of how incident shock wave characteristics and geometrical factors affect the reflected pressure profile.

With the identification of surface level specimen loading, the next step is to investigate how surface loading transmits into the specimen, and which parameters affect this transmission. In blast neurotrauma research, researchers typically focus on the primary injury, due to its persistent prevalence at greater distances away from the epicenter of the blast [30]. This allows for the investigation of injury in a controlled environment typically through the use of murine models. These models while providing insight to potential secondary cascades of injury, fail to accurately replicate the mechanics of insult undergone by humans in the field. In order to isolate the mechanical effects of shock on a body, researchers often take advantage of non-organic surrogates [8, 68]. These more complex surrogates (relative to the plates) play an important role in the investigation of the mechanics of insult without the variability of biological specimen. Thus, creating more accurate surrogates becomes pivotal when investigating bTBI. The difficulty in creating the said surrogates arises due to the increasing strain-rates on tissue during injury when compared to the commonly studied blunt injuries. This work continues the 2D plate experiments and through more complex 3D geometries, identifies potential brain simulants for the investigation of blast research. Brain simulants were chosen from various materials that have been previously used in TBI research. By using a simple 3D geometry in conjunction with field relevant blast conditions, this work aims to accurately elucidate how these materials behave under blast conditions. The chosen materials may have shown functional accuracy in blunt or even ballistic injuries, but the mechanics behind blast neurotrauma is significantly different and therefore, materials need to be re-evaluated. This work also allows for the investigation of the effect skull thickness on shock loading. By varying the thickness of the structure, how these changes vary shock wave transmission can be investigated, without the confounding factors from using actual bone. The work presented in this aim step by step investigates how individual parameters effect shock loading.

2.1.1 Objective

The objective of this work in this chapter is to *determine how specimen size, material, and thickness affect pressure loading variation using simple geometry surrogates* (Specific Aim 1). Using simple geometry surrogates, parameters of size, material, and thickness were isolated and investigated independently.

2.2 Materials and Methods

2.2.1 Shock Tube

All experiments were conducted with the 20-foot-long, 9 x 9-inch (228.6 x 228.6 mm) square interior cross-section tube, described previously in detail [18, 43, 54]. Helium (ultra-high purity, 99.99%), or nitrogen were used as driver gases in the experiments. The driver gas was pressurized in the driver section. The driver section is separated from the driven section of the shock tube by Mylar membranes. Shock waves are produced when the pressure in the chamber exceeds a set value and the membranes fail, and the burst pressure intensity is determined by the thickness and quantity of these membranes. Tests were performed at three discrete nominal shock wave intensities: 70, 130, and 180 kPa (10.1, 18.8, and 26.1 psi) measured at the test section of the shock tube covering a typical range in military bTBI studies. Incident pressure profiles were measured using PCB Piezotronics (Depew, NY) Model 134A24 distributed along the length of the tube. Pressure data was recorded at 1.0 MHz sampling frequency with a total acquisition time of 50 milliseconds. Reflected pressure was measured using the plates shown in Figure 2.1 A-D. The pressure data signal was run through a signal conditioner prior to the DAQ, no filtering or other post processing was done to the data after data was initially collected.

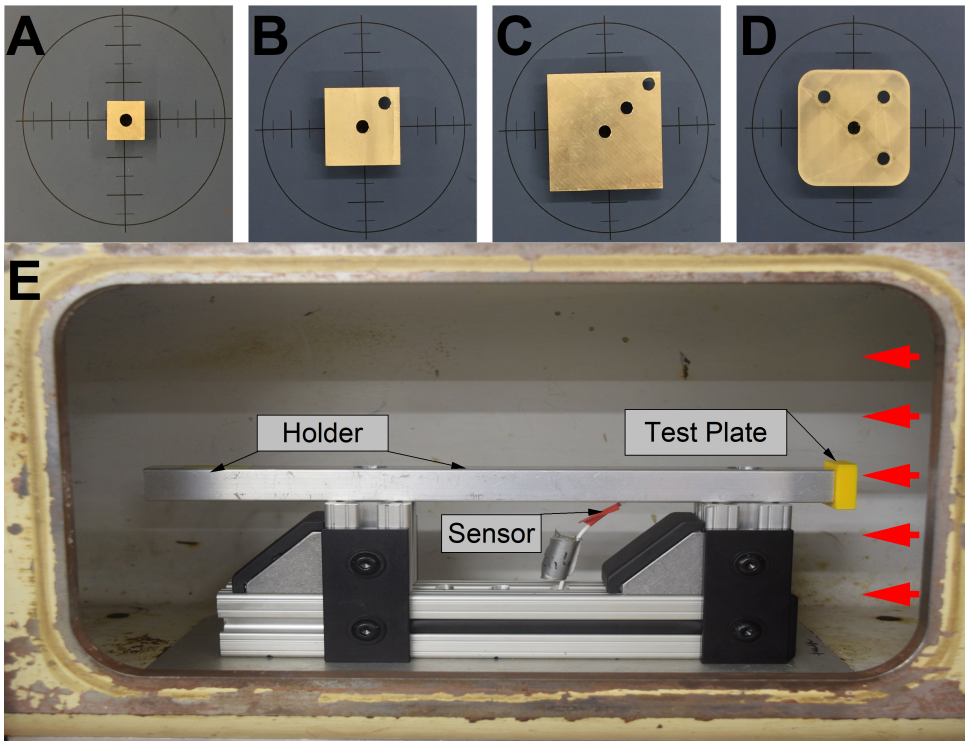

Figure 2.1 The test setup for the evaluation of the effect of the cross-sectional area on the reflected pressure. The aluminum plates with cross-sectional areas of: A) 1 in^2 B) 4 in^2, and C) 9 in ^{2} were mounted in the center location. D) A 9 in^2 PLA plate with rounded corners used in specimen location experiments. Rounded corners allowed for better fit in the various sensor locations. E) Test fixture at the test section of the shock tube holding an instrumented 1 in^2 PLA plate (yellow). The direction of the propagation of the incoming shock wave is indicated with red arrows.

2.2.2 Data Analysis

Various aspects of both the incident and reflected overpressure profiles were extracted from the data. The peak overpressure was determined manually by the peak of the initial rise of the pressure time curve (example shown in Figure 2.2G). This peak allows for consistent results that are independent of artifacts caused by reflections and motion, shown in the inset of Figure 2.2G. This is especially important for the reflected overpressure profiles where there are high peak artifacts during the flat top region of the reflected pressure time curve. Similar peaks have been reported previously in [69]. The risetime was calculated using OriginLab OriginPro and was based on the time to rise from 10% to 90% of the first peak described previously. The

duration was measured as the positive phase duration of the pressure time curves where t_1 is the time pressure rises above ambient pressure and t_2 is the time the pressure returns to a stable ambient pressure. The impulse was calculated as the integral of the pressure time curves during the positive phase duration.

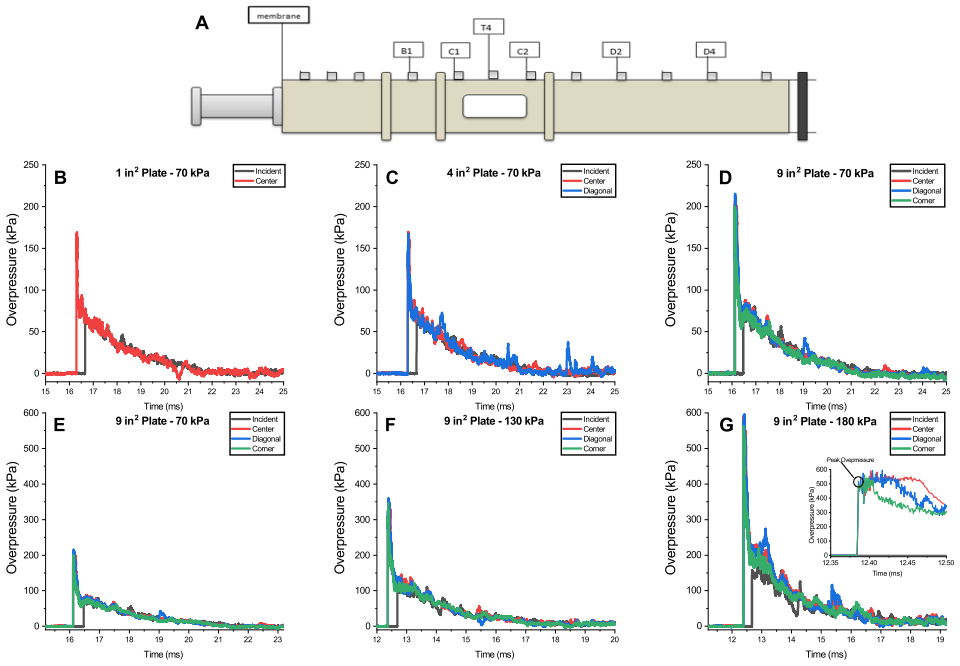

Figure 2.2 A) The diagram of the shock tube with the distribution and labeling of the pressure sensors measuring side on overpressure. Incident overpressure profiles shown are representative of those measured at T4. Incident and reflected overpressure profiles are shown for B) 1 in^2 plate, C) 4 in^2 plate, and D) 9 in^2 plate at a target 70 kPa incident overpressure. Incident and reflected overpressure profiles are also shown for 9 in^2 plate at a target incident overpressure of E) 70 kPa, F) 130 kPa, and G) 180 kPa. Zoomed in graph, shows the difference in the pressure profiles between three sensor locations on the plate.

2.2.3 Effect of Cross-sectional Area

In order to investigate the effect of specimen size on shock loading, three square aluminum plates were machined, and an additional three PLA plates were 3D printed with increasing cross-sectional area (H x W): 1 x 1 (1 in^2, Figure 2.1A), 2 x 2 (4 in^2, Figure 2.1B), and 3 x3 (9 in^2, Figure 2.1C). Plates of differing material were used to examine if differing material properties have significant effects on the pressure profiles and therefore, could be used interchangeably throughout the experiments. This was thought to be important for the corner sensor in the 9 in^2 plates where deformation in the PLA plates may affect measurements and cause changes to the dwell time of the reflected pressure. Plates were located in the shock tube at the test section approximately 3 meters (9.84 ft) from the breech (Figure 2.1E). The design of the plate holder was optimized to eliminate the vibration and other motion artifacts from the signal. The center of the plates were aligned with the central axis of symmetry of the shock tube to ensure flow field uniformity. The front surface of the plate was normal to the propagation of the incident shock wave. Each plate was instrumented with pressure sensors model 102B06 (PCB Piezotronics, Depew, NY), with the sensing element placed flush with the front face placed diagonally every .85 inches (21.59 mm), as size permitted. Each plate was exposed to the pressures described in Section 2.1 with helium as the driver gas.

2.2.4 Variable Duration

The breech length of the shock tube was adjusted, and nitrogen gas was used as the driver gas to develop a shock profile where the peak incident overpressure was constant while the duration increased as compared to the helium shots. For these experiments, only the 9in^2 (228.6 mm^2) aluminum plate was used. The plate was exposed to peak incident overpressures of 1) 130 kPa (18.9 psi) and 2) 180 kPa (26.1 psi) with incident impulses of 1) 440 Pa·s (63.8 psi·s), and 2) 720 Pa·s (104.4 psi·s),

respectively. Reflected overpressure profiles were compared with 9 in^2 plates exposed to standard helium shots (similar those described in Section 2.2) with peak incident overpressures of 1) 130 kPa (18.9 psi) and 2) 180 kPa (26.1 psi) and impulse of 1) 220 Pa s (31.9 psi·s), and 2) 330 Pa s (47.8 psi·s), respectively.

2.2.5 Specimen Location

In order to determine the effects of specimen location within a cross-sectional plane of the shock tube, a 3D printed PLA plate was instrumented as is shown in Figure 2.2D. Unlike previous plates, these plates were made with rounded edges to ensure there were no gaps between plate and shock tube walls. This plate was tested in three conditions: 1) center (aligned with the center axis of symmetry of the shock tube), 2) side (plate mounted symmetrically with the horizontal plane of symmetry and touching one wall), and 3) corner (placed in the corner of the shock tube). The plates were exposed to a single shock wave with 180 kPa (26.1 psi) BOP using nitrogen as the driver gas. The purpose of these experiments was to evaluate how the relative placement within the cross-section of the shock tube affects mechanical loading. This question assumes even greater emphasis considering animals are often placed in smaller shock tubes with these artifacts effecting the results.

2.2.6 Theoretical Calculations

Incident overpressure, sometimes referred to as side-on or static overpressure, describes the increase in pressure measured parallel to the incident shock wave relative to the ambient pressure P_x. It is most commonly used when describing shock waves and is directly related to the Mach number of the incident wave. The Mach number is the ratio of shock wave velocity to the acoustic velocity of the medium under similar environmental conditions including temperature, humidity, and altitude. Peak incident overpressure (P_y) can be theoretically solved for using Equation 2.1 (adapted

from [32]), where M_x is the Mach number of the incident wave. Mach numbers were calculated based on the arrival times of the shock front to closest incident pressure sensor and the arrival at the plate and accounting for differences in temperature and humidity measured pre-blast. Equations cited are based on idealized conditions for blasts through air. Comparison between theoretical and experimental values is shown in Figure 2.3.

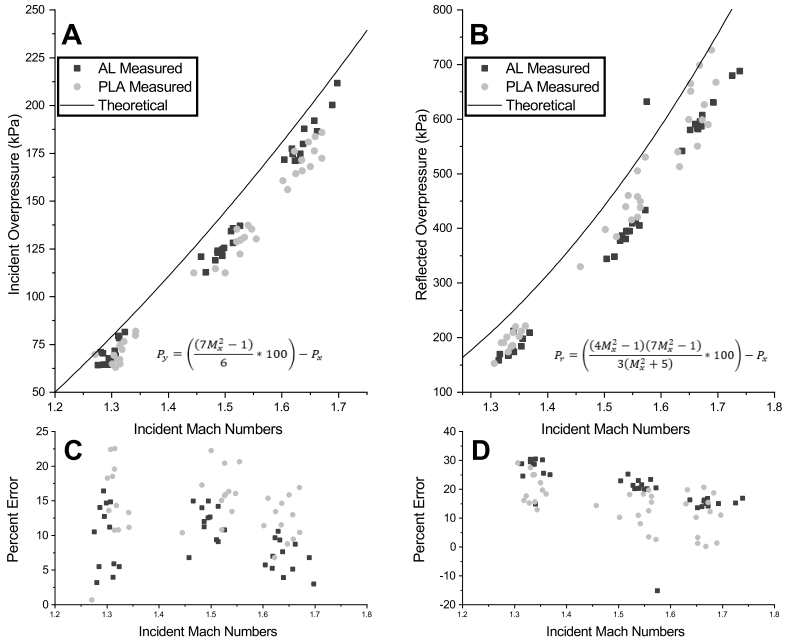

Figure 2.3 Comparison of A) the measured incident and B) reflected overpressure with the theoretical values calculated using Equations 2.1 and 2.2, respectively. (C) and (D) show the percent error at each data point.

$$P_y = \frac{7M_x^2 - 1}{6} \cdot 100 - P_x \tag{2.1}$$

The reflected pressure describes the increase in pressure on a surface impacted by a shock front. Reflected pressure is dependent on the angle of incidence, as well as M_x and is at its peak value when the impacted surface is normal to the incident shock wave. Due to plates being placed normal to the incident shock wave, the peak

reflected pressure equation can be simplified to Equation 2.2 adapted from reference [32]. It should be noted that these equations assume that the impacted surface is static and unyielding. Comparison between theoretical and experimental values is shown in Figure 2.3.

$$P_r = \frac{(4M_x^2 - 1)(7M_x^2 - 1)}{3(M_x^2 + 5)} \cdot 100 - P_x \tag{2.2}$$

The reflected pressure coefficient is the ratio of reflected overpressure and its respective incident overpressure. It can be used to easily make comparisons between blasts of varying overpressures. The reflected pressure coefficient for air can also be calculated from the Mach number using Equation 2.3 (adapted from [32]).

$$\frac{P_r}{P_y} = \frac{8M_x^2 + 4}{M_x^2 + 5} \tag{2.3}$$

When a shock wave interacts with a surface it creates a pressure build-up on the surface. This creates a region of relatively constant pressure in the reflected pressure profile, shown in inset of Figure 2.1G. The duration of this region is considered the dwell time. It is thought that this dwell is caused by the delay in the arrival of a rarefaction wave from the edges of the plate. However, these rarefaction waves, which should propagate with the velocity approximately the same as the speed of sound in the shocked medium, are elusive and difficult to characterize [32]. In simpler terms, the pressure buildup in the center of the plate is relieved by the pressure differential which exists between the center and the edges of the plate as the shock wave passes by. This flow from the high pressure to low pressure constitutes a rarefaction wave moving from the edges to the center of the plate [32]. With this parameter, dwell time or pressure relief time (t_r) can be estimated given Equation 2.4, where d is the shortest distance from the point of interest to the edge of the plate and u_x is the

acoustic velocity of the medium. It should be noted that this is just an estimate and in practice had been found to be sufficient for predictions [32].

$$t_r = \frac{d}{u_x} \tag{2.4}$$

2.2.7 Finite Element Modeling

A finite element model of the experimental setup with the shock tube and plates was created using a coupled Eulerian-Lagrangian modeling technique. This modeling technique has been shown to effectively simulate shock wave propagation within a shock tube and accurately recreates shock-structure interactions [70, 71, 72]. Two modeling domains were simulated, an air-filled Eulerian domain and the Lagrangian domain of the solid plates. The Eulerian shock tube model simulated a 3.8 m long Eulerian domain. This domain was filled with air at atmospheric pressure and temperature, modeled as an ideal gas with a specific heat ratio of 1.4. The length of the shock tube model was selected to simulate the section downstream from the first sensor closest to the breech, sensor B1 in Figure 2.1. The incident pressure signal from this sensor location was used as the input waveform for the simulations. The shock wave was modeled as a pressure-time waveform applied at the B1 location and was constrained at the shock tube walls and exit, where all translational degrees of freedom were constrained. The model was represented by a biased mesh, with a converged minimum element edge length of 4 mm at the region of interest, resulting in a system of over 857,000 linear hexahedral Eulerian elements. The Lagrangian domain consisted of models of plates based on the experimental specifications. The plates were modeled with a converged element edge length of 2 mm, with the 1 in^2, 4 in^2, and 9 in^2 plates having approximately 800, 2700, and 5750 linear hexahedral Lagrangian elements, respectively. Two additional models were created to simulate the rounded edge variations of the 9 in^2 plates used in the corner and side shock

tube locations. The plate was modeled as aluminum, approximated to be linear, elastic and isotropic with a density, elastic modulus, and Poisson's ratio of 2700 kg/m^3, 70 GPa, and 0.33, respectively. The plate locations were as specified in the experimental setup for validation of the experiment and all translational and rotational degrees of freedom were constrained on the posterior face of the plates, to mirror the experimental configurations. All the numerical models and computations were conducted by computation group at CIBM3 and is not part of the work carried out by the author of the thesis.

2.2.8 Simple Three-Dimensional Geometries

The box was constructed from a combination of polycarbonate (PC) and polytetrafluoroethylene (PTFE). The box was fixed to the 9-inch shock tube, previously described in [18, 43, 73], with an aluminum fin. The fin acts as an air foil to limit any additional interaction with the shock wave by reducing the potential reflections. To this end, the surrounding walls of the box were made extra thick compared to the front window to help limit shock wave transmission to the longitudinal axis. The box was filled with 10% VYSE Ballistic Gelatin (porcine based), 20% VYSE Ballistic Gelatin, 10% synthetic clear ballistics ballistic gel, and Sylgard 527 Silicone Gel. As shown in Table 2.1, where citations are listed, these materials were selected based on frequency of usage seen in recent literature. Specifically, 10% and 20% porcine gelatin were chosen as most common porcine gelatin brain simulants [74, 78, 83, 117]. Previously both 10% and 20% porcine gelatins have been tested and compared and have a relatively close match human brain depending on the temperature range [83]. Material selection does not necessarily presume these material are a one-to-one match for brain, and there may be materials or variations in composition that may be a closer match. Each of the materials selected have been previously used in order to study some modality of TBI and to some level have been shown to match brain tissue.

Boxes were 3x3x3 inches with an inside volume of approximately 2x2x2". In order to measure the transmitted pressure, two Millar 3.5F (SPR-525) catheter pressure sensors were embedded at various depths at the center and corner locations within the materials. Pressure sensors were supported by cannulas constructed from stainless steel tubing in order to limit motion artifacts and to protect sensors from damage. Throughout the study, in addition to varying the sensor depth and internal material, the incident overpressure and front window thickness were also varied between $1/8^{th}$ and $1/16^{th}$ in thick polycarbonate windows. A Kulite LLHT surface mounted pressure transducer was placed in the surface of the front window measuring the arrival of the shock front to the box. A strain gauge was also placed on the center of the window in order to see how deformation of the front window may change based on the materials behind it and how it may play a role on pressures measured inside the box.

Table 2.1 Brain Simulant Materials

Material	Citations	Count
Sylgard 527	[74, 75, 76, 77, 78, 79, 80, 81]	8
Sylgard 184	[82]	1
Animal Based Gelatin	[68, 74, 78, 83]	4
Synthetic Based Gelatin	[68, 84]	2
Agarose Gelatin	[78]	1
Agar/glycerol/water	[84, 85]	2
Agar/Glycerol	[84, 85]	2
Alginate	[84, 86]	2
Silicone Gel (unspecified)	[87]	1

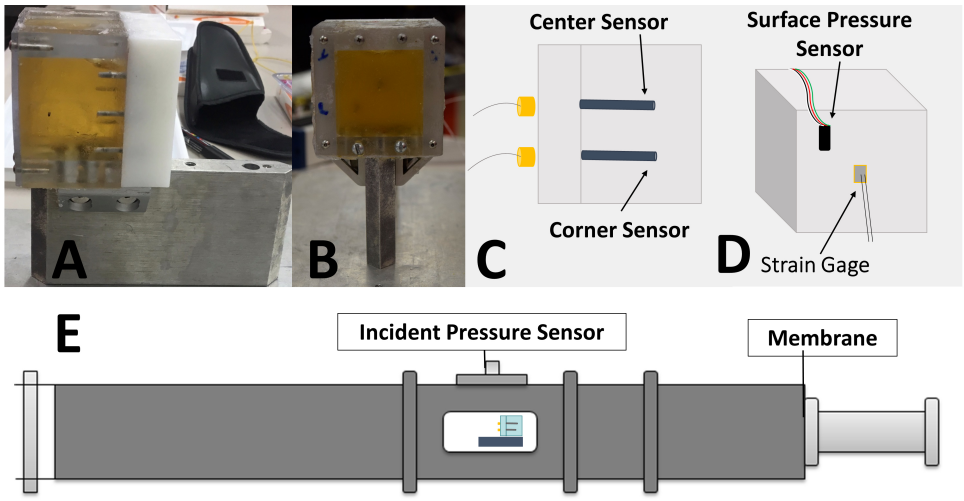

Figure 2.4 A) Side View and B) Frontal View of the box filled with 20% porcine gelatin. C) Pressure sensors are placed staggered and D) Strain gauges and surface pressure sensors are mounted front window. E) Specimen is placed within the 9x9 in shock tube.

2.2.9 Statistical Tests

Descriptive statistics were performed using OriginPro. A priori analysis based on preliminary data was performed using G*Power 3.1.9 [88] and found that an n value of 4 was sufficient. For the plate experiments, one-way ANOVA was performed using R Commander package of R and followed by post-hoc t-tests corrected using Tukey's Honestly Significant Difference (HSD) test to determine significance between groups also in R Commander [89, 90, 91]. Due to equal numbers in all groups, normality and variance were assumed. For the 3D geometry experiments, Factorial ANOVA was used for initial metric comparisons using SPSS 25, One-Way ANOVA for comparisons between the depths, and an independent samples t-test for comparisons between window thickness and gel concentrations. Finally, the post-hoc independent sample t-tests were run through Bonferroni corrections. In many cases data was normalized relative to it respective incident pressure parameter Material velocities were compared to literature values of brain [92]. This data base uses empirical data from multiple peer reviewed sources to identify the acoustic velocity of brain tissue using ultrasound.

This is thought to be sufficient for comparison because as the shock wave interacts with tissue it now behaves as a stress wave. Stress wave velocity is limited by the acoustic velocity if the medium.

2.3 Results for Two-Dimensional Geometries

A representative example of pressure profiles obtained during the experiments are shown in Figure 2.1. As expected, the peak reflected overpressures are multiple times higher than the peak incident overpressures. With the increasing size of the plate, the reflected pressure showed not significant change (Figure 2.1B-D), but does scale with incident BOP (Figure 2.1E-G). Also, as shown in the inset of Figure 2.1G, differences in dwell time (t_r) for different sensor locations are visually represented.

2.3.1 Effects of Cross-sectional Area

In order to determine if a more pliable material would affect the reflected pressure profiles throughout the plate, shock wave exposure tests using two 9 in^2 (228.6 mm^2) plates made of aluminum (Young's modulus: 69 GPa, tensile strength: 110 MPa) and PLA (Young's modulus: 3.5 GPa, tensile strength: 50 MPa) were performed. As shown in Figure 2.5, there was no significant difference between peak reflected overpressures or the impulse values when comparing two tested materials. While the stiffness varies greatly between the two materials, it seems that at the incident shock wave intensities used in this study, the PLA mechanical properties are sufficiently stiff to yield comparable results to that of the aluminum plate. This result is important from the materials selection perspective in the rest of this study, as now the two materials can be used interchangeably with confidence that no significant changes will occur due to the two differing materials.

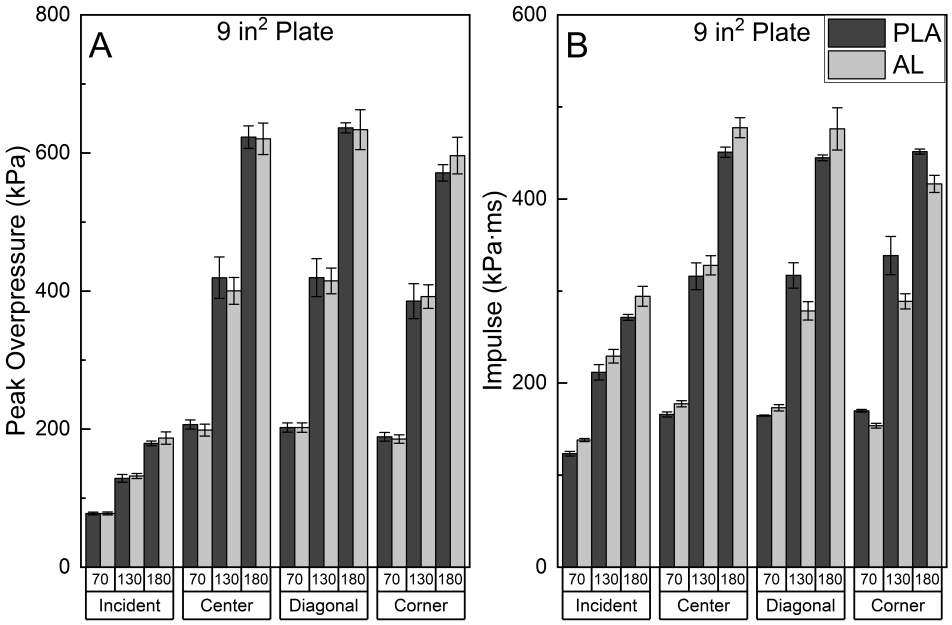

Figure 2.5 Comparison of A) the peak overpressure and B) impulse distribution at three sensor locations mounted in the PLA and aluminum plates. Data are presented as average ± SEM. No significant difference was seen between materials.

ROP distribution was evaluated using 9 in^2 (228.6 mm^2) square cross-section plate with three sensors mounted flush (Figure 2.6A). It is obvious that for the peak reflected pressure (Figure 2.6B), there are is no significant differences between sensor locations at any of the incident overpressures. However, the impulse values (Figure 4C), differed significantly between groups at each incident overpressure (one-way ANOVA, 70 kPa: $F(2,9) = 16.45$, $p = 0.00098$, 130 kPa: $F(2,9) = 7.33$, $p = 0.0129$, 180 kPa: $F(2,9) = 5.006$, $p = 0.0345$), despite no significant difference seen in the positive phase duration (not reported). As the sensor location approaches the edge of the plate, the impulse showed a significant decrease at 70 kPa ($p = 0.00133$, $p < 0.000422$) and 130 kPa ($p = 0.0440$, $p = 0.0139$) as shown in Figure 2.6C.

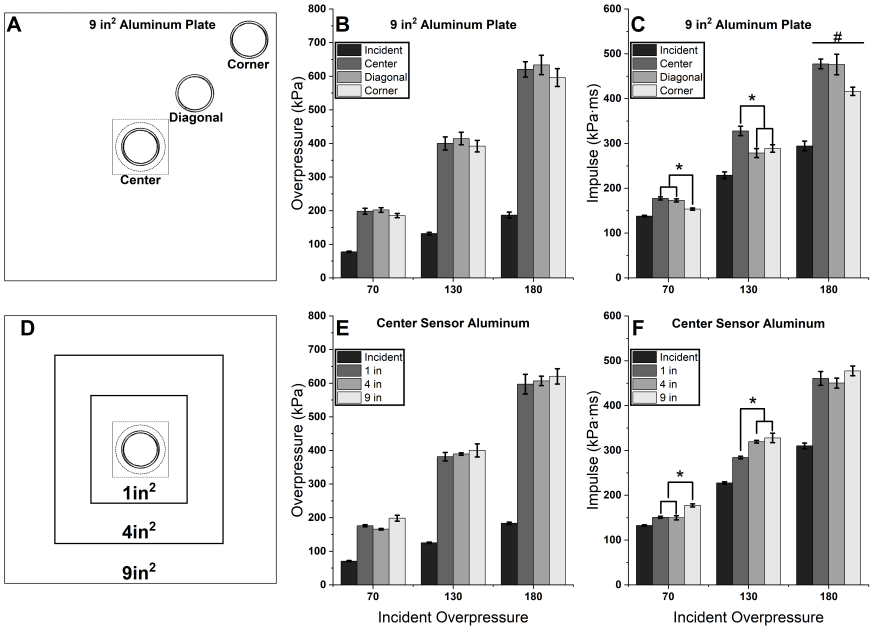

Figure 2.6 A) Diagram of 9 in^2 plate showing naming conventions for each sensor location. The effect of the sensor location on B) the peak reflected overpressure and C) impulse as a function of three discrete BOPs. D) Diagram of different the plate sizes. E) The peak reflected overpressure and F) impulse measured at three discrete BOPs by the sensor in the center of each plate.The asterisk (*) denotes significance in HSD post-hoc test, while the hash symbol (#) denotes significance in one-way ANOVA. Data are presented as mean ± SEM.

To evaluate the effect of the increased surface area, the values reported by the center sensor for all three plates (Figure 2.6D) were compared. Similar to the results described in the previous section, the peak ROP showed no significant difference between the plates (Figure 2.6E). The positive phase duration also showed no significant differences between plates with different surface areas (results not shown). However, the impulse values differed significantly between plates at 70 and 130 kPa (Figure 4F, one-way ANOVA, 70 kPa: $F(2,9) = 19.05$, $p = 0.000582$, 130 kPa: $F(2,9) = 12.86$, $p = 0.0023$). The statistical analysis revealed differences between 1 in^2 and 9 in^2 plates ($p = 0.00112$) and between 4 in^2 and 9 in^2 plates ($p < 0.001$) at 70 kPa, and between 1 in$_2$ and 4 in^2 plates ($p = 0.00961$) and between 1 in^2 and 9 in^2

plates ($p < 0.00264$) at 130 kPa. Interestingly, no significant differences were found at 180 kPa.

2.3.2 Exposure to Variable Duration Shock Waves

Representative pressure profiles for this set of experiments are shown in Figure 2.7A-D. Short duration shock waves have durations of approximately 5 milliseconds (Figure 2.7), while long duration shock waves have closer to double the duration of the short duration shocks, i.e., approx. 10 milliseconds (Figure 2.7). Note that while the duration of the shock wave has changed, the peak incident overpressure remains relatively constant. This feature is critical, considering that this level of control over the shock wave profile allows the isolation of the effects associated with the shock wave intensity vs. these associated with the impulse.

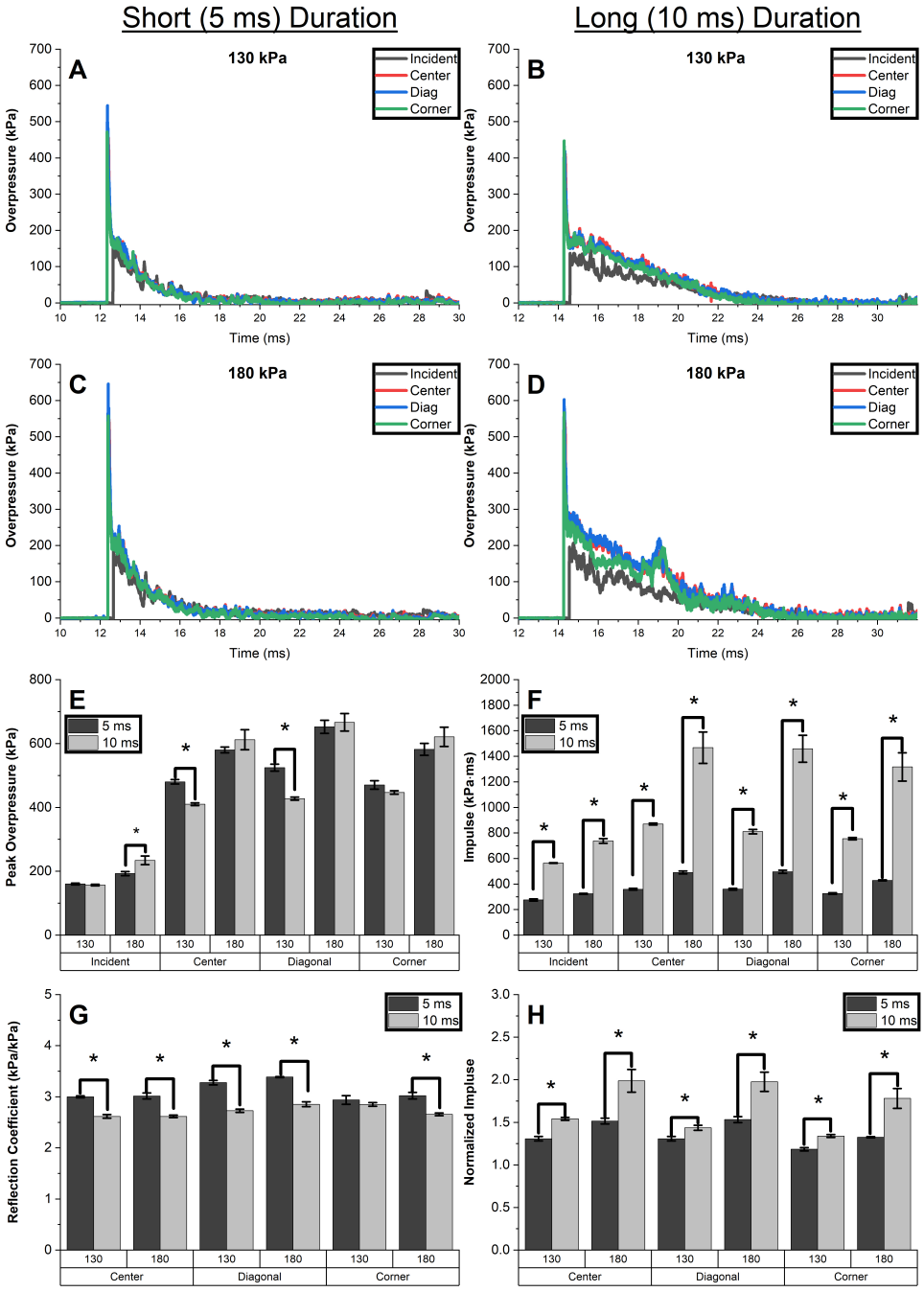

Figure 2.7 The overpressure waveforms for A) 130 kPa 5 ms, B) 130 kpa 10 ms, C) 180 kPa 5 ms, and D) 180 kPa 10 ms incident exposures. Quantification results of E) peak overpressure and F) impulse for short and long duration shock waves as a function of sensor location on the 9 in^2. plate. G) Normalized peak overpressure, and H) impulse comparison for both BOPs and three sensor locations.

As shown in Figure 2.7E, for 130kPa incident exposure there was a significant decrease in the peak reflected overpressure measured at the center and diagonal sensors. This was not seen for 180 kPa target incident overpressure where the long duration shock wave profiles showed a slight, but significant increase in peak incident overpressure compared to the short duration counterparts. This means there could be some differences in loading, and to account for these discrepancies, the reflected pressure values were normalized based on the respective incident pressure values (Figure 2.7G), thus using the reflection coefficient (Equation 2.3) instead. With the increase in the duration of the blast, a significant decrease in peak reflected overpressure are seen in Figure 2.7E at 130 kPa, and at each normalized overpressure shown in Figure 2.7G (Independent samples t-test, $t > 8.3$, $p < 0.00017$ and $t > 5.1$, $p < 0.0021$ respectively), which is counter-intuitive. As expected, there is a significant increase in the incident impulse when increasing the duration. This increase in impulse is further amplified when looking at the reflected impulse on the surface of the impacted plate as both the duration of the dwell time and the overall waveform are increased. As seen in Figure 2.7F and Figure 2.7H, the reflected impulse increases in all tests as compared to the short duration exposure conditions (independent samples t-test, $t > 7.9$, $p < 0.000214$ and $t > 3.3$, $p < 0.0164$, respectively).

2.3.3 Effect of Specimen Location

For these tests, round corner, square 3 x 3 in. plate was used with a different pattern of the pressure sensor distribution to capture the likely ROP changes resulting from the location of the plate within the shock tube (Figure 2.8D). The representative part of the pressure profiles is shown in Figure 2.8A-C. Pressure profiles are enlarged to similar regions near the peak of the pressure profile, where the most significant fluctuations in the pressure waveform are noticeable. It should be noted that the peak overpressure was not measured at the absolute peak of these fluctuations but rather,

the peak pressure of the initial sharp rise characteristic of a shock wave. The pressure values measured during the dwell time seem to be more sensitive to artifacts due to motion in the system. In order to prevent the data from skewing, peak in the dwell region of the reflected pressure profile were ignored. For the middle location (Figure 2.8A), the flow field is symmetrical, and therefore, little difference is seen in the ROP waveforms reported by peripheral sensors. In comparison, as seen in Figure 2.8B and Figure 2.8C, as the plate approaches the walls of the shock tube, the pressure profiles deviate from this pattern. As shown in Figure 2.8E, these changes in a position do not affect the peak overpressure, but in contrast, the impulse varies at specific plate positions. Although trends in Figure 2.8F appeared to be strong, significant difference was only seen in the top right sensor location (one-way ANOVA, $F(2,9) = 17.73$, $p < 0.001$). Specifically, the corner specimen location showed significantly decreased impulse values compared to both center and side locations (Tukey's HSD, $p = 0.00114$, $p = 0.00114$, $p = 0.00255$, for 70, 130 and 180 kPa incident BOP, respectively).

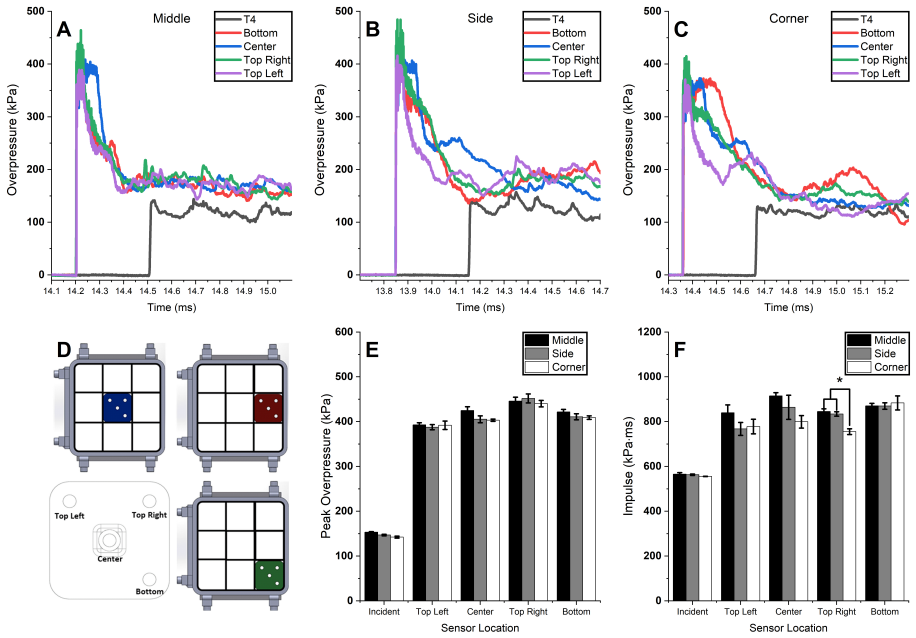

Figure 2.8 A) Overpressure profiles for the middle plate location (blue plate in Figure 2.8D) B) Overpressure profiles for the side plate location (red plate in Figure 2.8D) C) Overpressure profiles for the corner plate location. D) Diagram of the plate positioning used for evaluation of the effect of specimen location within the cross-sectional area in the test section of the shock tube. E) Comparison of peak overpressure and F) impulse values between four sensor locations (Bottom, Center, Top Left, and Top Right) at three plate positions (Middle, Side, and Corner).

2.3.4 FEA Modeling

Observations from the experiments were validated with the pressure-time data from the simulations. The results between simulations and experiments agree well with regards to duration and arrival times. While there is a slight discrepancy in the peak pressure values, the general trend of the pressure-time relationships at the center, diagonal and corner sensor locations are replicated with good fidelity.

The effect of the specimen location was also investigated, and respective heat map for the 9 in^2 plate at the middle, side, and corner locations were generated (Figure 2.9). The heat map values were normalized with respect to incident pressure values and ranged between 0 and 1 to allow for comparison between the different plate sizes. These heat maps illustrate how the disturbed symmetry of the flow field

around the plate affects the distribution of the reflected pressure on the surface. Heat maps showing changes in peak and impulse distributions for plate size and short and long duration exposures can be seen in Figures 2.10 and 2.11. For the plate in the middle location (Figure 2.8D) the center sensor has the highest BOP and impulse, and the remaining three sensors (top left, top right, and bottom) report equivalent values. When the plate is mounted on the side location the load changes in the following order: center > top right, bottom > top left, while for the corner location it is center, bottom > top left, top right. These results indicate that, not only the geometry is affecting the surface load, but also, the location of the specimen within the cross-sectional area of the shock tube. Again results shown are those completed by the computation group at CIBM3, based on the experimental data above.

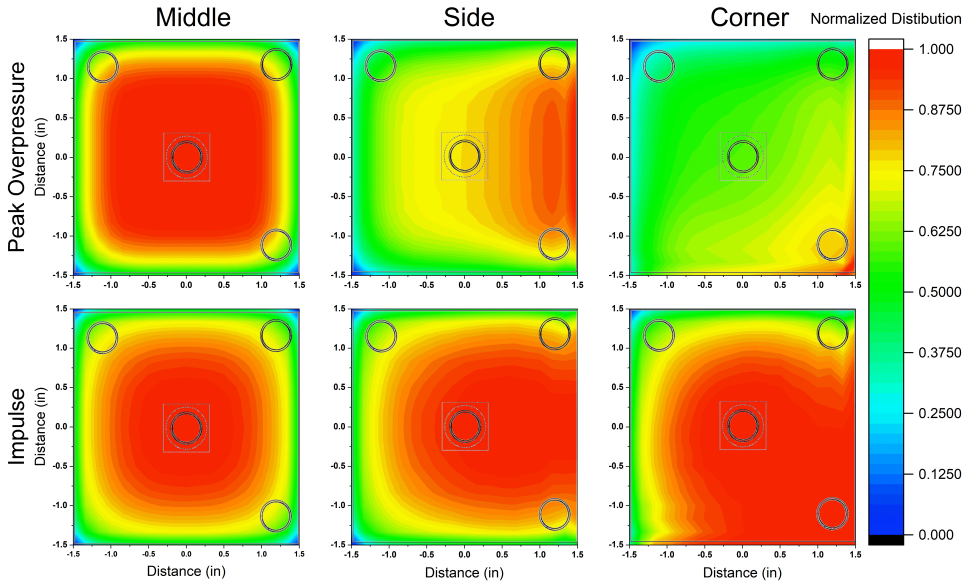

Figure 2.9 Heat maps of normalized peak reflected overpressure and impulse for the 3 x 3-inch plate exposed to a shock wave with a long duration. The effect of the plate location within the cross-sectional area of the shock tube is illustrated (see Figure 2.8D for the diagram of plate locations).

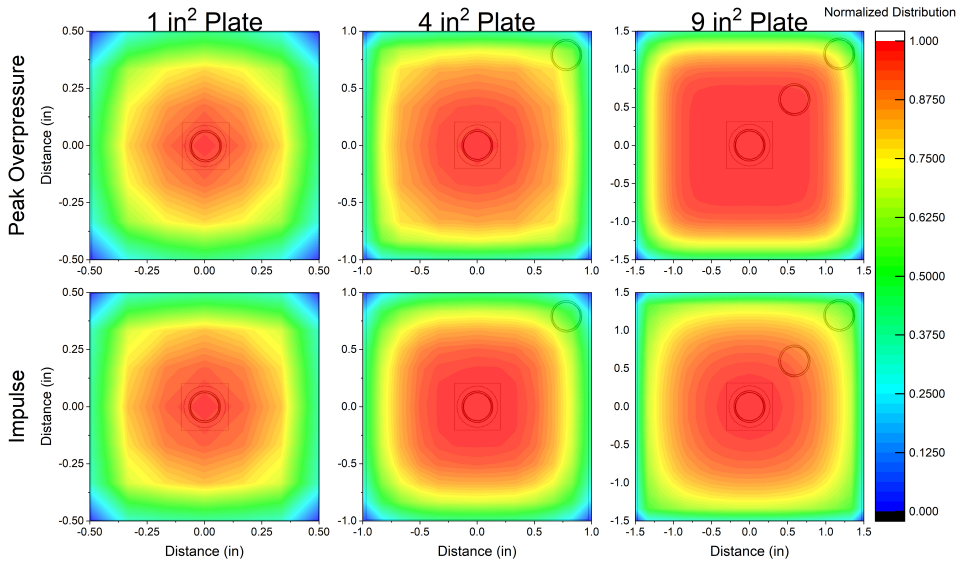

Figure 2.10 Heat maps of normalized peak reflected overpressure and impulse for the each plate exposed to a 180 kPa shock wave. The experimental outcomes can be seen in Figure 2.6.

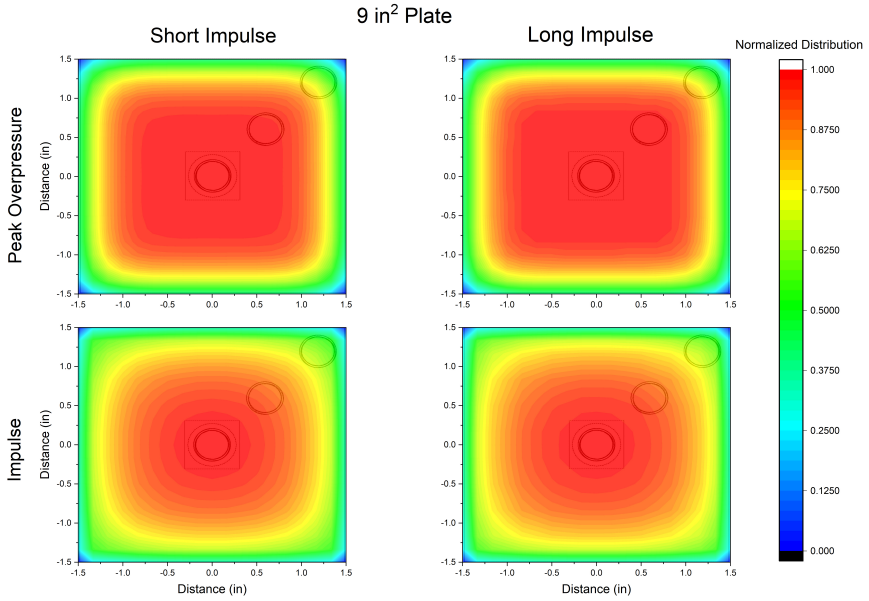

Figure 2.11 Heat maps of normalized peak reflected overpressure and impulse for the 3 x 3-inch plate exposed to either a short (5 ms) or long (10 ms) duration shock wave. Experimental results can be seen in Figure 2.7.

2.4 Results for Simple Three-Dimensional Geometries

Representative pressure profiles are shown in Figure 2.12, for each material that was tested. These profiles are compared and used throughout this study to investigate the effect materials. Differences in peak overpressure, duration, risetime, and impulse were all used. Initial inspections show clear differences between the pressure profiles between each of the materials. Comparing synthetic materials (Figure 2.12 C, D) to animal-based materials (Figure 2.12 A, B), synthetic materials show a much larger peak pressure compared to natural gelatins. Differences in the non-linear decay as seen specifically in Figures 2.12B, 2C were also observed. The differences in these profiles were quantified in the following sections Switching from qualitative to quantitative data, factorial ANOVA showed significant effect of sensor depth, material, thickness and sensor location ($p < 0.05$). Note due to equal n, normality and variance was assumed. These trends remain constant independent of incident overpressure.

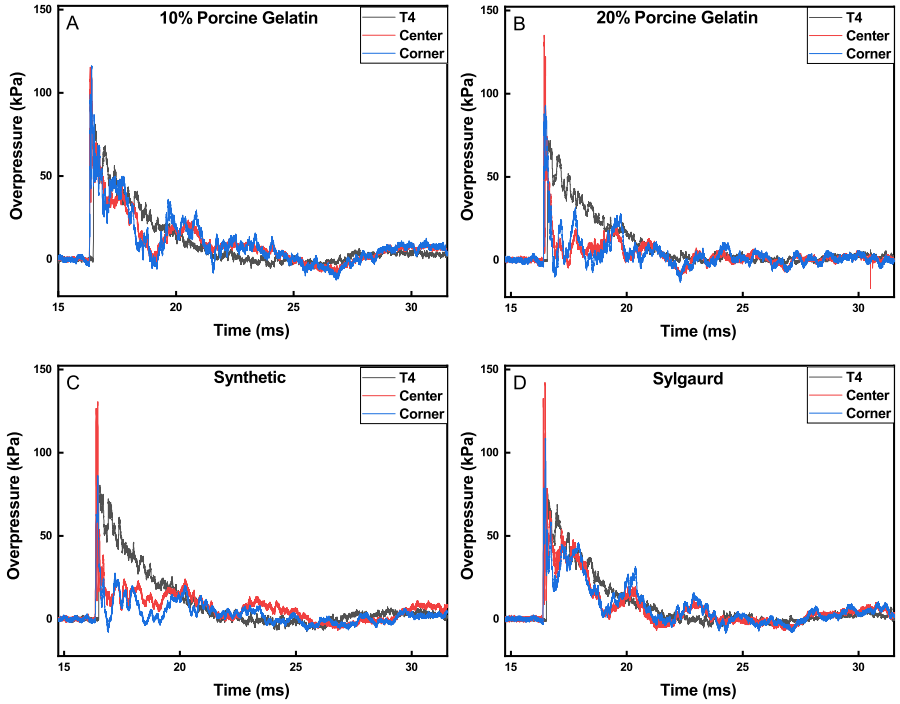

Figure 2.12 Representative pressure profiles for 130 kPa incident overpressure. In this case pressure sensor was placed, 1 in from the back of the box. A) Shows incident pressure profile, as well as center and corner pressure sensors, measuring the pressure within 10% Porcine Gelatin. B) Shows incident pressure profile, as well as center and corner pressure sensors, measuring the pressure within 20% Porcine Gelatin. C) Shows incident pressure profile, as well as center and corner pressure sensors,measuring the pressure within 10% Synthetic Clear Ballistics Gelatin. D) Shows incident pressure profile, as well as center and corner pressure sensors, measuring the pressure within Sylgard 527.

2.4.1 Effect of Material

The differences in the effect of materials are shown in Figure 2.12. Differences between pressure profile metrics (peak overpressure, impulse, duration risetime), are shown in Figure 2.13. As shown in Figure 2.13 A and B, there were significant differences seen in the incident pressure profiles. This implies that certain tests showed different loading patterns. To account for this, peak overpressure and impulse were normalized by their respective incident values and new comparisons were made as shown in Figure 2.14. ANOVA results showed significant differences between each of the brain simulants,

in virtually all metrics. Comparisons were made between each material (post hoc independent sample t-test with Bonferroni correction, adjusted $p<0.003125$). Note for figure clarity in the figures comparisons that showed no significant difference were denote by (ns). While this is not typical, this was done because far more comparisons showed significance. All other pair wise comparisons can be assumed to have shown significant difference.

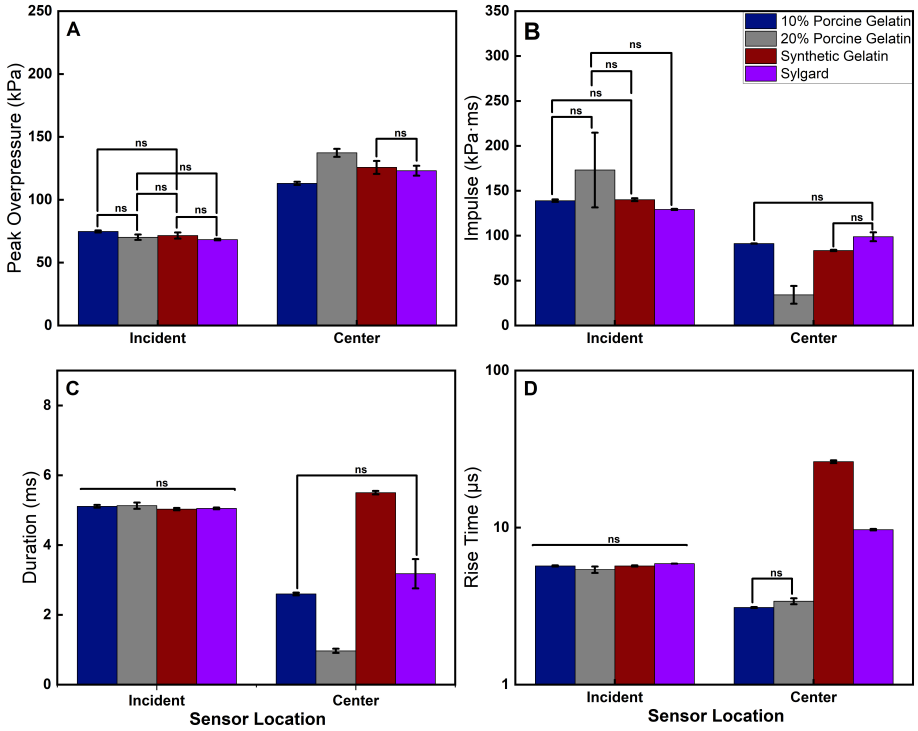

Figure 2.13 Representative comparison between the different materials at an incident overpressure of 70 kPa. (ns) denotes that no significant difference was found between groups. Significance threshold for post-hoc t-tests were adjusted $p < 0.003125$. A) Shows the comparison between peak overpressure. B) Shows the comparison in the impulse C) Shows the comparison in duration. D) Shows the comparison in risetime.

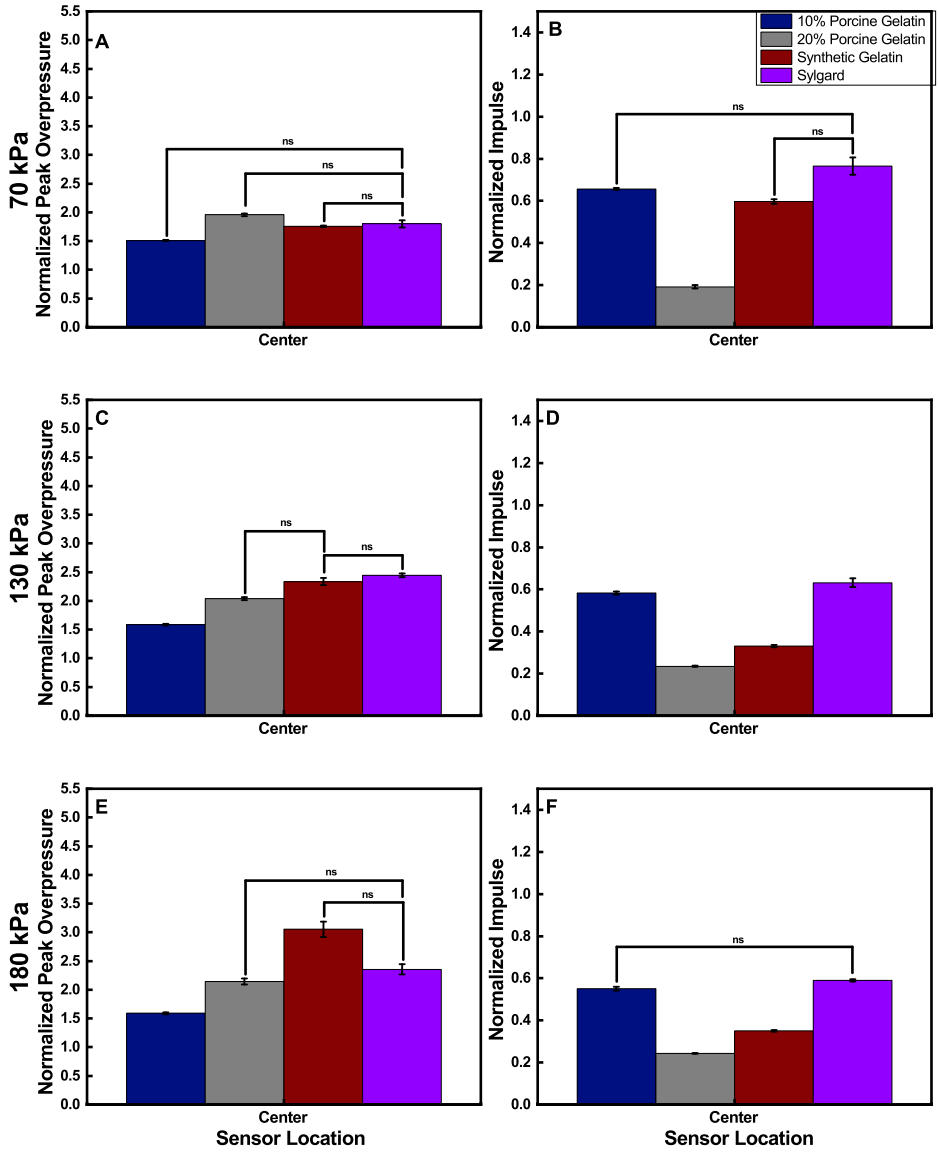

Figure 2.14 Normalized peak overpressure and impulse comparison for each incident overpressure. A) Shows the difference between in normalized peak overpressure at 70 kPa. B) Shows the difference between in normalized impulse at 70 kPa. C) Shows the difference between in normalized peak overpressure at 130 kPa. D) Shows the difference between in normalized impulse at 130 kPa. E) Shows the difference between in normalized peak overpressure at 180 kPa. F) Shows the difference between in normalized impulse at 180 kPa.

2.4.2 Effect of Window Thickness

As seen in Figure 2.15, the window thickness has the greatest effect on the impulse of the internal pressure waveforms. There is a significant decrease in internal impulse as the window thickness is increased (post hoc independent sample t-test with Bonferroni correction, $p < 0.003125$). Interestingly, the changes in the pressure profiles do not translate to peak overpressure. 10% porcine gelatin is the only material that showed significant decrease in peak overpressure (post hoc independent sample t-test, $p < 0.003125$) as the front window thickness increased.

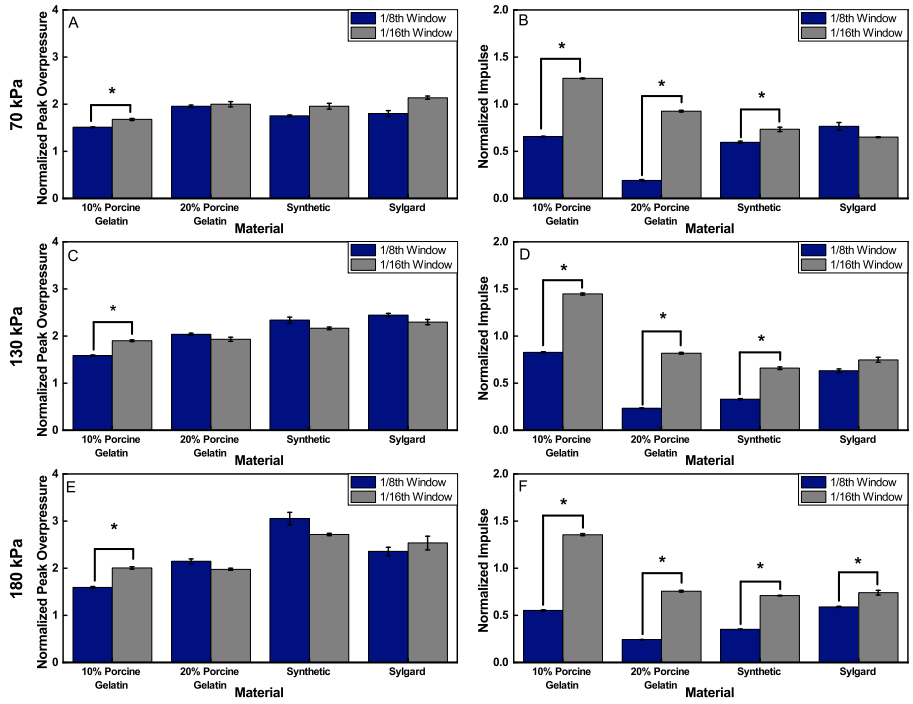

Figure 2.15 Comparison between $1/16^{th}$ and $1/8^{th}$ in windows. A) Shows the difference between normalized peak overpressure at 70 kPa. B) Shows the difference between normalized impulse at 70 kPa. C) Shows the difference between normalized peak overpressure at 130 kPa. D) Shows the difference between normalized impulse at 130 kPa. E) Shows the difference between normalized peak overpressure at 180 kPa. F) Shows the difference between normalized impulse at 180 kPa.

2.4.3 Effect of Sensor Location

There seems to be a significant drop (post hoc independent sample t-test with Bonferroni correction, $p < 0.003125$) in the pressure between the reflected and internal pressures measured. It should be noted that the reflected pressures were taken from measurements on a plate of similar area. In addition, as seen in Figure 2.16, in all cases there is a significant drop between the center and corner sensors in all cases. Independent of incident overpressure, there was a significant drop in both peak over pressure as well as impulse. The extent of the changes is very much dependent on the material of the potential brain simulants. Sylgard 527, for example, does not show as large of a change as other materials.

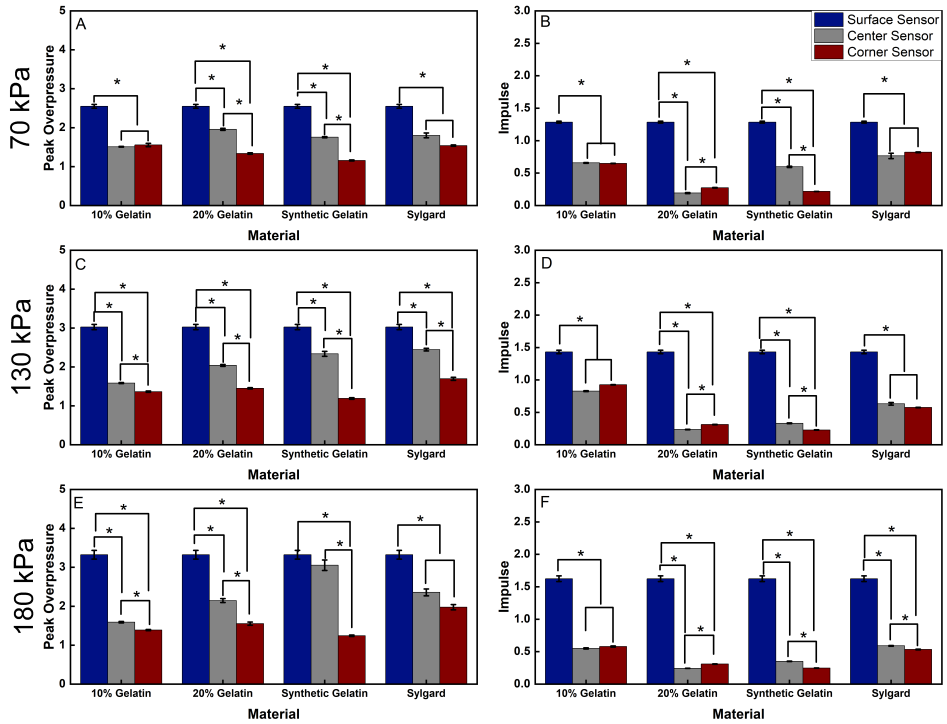

Figure 2.16 Comparisons in normalized peak overpressure and impulse at varying sensor locations. A) Shows the difference between normalized peak overpressure at 70 kPa. B) Shows the difference between normalized impulse at 70 kPa. C) Shows the difference between normalized peak overpressure at 130 kPa. D) Shows the difference between normalized impulse at 130 kPa. E) Shows the difference between normalized peak overpressure at 180 kPa. F) Shows the difference between normalized impulse at 180 kPa.

2.4.4 Front Window Strain Comparison

The strain on the front window, as expected, shows major differences due to the thickness of the front window (Factorial ANOVA, $p < 0.05$). This trend is seen regardless of material being tested. The metric for strain in these cases is the peak differential strain (maximum – minimum strain). The effect of material on strain seems to be dependent on the rate or intensity of the incident shock wave. While at 70 and 130 kPa, there was no significant difference in strain as a result of material (post hoc independent sample t-test with Bonferroni correction, $p > 0.0083$), at 180 kPa results begin to show significant differences due to the changes in material (post hoc independent sample t-test with Bonferroni correction, $p < 0.0083$). This is shown in Figure 2.17, where independent of window thickness, there is significant differences due to the material in the box.

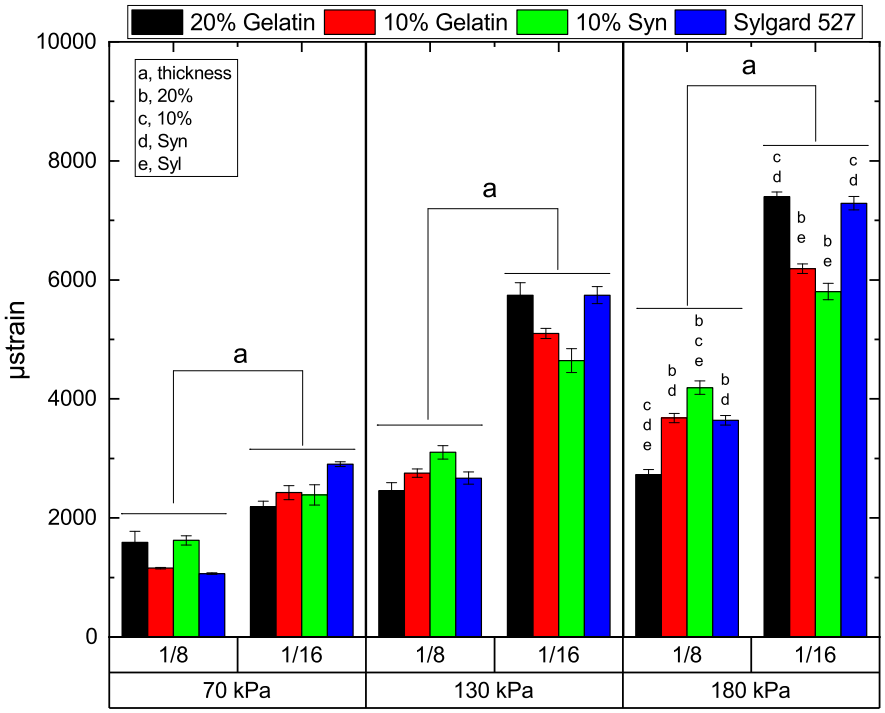

Figure 2.17 Comparison of the maximum differential strain on the front window. Comparisons were not made between incident overpressures. Significant differences were seen between windows with different thicknesses in all blast conditions. Interestingly in 180 kPa, significant differences begin to develop dependent on materials within the box.

2.4.5 Velocity Comparison

Because part the aim of this work is to identify which materials can be a usable brain simulant, the acoustic velocity of the materials was measured and compared to the value of brain acoustic velocity reported in literature. The velocity within the materials was measured based on the arrival times of the sensors within the box. Velocities measured within the box were averaged and compared to an average brain value acquired from a literature search [92]. The results shown in Figure 2.18 show that the synthetic material showed the greatest difference compared to the other materials (One sample t-test with Bonferroni correction $p < 0.002$). In contrast, velocities measured in porcine based gelatins were most similar to brain. Table 2.2 shows how the results of this work compare to literature.

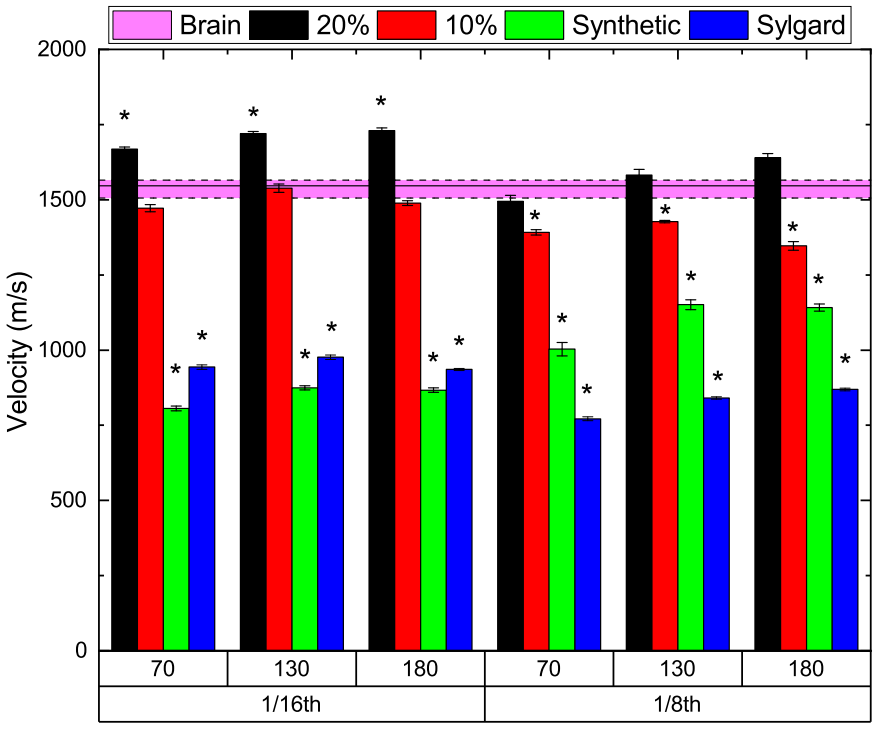

Figure 2.18 Comparison of acoustic velocity measured within the different materials. The band across the screen denotes the range seen in literature for the acoustic velocity of brain. (*) denotes significantly different acoustic velocities from brain.

Table 2.2 Acoustic Velocity Comparison

Material	Acoustic Velocity (m/s)	Source
Sylgard 527	951.93	Measured
	1020	[93]
Porcine Based Ballistic Gel	1572.26	Measured
	1501	[94]
	1520-1650	[95, 96]
Clear Ballistics Synthetic Ballistic Gel	1098.61	Measured
	1480-1580	[95]
Brain	1562	[97]
	1560	[95]
	1562	[98]

2.5 Discussion

The effects of the specimen geometry are important factors to be considered in shock tube testing. While many studies have looked at the effects of incident angle [99, 100] on loading, only a few have experimentally examined how the size of the specimen affects the ROP profile, the temporal evolution of the pressure distribution on the surface of the specimen or the transmitted pressure (the loading inside of the specimen). This work expands on previous studies, by not only changing size and placement within the shock tube, but also changes to the incident BOP duration independently. These questions remain largely unanswered and are vital for the understanding of the biomechanics of the bTBI, i.e., the propagation of the pressure wave inside of the body and subsequent causation of acute injury mechanisms. Though incident pressure profiles (peak pressure, duration, and impulse) can be used as a reference, it is not enough to predict the surface pressures and consequently mechanical loading. It is this mechanical loading that determines the

response of a structure or the injury state of a live specimen. Typically, a specific research question dictates that the specimen is instrumented with a set of pressure sensors distributed strategically on the surface to measure the ROPs [18, 101, 102]. The surface pressure histories are compared against the intracranial pressure (ICP) [16, 101], or surrogate brain tissue deformation [102, 103], to give insight into the acute biomechanical loading of the specimen. These measurements are of vital importance in the development of the validated numerical models of bTBI [14, 104, 105].

2.5.1 Increase in Cross-sectional Area

As the size of a specimen increases the magnitude of shock loading (defined by the reflected pressure profile) on that specimen increases. The dynamic component of the shock wave is thought to have a more pronounced effect on the specimen with a larger cross-sectional area, and on the shock wave flow field [106, 107]. This effect is seen as the longer dwell time at the center of the surface of the specimen (Figure 2.1D). Results presented in Section 2.3.1 show that the peak and the duration of the ROPs are not affected by the size of the specimen while the impulse varies significantly (Figure 2.7E, F). This increase in impulse is due to the increase in dwell time (tr) since it is the only noticeable difference between ROP waveforms. The shorter dwell time near the peak of the ROP waveform can also explain the decrease in impulse seen as the pressure measurements are taken closer towards the edge of the plates. At the edge, the ROP profile is not affected by the plate geometry (presented area) as strongly as in the center due to the much shorter time for the rarefaction wave to relieve the pressure. By extrapolating these finding to more complex geometries, such as those seen in a biological specimen, it can be argued that based on the size of the specimen, species with larger body surfaces normal to the shock front should experience larger biomechanical load, assuming that the reflected pressure translates into the level of transmission inside the specimen [14, 108]. Based on results

above, when a larger area of the body is impacted by the shock wave it will result in significantly different loading profiles compared to smaller bodies. These effects were demonstrated for the body and ICP dependence on the specimen orientation [109, 108]. Furthermore, an increase in loading on a specimen will translate into an increased injury purely due to geometrical factors. The temporal variations in reflected impulse on the surface of the specimen also imply that purely due to geometrical aspects, the loading of the specimen may not be uniform, even for a specimen with as simple geometry as a 2D planar plate.

2.5.2 Effects of Variable Duration

The vast majority of papers studying blast TBI, only rely on the incident peak overpressure as a sole exposure/injury predictor [66]. It is surprising, considering the well-known survival curves developed in the 1960s for long- (180-400 ms) and short-duration (2.1-4.6 ms) shock waves (the Bowen curves) using many species [110], incorporate both peak overpressure and duration as survival predictors. This work is even further expanded more recently for blast injuries [6, 51]. Despite the evidence that longer incident durations can contribute to more damage there had been little experimentation on how changes in solely duration can affect specimen loading. Results indicate that by increasing the duration by order of two, the impulse is also doubled (Figure 2.8A-D). This turn also changed significantly the loading experienced by the specimen (Figure 2.8E-F). These results demonstrate that the peak incident overpressure should not be the only metric to describe the biomechanical loading associated with blast exposure. By changing the duration of the incident waveform both the peak and the impulse ROP vary, given the same incident peak overpressure.

Interestingly, for the same peak BOP, the long duration shock wave had lower reflected pressure ratio but higher impulse ROP values, as evidenced by both plots of the normalized data (Figure 2.8G, H). The specimen loading scales with the incident

BOP, and in the most extreme cases there was a 20-30% increase in the surface load compared to the incident shock wave. This effect is seen by the normalized impulse values in Figure 2.8H. These effects have been demonstrated for the first time within this work.

2.5.3 Specimen Location, Blockage, and Flow Field Obstruction

The placement of the specimen within the shock tube influenced the surface loading morphology, as evidenced by the results of experimental (Figure 2.9) and computational studies (Figure 2.10). The flow field symmetry around the 9 in^2 (228.6 mm^2) plate was decreased by changing the position from the middle towards the shock tube wall (side location) and finally by placing it in the corner (Figure 2.9D). The presence of an additional obstruction in the form of the shock tube wall (extra effort was made to ensure there were no gaps between the edge of the plate and the wall) disturbs the 'normal' flow of the shock wave seen as symmetrical ROP distribution on the plate in the middle position (Figure 2.10). However, while these results are compelling evidence of the obstruction of the flow field affecting the surface pressure distribution, the role of distance between the specimen and the shock tube wall where the heterogeneity of the ROP characteristics disappears was not investigated. This is despite visually and quantitatively seeing differences in the dwell time at each sensor, but it appears that the differences were not enough to see changes within the reflected pressure profiles. These effects were studied computationally in the early 1980s [106, 107] for shock wave profiles which are relevant for the nuclear explosions (e.g., 70 kPa BOP, and 80 ms duration, corresponding to the nuclear blast originating from the detonation of a charge equivalent to 0.1 kilotons of TNT). These authors noted that the blockage effects (obstruction of the 20% of the area of the shock tube) were more pronounced for the step shock wave (also known as a flat top waveform) than for rapidly decaying shock wave with 80 ms duration. In this case, where the

goal of the study is to simulate field explosions of the high explosives, the durations are in the below 10 ms range. Thus, to see measurable blockage effects in these exposure conditions, the specimen would need to occupy a much larger area of the shock tube, i.e., most likely larger than 20%, provided the there is no contact between the specimen and the shock tube.

2.5.4 Simple Three-Dimensional Geometries

One of the first phenomena observed is the nonlinear acoustic velocity shown in the materials. The stress wave measured along the propagation of the material seems to accelerate. This is most likely due to the material itself compressing as the wave is propagating through the material. Based on the average velocities of the waves moving through the materials, the porcine based ballistic gelatins seem to behave the best, with similar acoustic properties compared to the brain. Results also show how these materials behave under shock loading. Based on the results shown above, the peak of the blast seems to remain the same as a function of window thickness. Despite this, the impulse or energy transmitted through differed significantly. The thinner window allowed for more of the energy to be transmitted through. If these results are extrapolated to biological systems, the skull thickness seems to be a protective measure when determining injury. The thicker the skull the less energy is transmitted to the brain, but the peak stress may not be affected, while the impulse may be.

2.5.5 Conclusions

In summary, throughout this chapter, the effects of size, material, and thickness were investigated. Using simple geometry plates, size was determined to have a significant effect on the loading patterns seen on the surface of specimen. In addition, Aluminum and PLA were compared and it appears even materials as different as Al and PLA show no significant difference in mechanical loading. Moving forward to 3D geometries, material and thickness were shown to significantly affect internal

mechanical loadings. By increasing the front window thickness, a proportionate decrease in internal mechanical loading was seen. Initial findings also point to porcine based gelatins being a reliable brain simulant as compared to the others being tested.

CHAPTER 3

EVALUATION OF BRAIN SIMULANTS

3.1 Background and Significance

To identify the mechanisms of bTBI, a plethora of animal studies have been carried out investigating the effects of blast exposures [48, 63, 111, 112]. Based on a recent survey of 70 studies, the vast majority of cases focused on the biological secondary mechanisms and behavioral responses to blast rather than the biomechanical response to blast [52]. Much of the work investigating the biomechanical response of blast relies on Finite Element Models (FEM). In the literature, these studies use a wide range of material properties to try and replicate the blast insult. As seen in Chapter 1 and Chapter 2, it is crucial to experimentally identify the biomechanical response of brain tissue, as well as, materials that can act as biological simulants to not only understand their effects, but also facilitate more accurate numerical modeling.

The complexity in modeling biological materials arises from the fact that they are highly heterogeneous at different length scales. Various cell types, morphological characteristics, and boundary conditions all contribute to a more complex shock wave interaction with the brain and surrounding tissue. The brain is considered to be a nonlinear, anisotropic viscoelastic material [113]. Even this profound classification is simplified as the mechanical properties varies across different length scales of cells, tissues, and organ systems. To simplify the problem, researchers employ several brain simulants to varying levels of success. Animal based gelatins are commonly used as brain simulants [73, 83, 84, 114, 115], but have limitations such as temperature sensitivity and a relatively short shelf-life. Synthetic ballistic gelatins have been tested as well to some success without the degradation issues found in animal based gelatins [68, 84]. They have also shown similar acoustic properties to soft tissue in ultrasound testing [96, 116]. It should be noted that the mechanical properties of

many brain simulant materials are yet to be characterized, especially at the high strain rates expected during blast events. In addition, while some of the materials have shown success in replicating blunt models of TBI, a thorough investigation of their relationship to blast TBI has yet to be done. This creates the need for testing these materials specifically under blast conditions in order to investigate how they respond to shock wave loading and how this relates to the response of brain tissue.

To this end, this work investigated potential brain simulants to understand shock biostructure interactions. Using similar techniques to Postmortem Human Subject (PMHS) experiments [83, 117], 10-week-old Sprague-Dawley Rats, were used as the point of reference when comparing simulants to living tissue under shock loading. Specimens were exposed using a compressed gas driven shock tube, the most common source for replicating blast [52]. In addition, more complex surrogate models were formed to investigate the possible effects of skin material on shock wave transmission. Full surrogate models, with both skin and brain simulants were tested and compared to the live rat models to provide gross insight into how skin material affects shock wave propagation through the specimen. As a measure of comparison, intracranial pressure (ICP) was used as a metric of shock loading in the brain and brain simulants. ICP is a common insult metric for numerical simulation, surrogate, and animal work [48, 75, 118] in the study of biomechanical loading in bTBI research. In addition, skull strain values were also measured and compared between models.

3.1.1 Objective

The goal of this chapter is to *determine how material affects pressure loading variations within brain and brain simulants* (Specific Aim 2). Using increasingly complex surrogates, the brain simulant that most closely resembles live brain under blast conditions needs to be identified. This chapter takes an important first step towards the investigation of how soft tissue interacts with shock waves.

3.2 Materials and Methods

3.2.1 Live Rat Preparation

10-week-old male Sprague-Dawley rats (Charles River Laboratories) weighing between 300-350g were exposed to blast. Animals were used in accordance with protocols approved by Rutgers University Institutional Animal Care and Use Committee (IACUC). Animals were housed at 22 degrees C with free access to food and water in a 12-hour dark-light cycle. Prior to blast, surgeries were performed in order to fix two cannulas at the base of the skull, as described in reference [64]. Cannulas were formed from 16-gauge flat tipped fill needles. These cannulas held the two Millar 3.5F (SPR-524) Mikro-Tip Catheter Transducer pressure sensors in each hemisphere of the rat brain as shown in Figure 3.1A. The cannula in the left hemisphere placed the sensor 11 mm deep from base of the skull; while, the cannula in the right hemisphere placed the sensor 6 mm deep. Two strain gauges were also fixed to the skull of the rat at the Lambda and Bregma locations. The flesh of the rat was then pulled over the strain gauges limiting direct exposure to the shock wave.

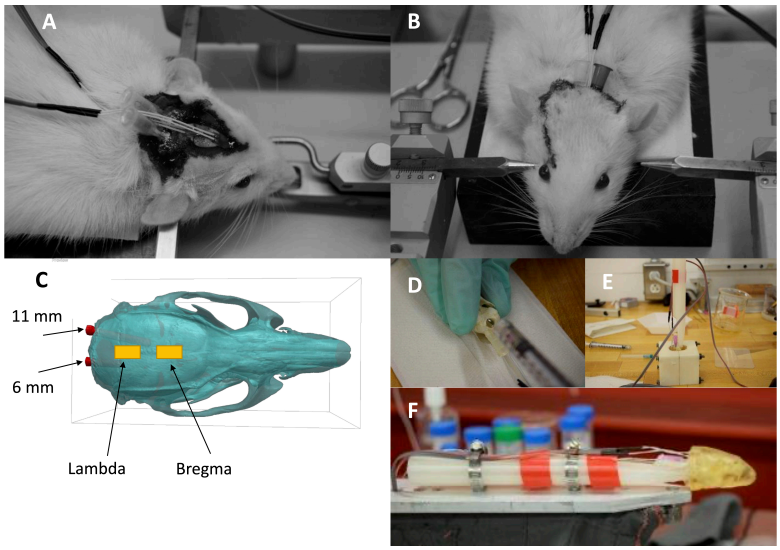

Figure 3.1 A) Typical 10-week-old Sprague-Dawley rat during instrumentation and brain replacement surgery. Cannulas are placed through the occipital bone as shown. Skulls were cleaned as best as possible in order to fix the strain gauges as shown. B) Post surgery for the Rat model. C) Reconstructed micro-CT of rat skull with cannulas, showing the approximate location of strain gauge placements. D) Filling process for full surrogate models E) Mold for the soft tissue simulant for full surrogate model. F) Mounting and instrumentation for full surrogate model before blast.

3.2.2 Semi-Surrogate Preparation

Postmortem 10-week-old male Sprague-Dawley rats weighing between 300-350 g were used. Immediately after animals were sacrificed, the brain was autolyzed using Ripa Lysis Buffer and sonicator and was removed via the foramen magnum and replaced with either 10% and 20% porcine gelatin (VYSE Ballistic Gelatin) common brain simulants [74, 78, 83, 117]. Previously both 10% and 20% porcine gelatins have been tested and compared and selected to closely mimic brain depending on the temperature range [83]. Similar to the Live Rat models, surgeries were performed to place cannulas for two Millar 3.5F (SPR-524) Mikro-Tip Catheter Transducer pressure sensors inside the gelatin. Two strain gauges were also placed on the Lambda and Bregma of the skull. The flesh of the rat was then pulled over the strain gauges limiting their direct exposure to shock. It should be noted that aside from the brain

of the rat, the skull and other tissues were kept as intact as possible as seen in figure 3.1B.

3.2.3 Full Surrogate Preparation

Rat skulls were purchased from The Bone Room LLC. Holes were drilled in the base of the skull for the cannulas, where two Millar 3.5F (SPR-524) Mikro-Tip Catheter Transducer pressure sensors would be fixed. The skulls were then filled with either a synthetic gelatin brain surrogate [84], in this case 10% Clear Ballistics Synthetic Ballistic Gelatin, or one of two concentrations (10% and 20%) of Porcine Ballistic Gelatin (VYSE Ballistic Gel). After the brain surrogate materials cured, the model was attached to the 3D printed PLA necks. Necks were not intended to be biofidelic and served only to hold the surrogate rat head in place and to eliminate as much motion of the head as possible while allowing enough clearance for the sensors. The skin was then added using a negative mold of the head created from a CT scan of a rat head. Skin was made from materials that varied from 10% Synthetic gelatin to 20-25% porcine gelatin. A completed model is shown in Figure 3.1F. Below 20% proved to be difficult to hold shape and/or survive blast loading.

3.2.4 Blast Exposure

All specimens were exposed to three discreet incident overpressures of 70, 130, 180 kPa, as well as two different durations (4 ms and 8 ms) for the 130 and 180 kPa overpressures. Helium was used as the driver gas in the shorter duration tests to provide durations of approximately 4-5 milliseconds. Nitrogen was used to provide Friedlander pressure profiles of equal peaks but with duration of 8-10 milliseconds. Specimens were fixed to the surfboard in the test section of the shock tube shown in Figure 3.1F and has been previously described in [64]. In addition to ICP measurements, incident overpressure measurements were taken throughout the length of the shock tube. Pressure measurements were recorded at 1.0 MHz for a duration

of 50 milliseconds, where 10,000 pre-trigger samples were saved to ensure capture of shock wave. Strain measurements were recorded using NI-cDAQ9188 strain gauge system for 100 milliseconds. Strain gauges were set in a Quarter Bridge set up with a 350Ω reference resistor. Strains were recorded at 50,000 samples per second, the maximum of the NI-cDAQ9188 system.

3.2.5 Statistics

All data was postprocessed and organized using OriginPro from Originlabs. Statistics were performed using SPSS 25. Because of failures in normality (Shapiro-Wilk, $p > 0.05$), Kruskal-Wallis tests were performed, followed by a Mann-Whitney post-hoc test with a Bonferroni correction (adjusted $p < 0.0083$). Comparisons were made between models at similar sensing location, and metrics were only compared to investigate whether models differed significantly from live rat. There is a differing n number between groups due to the removal of some specimen data due to failure of sensing elements during specific trials.

3.3 Results

As seen in Figure 3.2, the ICP profiles measured are approximately equal to the peak incident blast overpressure (BOP) at 70 kPa BOP which is also in the Friedlander waveform. This trend remains consistent for all incident overpressures tested. Qualitative observation shows peak ICP values begin to deviate from incident pressure as the BOP increases at a slower rate. Generally, the left hemisphere shows a slight increase in the peak pressure compared to the right ICP, possibly since it is closer to the front. However, these differences were not significant overall. In Figure 3.2D, one can also begin to see that as the complexity of the surrogate increases, the pressure profiles begin to further differ from the Friedlander waveform.

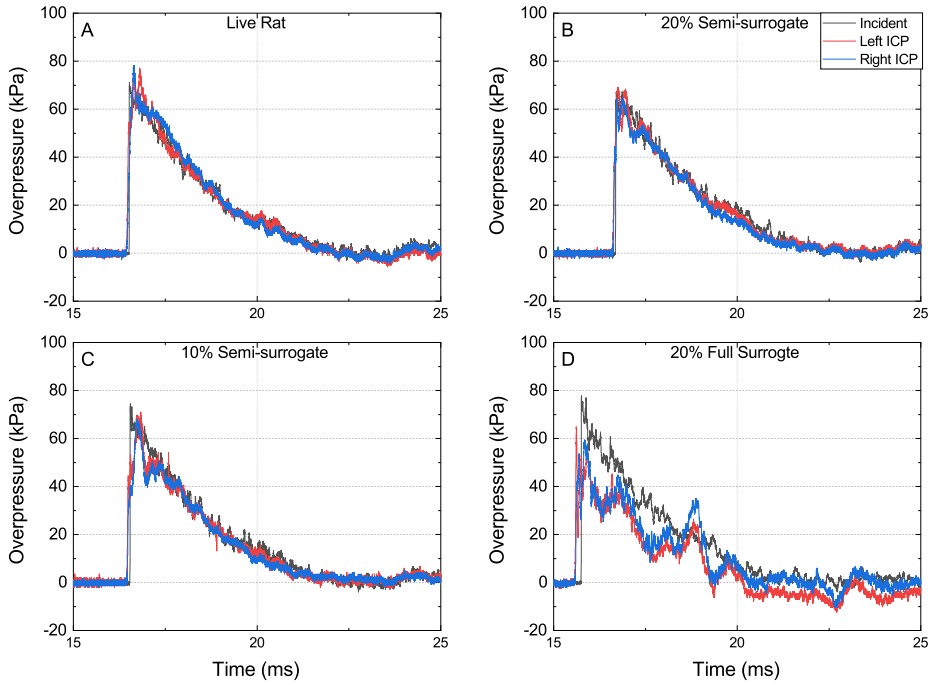

Figure 3.2 Representative overpressure profiles measured during nominal 70 kPa exposures. A) Shows Live Rat incident exposure as well as the left and right ICP measurements. B) Shows 20% Semi-surrogate incident exposure as well as the left and right ICP measurements. C) Shows 10% Semi-surrogate incident exposure as well as the left and right ICP measurements. D) Shows 20% Full Surrogate incident exposure as well as the left and right ICP measurements.

When comparing the peak ICP of different models (figures 3.3-3.5A), there were significant differences between materials and live tissue (p-values reported in Table 2). It should be noted that the comparisons were only made between live tissue and different materials. Figure 3.3 shows the results for 70 kPa incident overpressure, the lowest incident pressure tested. Here the 20% porcine based gelatins showed the least significant difference in all parameters. Surrogates made from the 10% synthetic gelatin, conversely, did not perform satisfactorily across the board. These surrogates show significant differences in ICP and intracranial impulse (ICI) values across virtually all test conditions (Mann-Whitney with Bonferroni Correction, adjusted $p < 0.0083$). As the incident overpressures increases, these trends remain relatively constant. The intracranial impulse is the most difficult parameter to match.

Each of the surrogates underestimated the insult that would be present in live rats. Although, based on the results shown in figures 3.3-3.5B, the 20% semi surrogate showed consistently the least deviation from our rat model. Table 3.1 shows the count for each significantly different parameter investigated. Raw data included: peak overpressure, duration, rise time, and impulse. Normalized data included peak overpressure and impulse. Overall if all parameters are considered, the 20% porcine gelatin semi surrogate shows the best match to live animal data as shown in Table 3.1. This model shows the lowest score and therefore, is the most similar to live tissue. The score of raw data is dependent on the number significantly parameters, including peak overpressure, impulse, duration, and risetime. The score of normalized data is based on differences in peak pressures and impulse. It should be noted that 20% gelatin does still underestimate the intracranial impulse. In addition, in some cases there were significant differences between the incident pressure profiles.

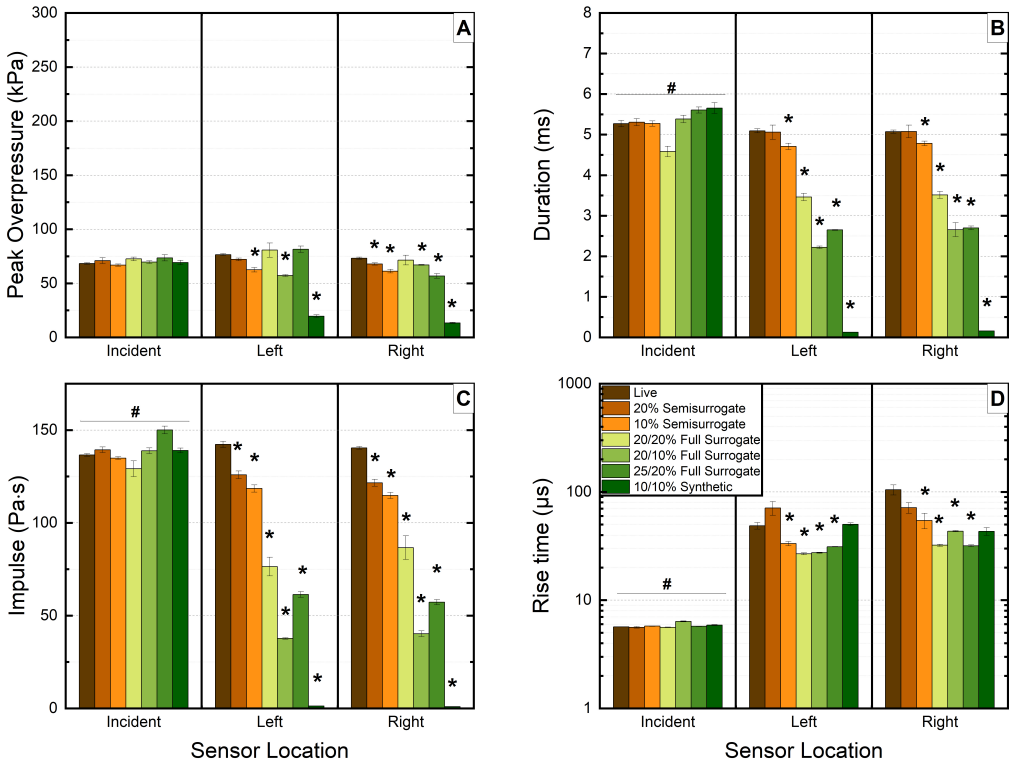

Figure 3.3 Results for 70 kPa Incident BOP. Error bars are ± SEM. (#) Denotes solely passing Kruskal-Wallis test. $p < 0.05$, (*) denotes passing of Mann-Whitney test with Bonferroni Correction adjusted $p < 0.00833$. A) Comparison of peak overpressure between live rat and each of the models. B) Comparison of duration between live rat and each of the models. C) Comparison of impulse between live rat and each of the models. D) Comparison of rise time between live rat and each of the models.

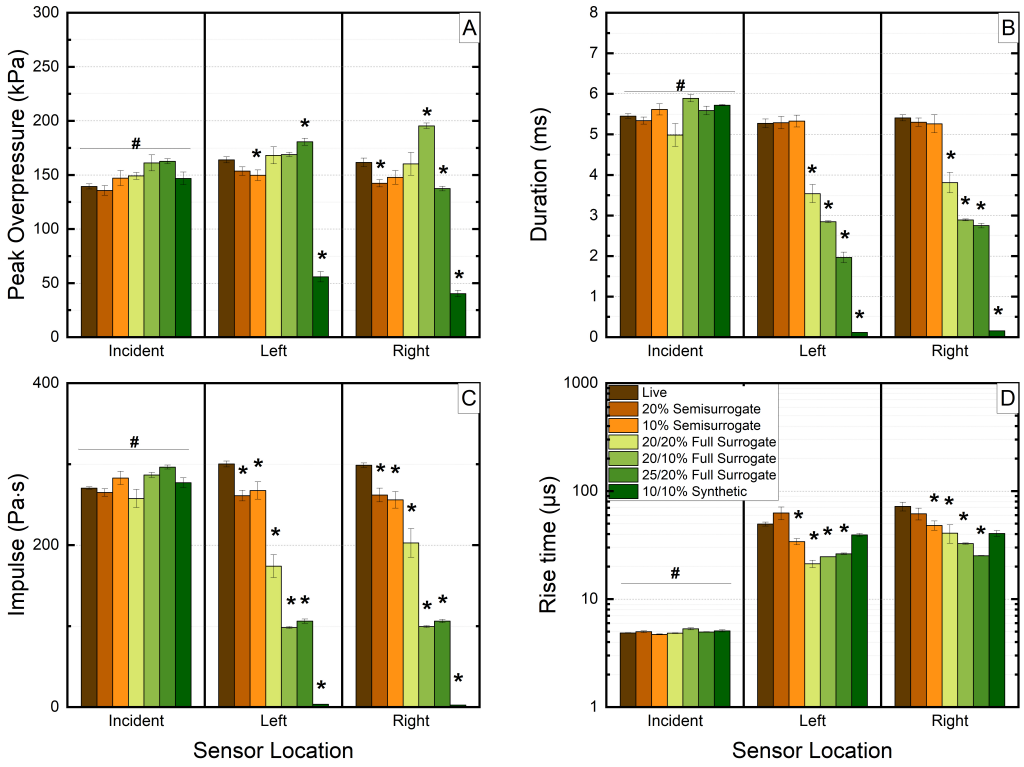

Figure 3.4 Results for 130 kPa Incident BOP. Error bars are ± SEM. (#) Denotes solely passing Kruskal-Wallis test. $p < 0.05$, (*) denotes passing of Mann-Whitney test with Bonferroni Correction $p < 0.00833$. A) Comparison of peak overpressure between live rat and each of the models. B) Comparison of duration between live rat and each of the models. C) Comparison of impulse between live rat and each of the models. D) Comparison of rise time between live rat and each of the models.

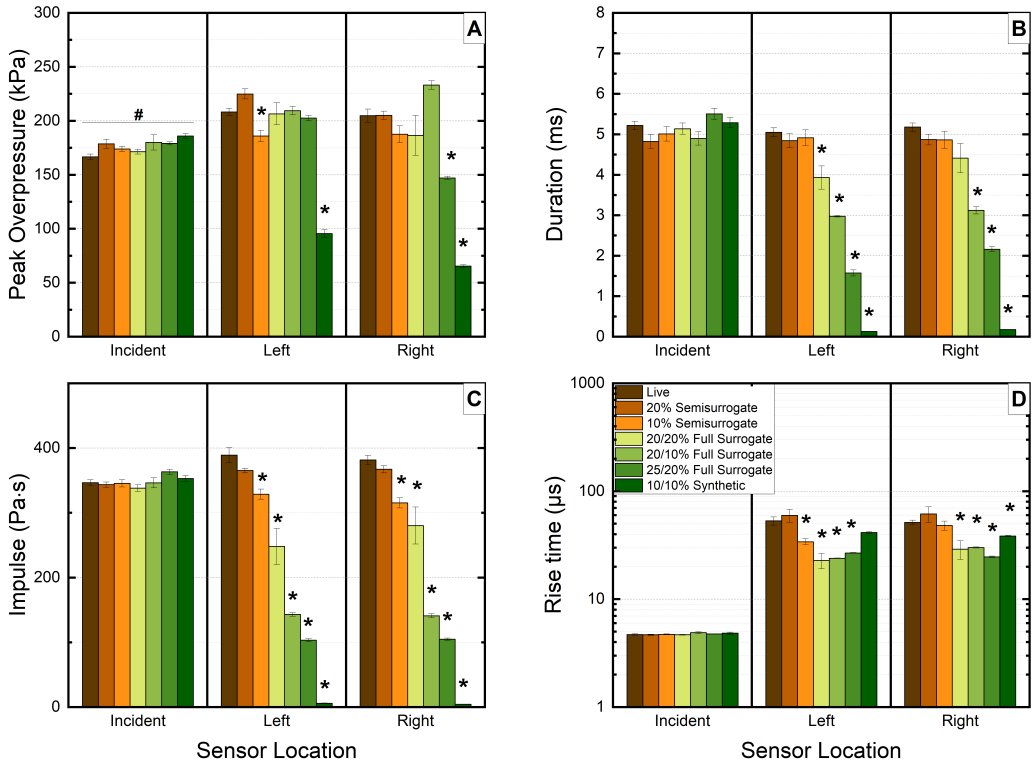

Figure 3.5 Results for 180 kPa incident BOP. Error bars are ± SEM. (#) Denotes solely passing Kruskal-Wallis test. $p < 0.05$, (*) denotes passing of Mann-Whitney test with Bonferroni Correction $p < 0.00833$. A) Comparison of peak overpressure between live rat and each of the models. B) Comparison of duration between live rat and each of the models. C) Comparison of impulse between live rat and each of the models. D) Comparison of rise time between live rat and each of the models.

Table 3.1 Surrogate Scoring

Surrogate	**Raw Data Score (max=24)**	**Normalized Data Score (max=12)**
20% Porcine Gelatin Semi	7	6
10% Porcine Gelatin Semi	16	12
20% Porcine Full	16	6
20%/10% Porcine Full	21	7
25%/20% Porcine Full	22	10
10% Synthetic	18	12

Lower score equals closer match

In order to correct for variations seen in the incident pressure profiles, peak pressures and impulses were normalized by their respective values. With this accounted for, the 20% semi surrogate remains the best brain replicant. When comparing peak overpressures, the surrogates brain simulants made of porcine gelatin outperformed especially when compared to synthetic materials. Through both insult metrics (peak pressure and impulse) 20% semi surrogate and 20% full surrogate showed the best match to brain, having the least amount of significantly different outcomes. 20% full surrogate model performs well when matching solely the peak overpressure but strongly underestimates the impulse seen in living brain tissue, as seen in Figure 3.6(B, D, F). Conversely, while at lower pressures the 20% surrogate slightly underestimates pressure, it does much better at estimating impulse.

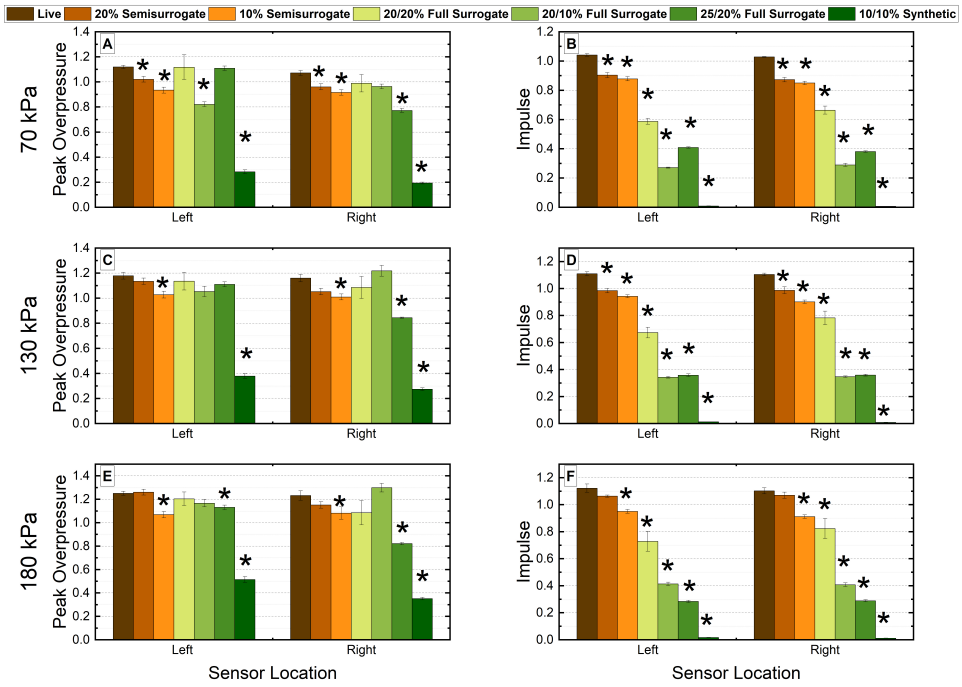

Figure 3.6 Normalized Results for 70, 130, and 180 kPa BOP. Error bars are ± SEM. (*) Denotes significant difference of post-hoc Mann-Whitney tests. A) Comparison of peak overpressure between live rat and each of the models exposed to 70 kPa. B) Comparison of impulse between live rat and each of the models exposed to 70 kPa. C) Comparison of peak overpressure between live rat and each of the models exposed to 130 kPa. BD Comparison of impulse between live rat and each of the models exposed to 130 kPa. E) Comparison of peak overpressure between live rat and each of the models exposed to 180 kPa. F) Comparison of impulse between live rat and each of the models exposed to 180 kPa.

The skull strain proved to be more difficult to compare between models. As seen in Figure 3.7, comparisons were only made for the models with the best matched pressure profiles. Results show that there is a significant difference between groups (Kruskal-Wallis Test, $H \leq 10$, $p < 0.02$). Despite this, no significant difference in the post hoc Mann-Whitney tests was found in any of the cases. While visually the 20% semi-surrogate was the closets in to matching Live rat once again, this conclusion cannot be made with certainty.

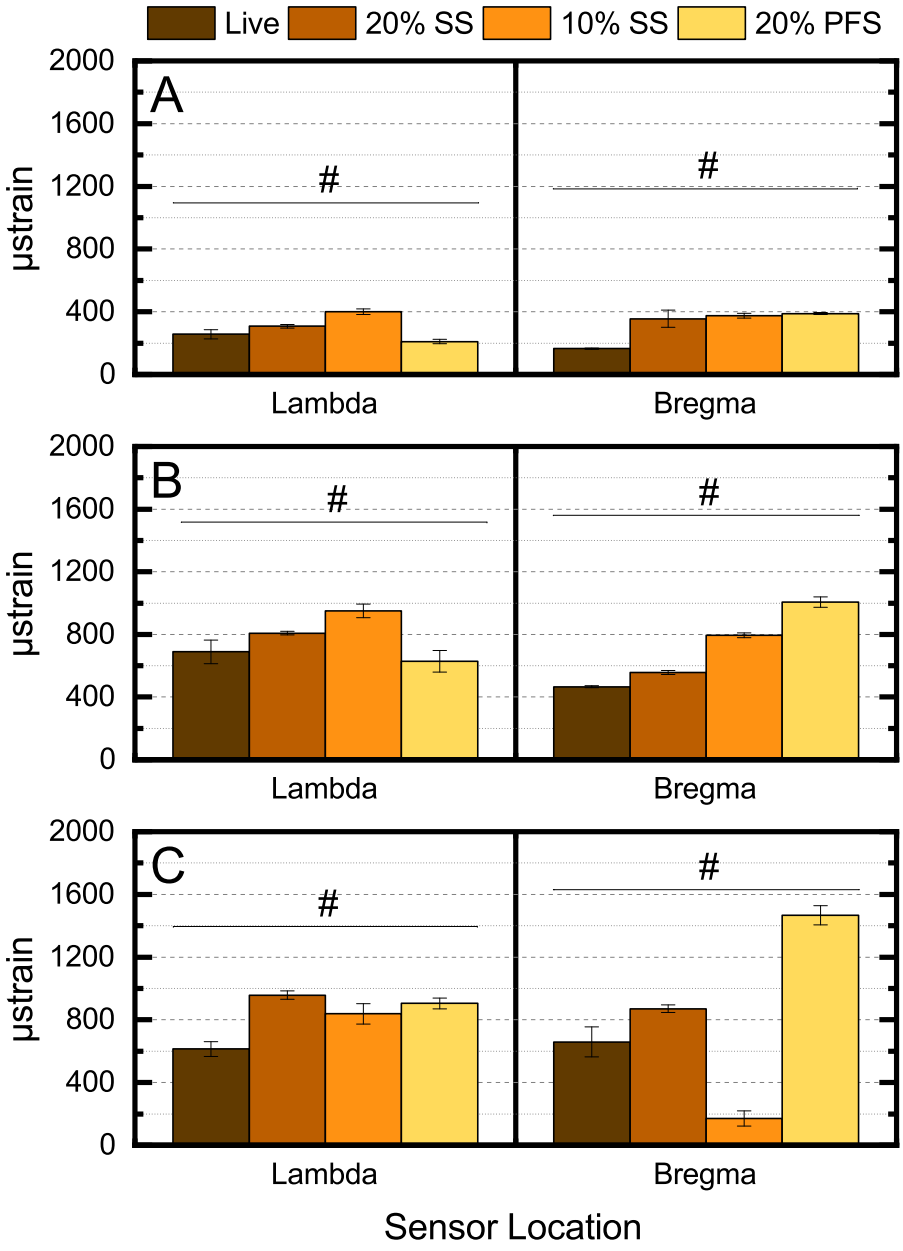

Figure 3.7 Strain results for A) 70, B) 130, and C) 180 kPa BOP. Error bars are ± SEM (#) denotes significant difference between groups using Kruskal-Wallis test. Despite significant differences being found pair-wise comparisons showed no significant difference between the groups.

Even when changing the duration of the blast, similar trends can be seen between the actual brain tissue and the porcine gelatin brain simulants as seen in Figure 3.8. Again, only selected cases were compared between the materials for which ICP profiles showed the least significant difference to that of live rat. Here again results show that the 20% semi-surrogate is the closest match to the live rat showing no significant difference.

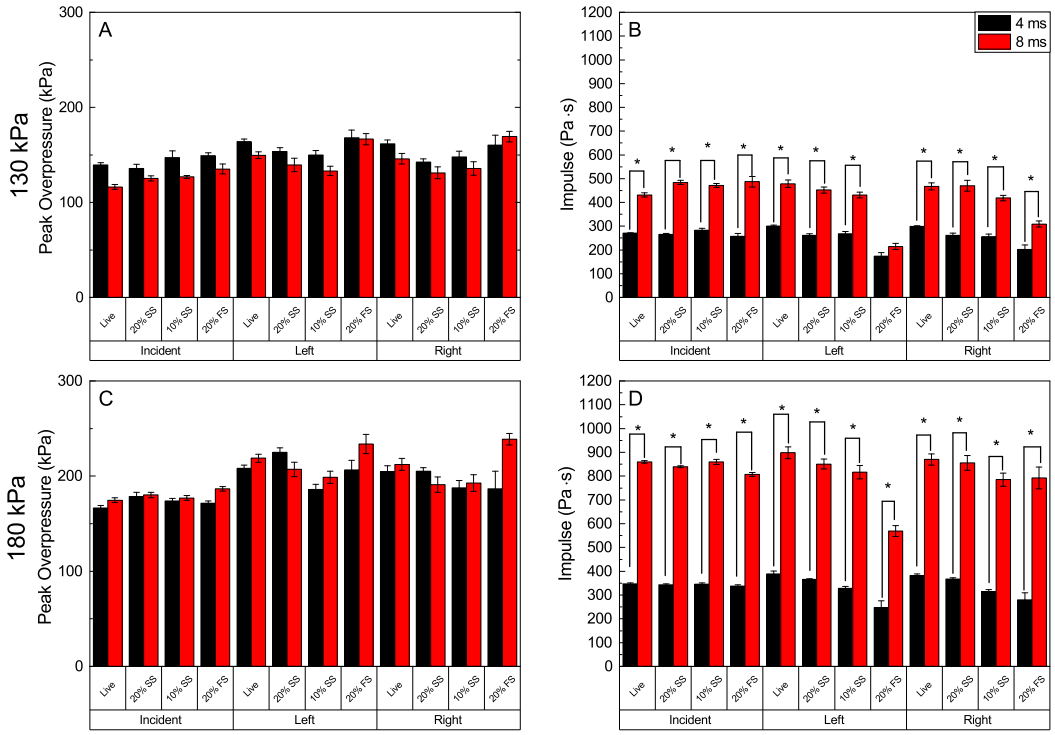

Figure 3.8 A) Peak pressure and B) impulse results for 130 kPa peak BOP comparing short and long durations. C) Peak pressure and D) impulse results for 180 kPa peak BOP comparing short and long durations. Error bars are ± SEM. (*) Denotes significant difference long (8 ms) and short (4 ms) duration exposures.

3.4 Discussion

Based on results shown, it is clear that the semi surrogate models outperform their full surrogate counterparts in terms of matching injury metrics to live rats. As seen in Table 3.1, models with 20% brain simulants typically outperformed other surrogate materials. With the 20% semi-surrogate performing the best, 20% porcine gelatin

seems to be the brain simulant, traditionally used by many investigators, matching in most injury metrics independent of BOP or impulse. The synthetic ballistic gel damped the transmission of the shock wave almost completely. This may be due to its combination of low density and high elastic modulus [113]. This would result in very different acoustic properties to those found in either skin or brain. The failure of the full surrogate models and relative success of the semi-surrogates shows the importance of flesh materials in dampening the effect of the shock front. Even with minor changes to skin material properties, for example from 20% to 25%, porcine gelatin resulted in very different pressure profiles. This suggests that the properties of the flesh play an important role in how shock waves transmit to the brain. By increasing material stiffness, results have shown that the shock wave has more difficulty transmitting in terms of impulse to the brain, i.e., the stiffer surrogate materials seem to reduce the amount of energy that is transmitted into the skull. Over all, this work validates previous PMHS work that used 20% porcine gelatin [83]. Although, the ICI results previously discussed show that impulse measured using porcine gelatin underestimates the actual loading taking place. Of the common brain simulants tested, 20% porcine gelatin is the closest based on strain values. While it is shown that brain material properties change the strain measured, the results showed high variability for the post-hoc tests. Strain measurements, in addition to being dependent on material, also proved to be sensitive to how strain gauges are mounted. The amount of glue, humidity under the skin, and other factors led to inconsistent data. These data were removed due to shorting of strain gauges and/or slipping of strain attachment.

Overall, this work has shown the importance of flesh/facial tissue on the ability for a specimen to dampen shock loading. While this work was unable to find a potential skin surrogate, results indicate that this layer will be crucial for the development of accurate surrogates in the future. This work has also shown that 20% porcine gelatin adequately replicates shock loading within the cranium. It also

corroborated FEA results to some experimental data and shows that small changes in material properties can have a drastic affect. This is an important step towards the development of better models of bTBI and allows for the use of surrogates that can mimic brain tissue.

In summary, this chapter focused on determining the effects of material on the biomechanical loading of brain and brain simulants. Stiffer and more elastic materials were shown to underestimate mechanical loading as compared to live brain tissue. In addition, out of all the simulants tested, 20% porcine gelatin was solidified as the brain simulant most similar to living brain tissue.

CHAPTER 4

POSTMORTEM HUMAN SURROGATE EXPOSURES TO SHOCK LOADING CONDITIONS

4.1 Background and Significance

One of the main issues in comparing bTBI between species is injuries in the field are typically self-reported with no specific reference to blast loading conditions in terms of the blast strength or standoff distance. These data will allow the prediction of overpressure-time curves typically used in animal testing. Measures, such as the Glasgow coma scale, are very subjective and are dependent on the responses of the patient and the interpretation by the physician [34]. In most cases, the parameters that could characterize injury in the field (standoff distance, orientation, etc.) are unknown. This differs significantly from animal models where animals are loaded in the same orientation, by the same blast, and injuries have more objective measures. In animal models it is possible to measure, for example, the intracranial pressure during a 70 kPa, 4 milliseconds, shock wave impacting head on, and identify how blast loads the brain and which histological, pathophysiological, cognitive, and behavioral outcomes correspond to this level of blast. Thus, fundamental questions in the study of bTBI are, how a controlled mechanical loading is transmitted into the human brain and how this compares to animal models with comparable shock loading in the lab. Assuming the ability to properly load specimen described in previous sections, it should be possible to investigate how shock loading differs between species.

To this end, PMHS are used in order to most accurately estimate the mechanical loading that takes place during blast exposure. PMHS have been used before to mixed results. Data typically rely on a low n number and the data have proven to be inconsistent between groups [83, 101, 117]. PMHS is the best option in order to elucidate the interspecies differences in loading.

4.1.1 Objective

The aim of the work, described in this chapter, is to detail the PMHS exposures and how the data compare to the what has been seen in rats. By loading PMHS to the same level of exposure as rats, one-to-one comparisons can be made between the loading conditions. The work in this chapter will then be used toward the development of interspecies transfer functions in Chapter 5.

4.2 Materials and Methods

4.2.1 Postmortem Rat Surrogate Preparation

Exposed rats are prepared as described in Section 3.3. Specimen brains were replaced with 20% porcine gelatin, based on outcomes of Chapter 2 and Chapter 3. Rats were exposed to three discrete overpressures with in the previously mild range of bTBI, namely 70 kPa, 130 kPa, and 180 kPa [119].

4.2.2 Postmortem Human Surrogate Preparation

Five Postmortem Human Surrogates were acquired from Science Care™. All subjects were male with an average age of 61.2 years old. Subjects had an average weight of 214.42 lbs (97.26 kg) making the mean BMI 29.29. Before the specimen shipment, CT scans were obtained for each specimen. Upon receipt, specimens were placed in -20 freezer for storage until ready for experiments. Two days before blast exposure, the specimens were removed from freezer and allowed to thaw. Excess flesh around the lower chin and neck were removed to expose the bottom of the skull and foramen magnum. From here, brain and dura matter were removed through the foramen magnum. After the brain was removed, it was replaced by 20% porcine gelatin (VYSE Ballistic Gelatin). Next, five holes were drilled into the occipital region of the skull. Cannulas were designed from 16-gauge steel tubing to place sensors at decreasing depths (5 in, 4 in, 3 in, 2 in, 1 in) from top to bottom in the midsagittal plane. Millar

3.5F (SPR-524) Mikro-Tip Catheter Transducer pressure sensors were placed at each cannula site as shown in Figure 4.1.

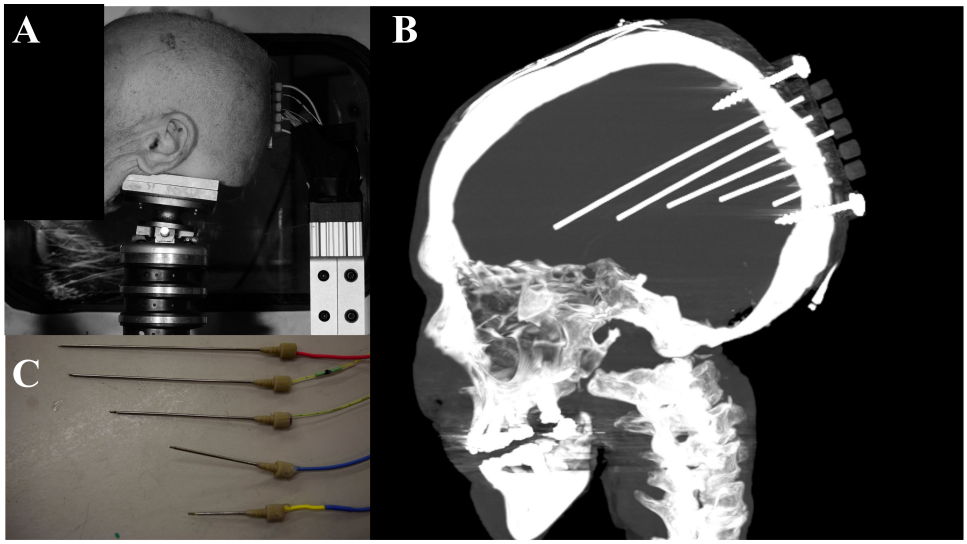

Figure 4.1 A) An instrumented PMHS model affixed to a Hybrid III neck. Face has been blocked out to protect the identity of the subject. B) Stacked post exposure CT scans used to show sensor locations. It should be noted that during post blast CT severed necks were placed next to head in scanner, neck was not attached during blast. C) Pressure sensors within cannulas, places with in the PMHS.

4.2.3 Blast Exposure

For the rodents, tests were performed as described in Chapter 3. To estimate human blast loading, PMHS were exposed in the 28-inch by 28-inch cross section shock tube previously described [18, 43]. PMHS were placed in the 28x28 in shock tube rather than the 9x9 inch tube to reduce the amount of area blocked by the specimen. Specimen were fixed so that they were as close to the central axis of the shock tube as possible, to remove any of the effects seen in Chapter 2. PMHS were affixed to the test section of the shock tube using a Hybrid III neck as shown in Figure 4.1. Specimens, regardless of species, were exposed to four times to each of the three discrete incident overpressures of 70, 130, and 180 kPa, covering the rodent mild range TBI. This would allow for a one-to-one comparison of ICP profiles between the species at each overpressure. ICP for PMHS measurements were taken simultaneously

at the five locations previously listed and BOP measurements were recorded at 1.0 MHz sampling frequency for a duration of 50 milliseconds.

4.2.4 Data Analysis and Statistics

After exposure, recorded PMHS data had high frequency noise in the signal which was accounted for during post processing using a 125kHz low pass filter applied. The filter was chosen to remove the high-frequency noise without removing the actual pressure data. The signal before and after preprocessing can be seen in Figure 4.2. This figure is used for illustrative purposes. It was also discovered, post CT, that one of the specimen had sensors mistakenly placed with the skull. Because of this, the specimen was removed from the study. The peak pressure and impulse of the ICP profiles were determined using OriginPro and used to compare between specimen, as well as, with the results of rodent experiments. Descriptive statistics were also performed using OriginPro. Both linear and nonlinear regressions were also performed using OriginPro. All ANOVAs and following post-hoc tests, as well as, multiple regression analysis was performed using SPSS 25.

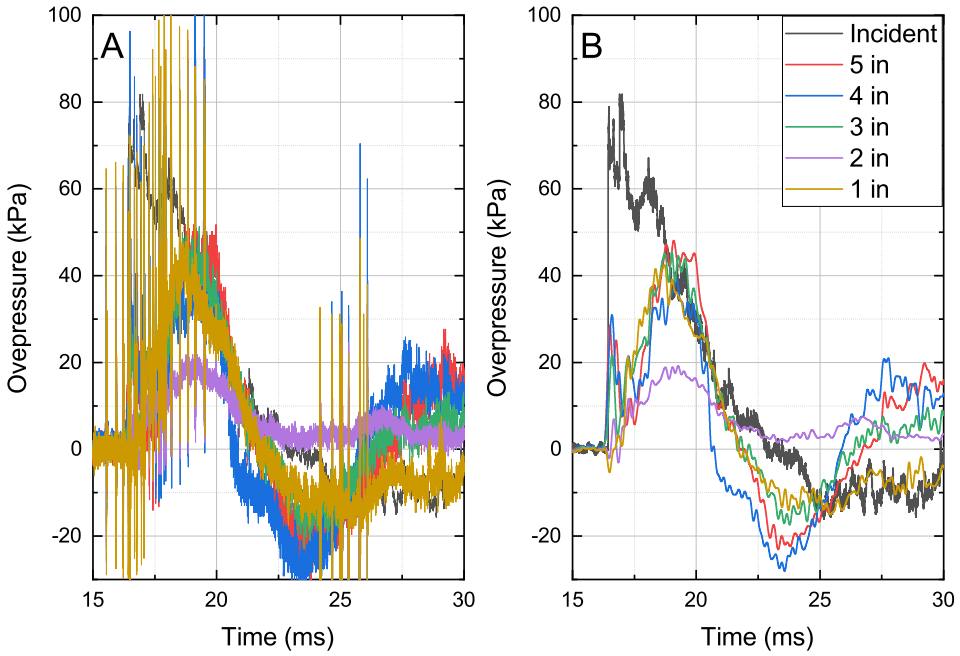

Figure 4.2 A) Raw data and B) filtered data from PMHS exposures.

4.3 Results

4.3.1 Postmortem Human Surrogate Exposures Blast

Results shown in this section, are those directly used in the development of the transfer function in Chapter 5 it should be noted that 1 specimen had to be removed from the data set due to errors with sensor placement. For a complete set of results for all specimen, please see Appendix A. Figure 4.3 shows the results for peak ICP and ICI for each individual specimen. Mean and Standard error of all four shots for each condition are shown. Between subject statistics were not performed. While patterns are similar, there is still noticeable variation from specimen to specimen. These variations can be attributed to the physiological differences between specimen (BMI, age, skull thickness, etc.). These variations were also investigated to provide further insight into shock-biostructure interactions. Initial observations show that unlike in rats, where ICP and ICI were similar to the incident BOP values, the ICP, as well as ICI, for the PMHS were significantly lower than the incident values, as seen in Figure 4.3. These trends are seen for all loading conditions.

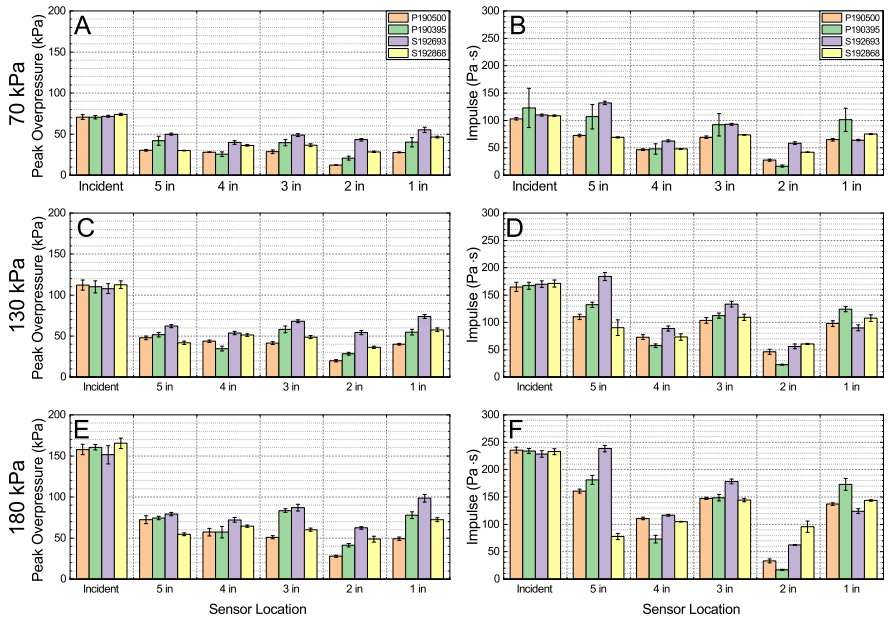

Figure 4.3 Results for peak overpressure and impulse, separated for each specimen. A) Shows the peak overpressure data for 70 kPa incident overpressure exposures. B) Shows the impulse data for 70 kPa incident overpressure exposures. C) Shows the peak overpressure data for 130 kPa incident overpressure exposures. D) Shows the impulse data for 130 kPa incident overpressure exposures. E) Shows the peak overpressure data for 180 kPa incident overpressure exposures. F) Shows the impulse data for 180 kPa incident overpressure exposures.

By combining the data in Figure 4.3, the plot accounts for the variations between subjects. The collection of data are shown in Figure 4.4. The data show a sinusoidal effect in the intracranial pressure and impulse as the pressure moves from the frontal lobe to the occipital lobe. As shown in Figure 4.4, there is no significant difference between the 5 in, 3 in, or 1 in sensor depths (post hoc independent samples t-test with Bonferroni Correction, $p > 0.005$) in terms of peak ICP and ICI. These locations are also where the highest ICP and ICI were found. This pattern remained consistent independent of the BOP exposures, as seen in Figure 4.4. With the data represented in this way, the dramatic drop relative to the BOP is clear. When looking at the differences between sensor locations, ANOVAs were performed separately for each BOP. In all the cases there were significant differences ($p < 0.005$) between sensors,

with post-hoc independent sample t-test showing that the 4 in sensor and 2 in sensor show significantly lower insult (ICP, ICI), compared to other sensor locations.

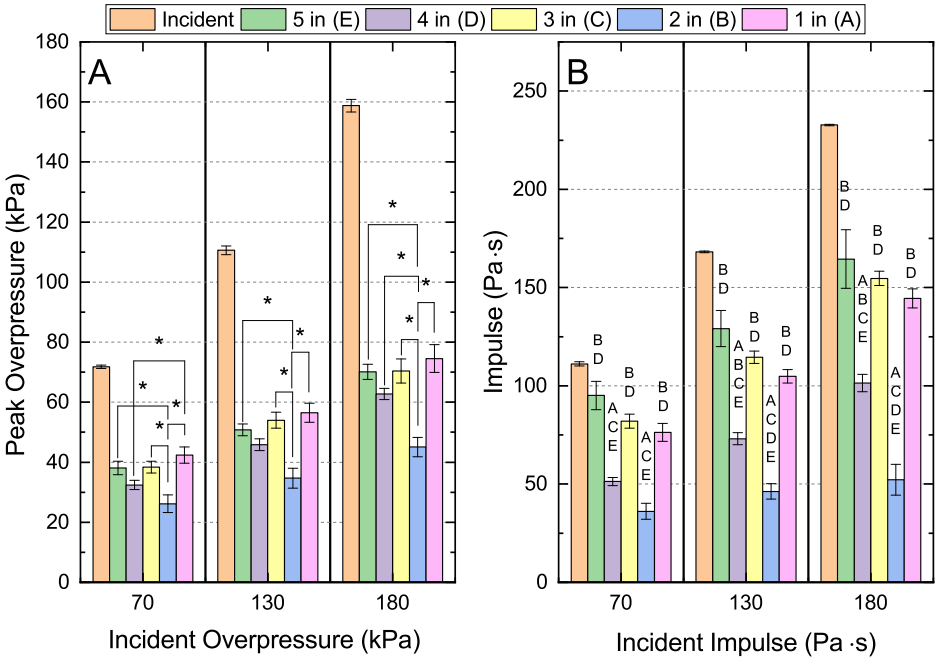

Figure 4.4 Collection of all of the peak ICP PMHS data. A) Shows differences in ICP between sensor locations (*) denotes significant difference in post-hoc tests. B) Shows the difference in ICI between sensor locations. Letters denote significant difference using post-hoc tests.

For further investigation of how shock wave transmission takes place, both ICP and ICI values were normalized by peak BOP and incident impulse, respectively. Results, expressed in Figure 4.5, show that as the BOP values increase, less of the wave is transmitted to the brain. Despite these clear trends shown in Figure 4.5, ANOVAs showed no significant difference between the three overpressures. This is most likely due to the low number of specimen able to be acquired at this time. Based on this data, a power analysis was performed using G*Power 3.1, and an n number of 7 specimen would be required to gain significance between the ICP/BOP Ratios shown in Figure 4.5.

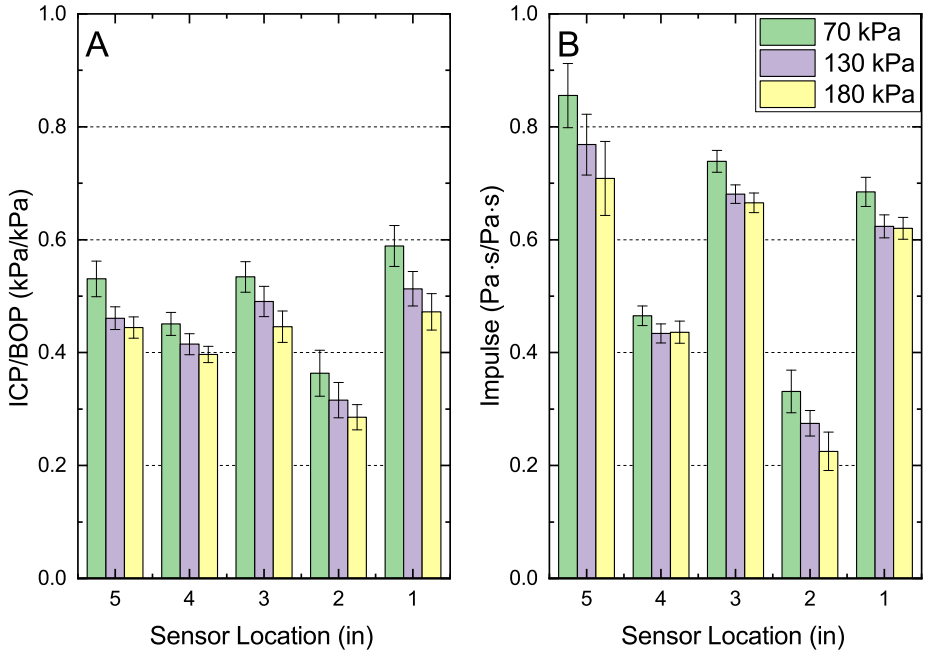

Figure 4.5 A) Shows normalized peak ICP values. B) Shows normalized ICI values. One-way ANOVA showed not significant difference at any of the sensor locations, despite downward trend.

4.3.2 Variation in Postmortem Human Surrgate Data

As shown in Figure 4.3, specimen variation in PMHS were much higher than those seen in rats. This is possibly due to the physiological differences between subjects (Age, Weight, etc.). In order to account for this variation, multiple linear regression was performed in IBM SPSS Statistics 25, to investigate the effect of shock and physiological parameters on the ICP and ICI. From the human data, certain parameters were selected, and multiple linear regression was performed for all parameters. Then, a stepwise analysis was performed to see if the addition of each individual parameters significantly increased the accuracy of the derived equations. Results for ICP are shown in Table 4.1. As shown in Table 4.1, BOP with an adjusted R^2 of 0.628, only accounts for an estimated 63% of the variation between specimens. The addition of skull thickness did not significantly account for any of the variation between the specimen and was removed from the analysis. This is most likely due to

the low between specimen variation within skull thickness. Both the addition of BMI and age significantly improved the amount of variation accounted for by the model totaling to 85%. These parameters are then combined into Equation 4.1. ANOVA determined that the equation developed significantly accounted for the variation in ICP between specimen ($p < 0.001$).

Table 4.1 PMHS Variation in ICP

Parameter addition	$\mathbf{R^2}$	**p-value significant change**
BOP	0.628	<0.001
Skull thickness[a]	0.622	0.654
BMI	0.656	0.036
Age	0.851	<0.001

[a]Skull thickness was removed due to lack of significance

$$ICP = 0.36(BOP) + 1.3(BMI) - 2.6(Age) + 131 \tag{4.1}$$

Results for ICI are shown in Table 4.2. As shown in Table 4.2, incident impulse alone already accounts for an estimated 88% of the variation between specimen. The addition of skull thickness again did not significantly improve the ability for the model to account for any of the variation between specimen and was removed from analysis. Similar to ICP, both the addition of BMI and age significantly improved the amount of variation that the model accounted for totaling 95% of between specimen variation. These parameters are combined into Equation 4.2. ANOVA determined that the Equation developed from this model significantly accounted for the variation in ICI between specimen ($p < 0.001$).

$$ICI = 0.56(Imp) + 2.1(BMI) - 1.8(Age) + 68 \tag{4.2}$$

Table 4.2 PMHS Variation in ICI

Parameter addition	**R^2**	**p-value significant change**
BOP	0.88	<0.001
Skull thickness[a]	0.87	0.587
BMI	0.93	<0.001
Age	0.95	<0.001

[a]Skull thickness was removed due to lack of significance

4.4 Discussion

From the perspective of biomechanical loading, the use of PMHS is as close to live human subjects as possible. PMHS truly represents all the geometric features of a live human, except the brain. It is also possible that the skin and skull may show a differential blast response compared to their live counterparts. However, the analysis of live and surrogate rodents identified that 20% porcine gelatin was capable of representing the brain biomechanically (see Chapter 3). By exposing PMHS and rats under similar loading conditions, the effect of loading is eliminated, and the observed differences should arise only from the geometry of the two species. Despite being an important step, PMHS experiments are not performed frequently to study blast TBI. Field experiments are very expensive to start with and require coordination between groups from explosive experts, to instrumentation engineers, to biological and physical scientists and engineers. In addition, preparing a PMHS in the field adds additional complexity. Thus, field experiments with PMHS exposed to blast are rarely done. Conducting research inside a shock tube is possible; however, a large sized shock tube with expertise is needed. Fortunately, such facilities are available at NJIT.

Interestingly, the intracranial pressure profiles, shown in Figure 4.1, measured deviated significantly from the pressure profiles seen in rats. While in rats ICP profiles resembled the Friedlander waves typically seen in incident profiles, this differs significantly in PMHS data. There is not nearly as sharp of a rise nor, a consistent nonlinear decay. The raises the question on whether rodent models are an adequate model for bTBI. This question has been previously raised for TBI in general [2]. From the sole consideration of biomechanics, primates and other higher order mammals would be expected to be a closer match to humans. With similar body plans, geometries, and brain structures, these would be ideal in order to investigate the biomechanical of shock loading as well as the down stream consequences. That being said the benefits gained do not outweigh the ethical and financial costs of using these species. It has also been suggested that the porcine model may be a superior model due increase physiological similarity compared to rats [59]. While argument are valid again the financial costs to perform statistically significant studies out weight the benefits Rodent models allow for accurate investigation of the downstream effects of injury while allowing for more control and lower cost.

Furthermore, PMHS pressure profiles deviated significantly from the Friedlander like waves seen in previous literature [83]. The measured profiles had significantly lower peak values as well. These differences may be due to differences in sensor placement or in the accuracy of sensing elements used between studies and/or differences in the volumetric dimensions between PMHS specimen. Despite these differences, the oscillatory pattern and negative countercoup pressure seems similar between this study and that of the others [83, 118]. The shape of the pressure profile measured closely resembles work published previously [48, 117] though there are some differences in the peak values. In addition, peak ICP trends of human being lower than rat do confirm trends previously reported [57].

It is postulated that the differences seen are due to two key factors. First, the greater skull thickness found in PMHS compared to rats forces stress wave reflections to take longer to interact within the brain. At each material interface, there will be reflections where a portion of the wave is transmitted and reflected [120]. It will take much longer for the reflection to return to the interface (restarting the process) in PMHS than the rat data. These compounding waves, in the rat model will interact with almost no phase shift, while in PMHS this will be significant. Second, due to volumetric differences between species, there are possibly three stress waves interacting within the PMHS brain, that are not seen in rats. These waves include; the wave passing through the skull at the forehead, the wave transmitting through the skull towards the back of the skull loading the brain from the rear, and the wave rising from skull flexure compressing and decompressing the skull, as the loading passes along the skull from front to rear. This may explain why the 1 in and 2 in sensors start with a negative pressure as the wave here is moving in the opposite direction. The interactions of these complex waveforms may create areas of the brain where constructive interference take place and others where destructive interference dominates. This is supported by the results shown by the 4 in and 2 in sensor, where loading is significantly lower in almost all categories.

The PMHS data collected were also relatively inconsistent when compared to the rat data. This is most likely attributed to intraspecies differences seen between specimen. While the rat subjects' weight, age, size, remained controlled and constant, the same parameters for the humans were not. Ages were relatively similar but there was large variation in weight, height, and BMI. Consequently, an investigation of which of these parameters affect loading variations was also performed. As shown in Tables 4.1 and 4.2, ICP and ICI are significantly affected by incident pressure profile, BMI, and age. BOP and incident impulse, of course, affect insult as measures of blast loading in the environment. The larger the BOP and/or incident impulse,

the larger the insult, as confirmed by the positive coefficient. Age itself is most likely not independently affecting the result, but rather, is a representative factor for bone density. As age increases bone density decreases and this loss in density within the skull contributes to loss in shock wave transmission due to internal reflections. This should explain the decrease in insult seen as the age of the specimen increases. Further detailed analysis needs to be performed to confirm this hypothesis. In wave transmission equations, transmission speed is inversely related to density of the medium and thus, provides some credence to this argument.

More interestingly, BMI shows a positive coefficient in both Equations 4.1 and 4.2. This implies that as BMI increases the level of insult also increases. Higher BMI, with known correlations to obesity, can be correlated to higher density of soft tissue around the head, including skin. As seen in Chapter 3, small variations in the flesh/soft tissue of a specimen can have significant effect on the internal loading of a specimen; though in this case the increase in soft tissue density caused a decrease in insult. The size of the specimen comes into play when determining BMI. Given the same weight but changing the height alters the BMI. These size changes may cause changes in the head cross sectional area. Taller subject will have proportionally larger head dimensions [121, 122]. These larger head dimensions, according to results in Chapter 2, should results in increased surface loading and increased internal mechanical loading.

In summary, PMHS showed significantly lower ICP and ICI when compared to rats exposed to the same conditions. These differences can possibly be explained by the geometric differences between the two species. By characterizing how loading changes based on interspecies differences, it should be possible to arrive at a more accurate scaling relationship between animal and human injuries.

CHAPTER 5

INTERSPECIES BIOMECHANICAL TRANSFER FUNCTION

5.1 Background and Significance

Some of the current scaling techniques are derived from mass scaling developed by Bowen et al. [55, 56] and the Lovelace foundation in the 1950's and 1960's. However, those studies focused on mortality rather than injury, and further they typically studied blast induced lung injury and not brain injury. The postulated functions scale between species based on differences in lung volume and body mass and was found to be sufficient for pulmonary blast injury. Nevertheless, these functions fail to account for the complexities of blast injury [6, 45, 57]. Body and brain mass scaling have also been proposed for brain injuries, but these transfer functions have also been ineffective [57, 58]. These functions ignore geometric or material differences that exist between species. For instance, vast differences between the percent mass of white matter between murine and human can cause changes in loading profiles [59]. In addition, the reflected pressure, the pressure measured on the surface of an impacted object during blast, varies based on the angle of incidence and stiffness of the material [32]. Another major issue is that most transfer functions rely solely on peak BOP and ignore the effect of blast impulse. While incident duration has previously been used as a metric [6, 51, 62], it has yet to be used in the mild range of TBI. Other transfer functions have taken inspiration from blunt injury models and are based on the acceleration [60]. Although the use of acceleration in HIC has been effective in reducing prevalence blunt injuries, it cannot be directly extended to blast loading nor to mild injuries since they were derived for skull fractures.

With recent technological advances, Finite Element Modeling (FEM) has been used to attempt the derivation of interspecies transfer functions. These attempts try to account for the differences in geometry and mechanical properties between species

and aim to fill the gaps left by current transfer functions [57, 58]. Using FEM, Jean et al. [57] was able to show that brain and body mass scaling [42, 62, 63] does not accurately represent bTBI. While providing some insight, many of these studies lack the validation of proper shock loading and material properties based on experimental data.

5.1.1 Objective

The aim of the work described in this chapter, is to *develop transfer functions between rat and human models of mild bTBI* (Specific Aim 3). The functions are based on experimental outcomes using postmortem surrogates for murine and human described in Chapter 4. Based on the parameters established in previous aims, two transfer functions, one for peak incident BOP and the other for impulse, have developed here. Using skull thickness as the main physiological parameter, in conjunction with incident shock parameters, these transfer functions for ICP and ICI can predict the level of insult regardless of species

5.2 Methods and Materials

5.2.1 Data Analysis and Statistics

Both linear and nonlinear regressions were also performed using OriginPro. All ANOVAs as well as multiple linear regression analysis was performed using SPSS 25. A MATLAB script (Appendix B) was written to perform a leave one out cross validation (LOOCV), a common machine learning technique to then validate the effectiveness of the data set to ensure that results were unbiased. This method was chosen because of the relatively low number of samples and low computation time.

5.3 Results

5.3.1 Transfer Function Derivation

Interspecies transfer functions were developed in two ways. First, linear regressions were performed to identify the relationship between rodent ICP and incident BOP; a similar relationship between intracranial impulse (ICI) and incident impulse was also developed (Figure 5.1). The same techniques were then performed on the PMHS data (Figure 5.2). It should also be noted that because no significant difference was found between the peak ICP or ICI values of 5 in, 3 in, and 1 in sensor locations (post-hoc Independent Samples t-test with Bonferroni correction, $p > 0.005$), the data at these locations was pooled for the derivation of interspecies transfer functions. These sensor locations were also chosen because they showed the highest level of insult out of any of the locations tested. This would create a transfer function for the worst case scenario given a specific incident overpressure. Using the linear regression equations at these locations with the highest adjusted R^2 values were chosen (Figure 5.3). Figure 5.3 shows the equations for rat and PMHS data. When comparing the equations for both ICP and ICI, insult in the rat is significantly higher than that of the PMHS.

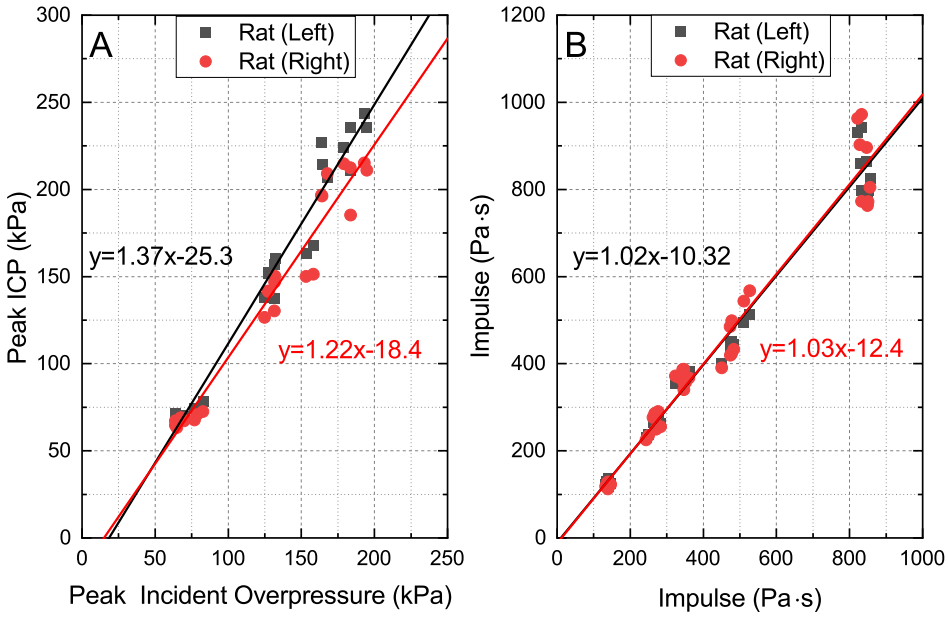

Figure 5.1 Linear Regression results for each sensor location. A) Shows relationship between peak ICP and peak BOP. B) Shows relationship between intracranial impulse and incident impulse.

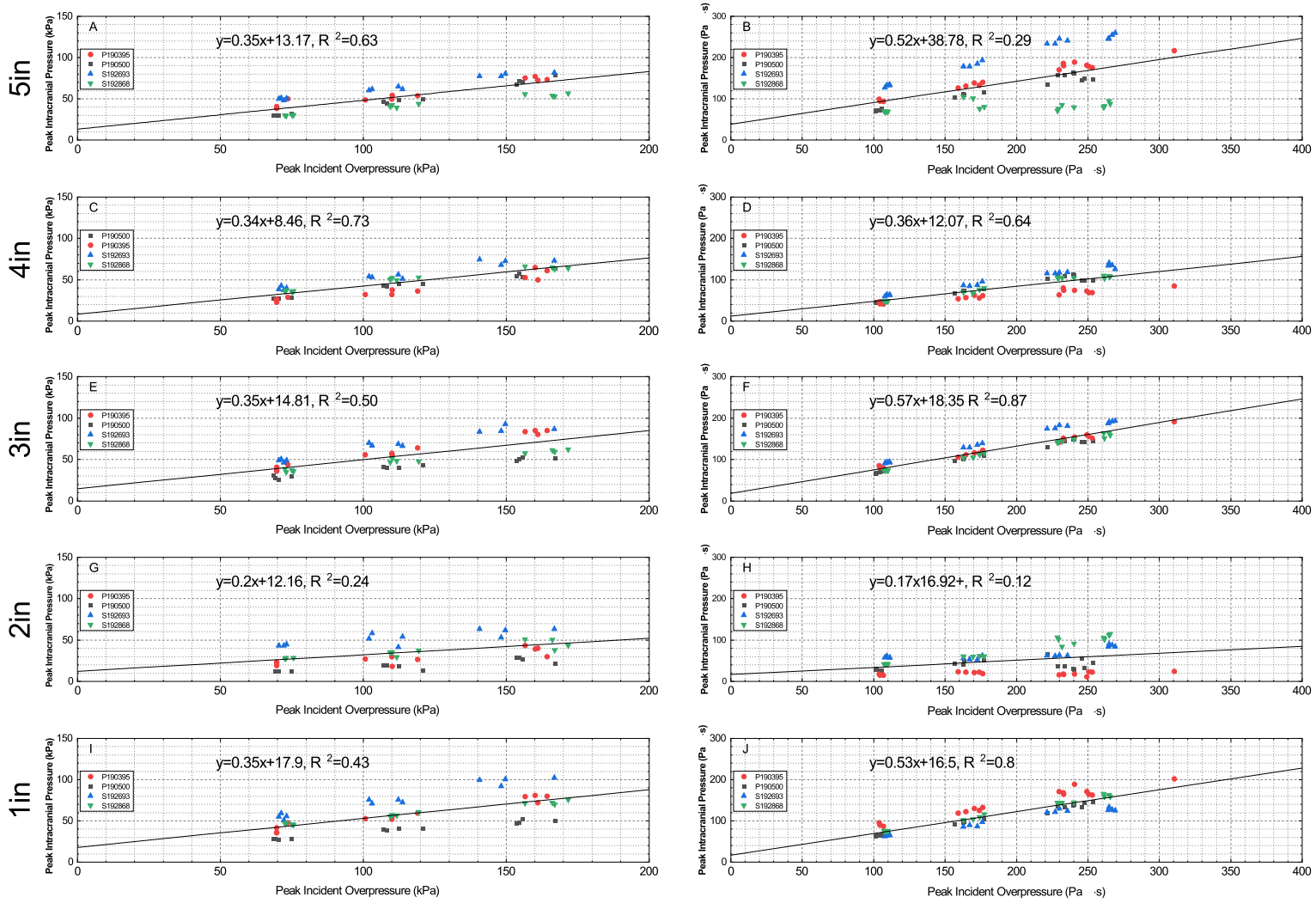

Figure 5.2 Linear Regression results for each sensor location for PMHS data. Left side shows relationship between peak ICP and peak BOP. Right side shows relationship between intracranial impulse and incident impulse.

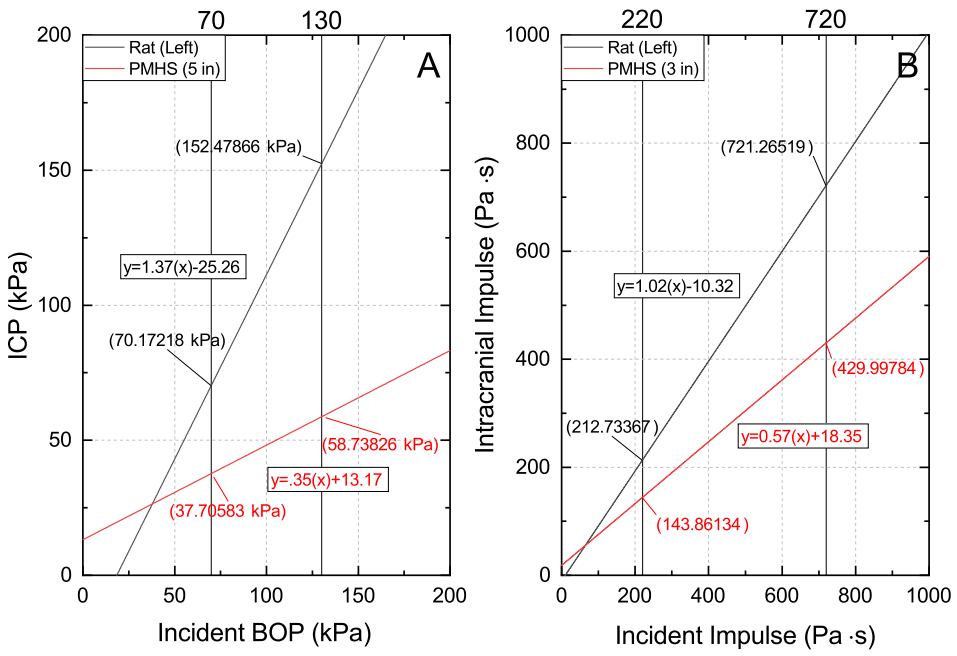

Figure 5.3 Linear regression equations for rat and PMHS data for both A) peak overpressure and B) impulse.

Two separate analyses were conducted to relate ICP and ICI. The equations and plots can be seen in Figure 5.4. As seen in Figure 5.4, peak ICP values have a more dramatic drop compared to the impulse values. Also, the work further shows that the relationship between rodent and human insult is nonlinear. For lower incident pressures and impulses, brain insults are close for the two species. Furthermore, both equations with an adjusted R^2 value of 0.99 account for 99% of the variation in their respective data.

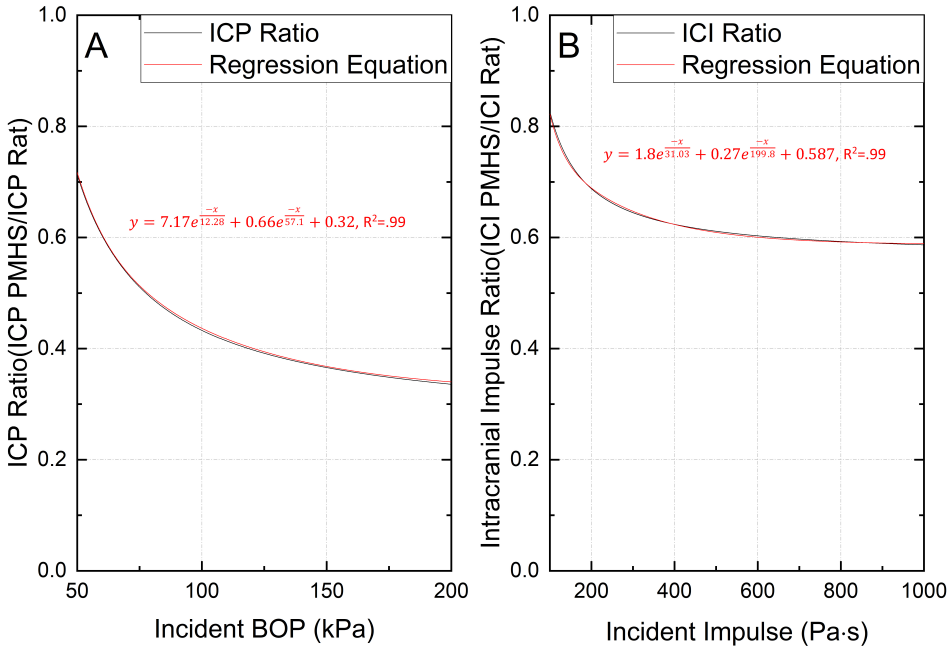

Figure 5.4 Plots for equations that provide conversion factors for A) peak overpressure B) impulse. Exponential decay equations derived using nonlinear regression.

5.3.2 Transfer Functions Based on Physiological Parameters

While the version of the interspecies transfer function, previously derived in Section 5.4.1, can relate rodent to human insults, it cannot be expanded to other species and fails to specifically include physiological differences between species. To this end, a second transfer function was developed that accounts for both physiological and incident loading parameters and output insults metrics, ICP or ICI. One of the main differences established between the two species is the skull thickness. While in Chapter 2 size was identified as potential target it was removed as it predicted an opposite affect than what than what was observed on Chapter 4. Using similar regression techniques used to investigate inter-specimen differences for PMHS, the combined effects of skull thickness and incident loading parameters on insults metrics were investigated. To estimate skull thicknesses, micro-CT for rats and CT scans for PMHS, were imported into Simpleware ScanIP. Masks were created for each skull,

for easier manipulation and analysis. Using the Simpleware ScanIP wall thickness tool, the mean skull thickness was estimated. Mean skull thickness was used due to the observed pressure profiles near the back of the skull. It should be noted that the values of skull thickness are most likely an underestimation due to the nature of the wall thickness function in Simpleware ScanIP. To adjust for this, thresholds were set to remove micron thick elements that were determined to be either unrealistically low or arising from noise in the CT scans. These values were plugged into SPSS 25 with the respective incident BOP or impulse, where multiple linear regression was performed. The derived equation for ICP had an adjusted R^2 of 0.85, meaning that 85% of variation in ICP was accounted for by Equation 4.3. ANOVA shows that the model significantly accounted for the observed variation ($p< 0.001$). The combination of skull thickness and incident impulse showed greater accuracy with Equation 5.2 accounting for 95% of variation, with ANOVA resulting in significant account of variation ($p < 0.001$).

$$ICP = 0.801(BOP) - 13.8(ST) + 53.9 \tag{5.1}$$

$$ICI = 0.98(IMP) - 10.6(ST) + 10.5 \tag{5.2}$$

With equations derived, validation must take place to ensure that multiple linear regression is not biased by the selected data. Accordingly, LOOCV was used to validate the equation derived. As a result, 72 iterations for ICP and 104 iterations for ICI were performed resulting in total RMSE (combined over all iterations) of 24.4 and 38.9, respectively. ANOVA consistently shows that the model significantly predicted the test data set. This combined with the relatively low RMSE, validates that the multiple linear regression given by equations 5.1 and 5.2.

5.3.3 Porcine Data Predictions

To test the robustness of the transfer function developed, the transfer function was used to predict insult metrics seen in literature for porcine models. Different species of pigs and mini pigs have been used in TBI research as an intermediate between rodent and human experiments [48, 57, 78, 111, 123, 124, 125]. It has even been argued that due to similarities in body mass and other parameters that pigs may be a more accurate model of TBI [59]. Because of this, porcine data were selected as an important step towards the validation of the transfer functions developed. Unfortunately, this came with challenges. As previously mentioned, the importance of impulse/duration in exposure is often ignored. Thus, only the ICP function was able to be tested. First, work from Shridharani et al. [126] was used. This paper was selected because it provided an average skull thickness of 9.75 mm for the porcine and complete incident blast conditions. As seen in Table 5.1, predicted ICP largely underestimated the ICP expected in brain injury. This work deviated significantly from the experiments described in Chapter 4. Most notably the incident overpressures far exceeded the range the equation was tested, because of this Table 5.1 was not considered towards the validation of Equation 5.1. Next, work from Feng et al. [48] was used. This work was selected for having more similar loading conditions with work done in Chapters 3 and 4. Unfortunately skull thickness was not directly given for the pigs used, instead the authors claimed that due to the pigs age, skull thickness should be similar to human skull thickness. Because of this, the average skull thickness for human in this work (6.65 mm) was used as the input for skull thickness. As seen in Table 5.2, predicted ICP was more accurate, but deviated as BOP exceeded the mild TBI range.

Table 5.1 Transfer Function Prediction for Shridharani et al. [126]

Reported BOP	Reported ICP	Predicted ICP	Error %
234	389.1	106.92	72.52
242	185.2	113.33	38.81
269	192.6	134.96	29.93
272	278.1	137.36	50.61

Table 5.2 Transfer Function Prediction for Feng et al. [48]

Reported BOP	Reported ICP	Predicted ICP	Error %
148.8	78.9	81.32	3.06
278.9	209.1	185.53	11.3
409.2	328.2	290	11.6

5.4 Discussion

The development of interspecies transfer functions is a key scientific and technological gap towards the understanding of blast TBI in humans for possible diagnostics, therapeutics, and prevention. Previous attempts did not account for the uniqueness of blast loading compared to other types and failed to correlate experimental data on animals of PMHS. The work described in this chapter identifies skull thickness as an interspecies insult metric that needs to be specifically incorporated in the development of the transfer function between animals and humans.

As shown from the PMHS data in Chapter 4, the insult for the same level of blast is much lower in humans compare to the rats. Both ICP and ICI values were significantly lower in PMHS than in rats. These lower insults imply that the resultant injuries are far less severe assuming the same external loading conditions. Because of this, parameters such as size (cross-sectional area) that were identified in previous aims were removed from consideration. While results indicate that there should be

an effect, it would not be as sensitive as the other parameters due to moving in the opposite trend of loading. To further examine the relationship between measured insults and predicted injury, equations derived above were used to equate injuries and determine the equivalent incident pressure profile metrics that would be needed to develop the same injury. To do this, dose-response curves were taken and equated to the predicted ICP values based on linear regression equations derived above. With the assumption that under the same level of tissue loading results in similar injury, the predicted ICP determines the severity of injury regardless of species. These ICP values were then used to find an equivalent incident pressure that would be required to develop the respective insult.

The first of these dose-response curves can be found in Figure 5.5. Here mortality data from the CIBM3 lab was taken from [119]. In the figure, the 24 hours survival (mortality) is plotted as function of various incident BOP and impulses. Based on the transfer functions developed here, equivalent dose-response curves for human mortality can be plotted given the following assumptions. The first is that the ICP measured in rat brain and human brain would result in the same downstream injuries that lead to mortality. The second is that mortality is caused solely by traumatic brain injury and not any other systemic effect. Last is human mortality rates assume an unprotected individual; no external protections in the form body armor or helmets (commonly used by military personnel during exposure) were considered. With this considered, as seen in Figure 5.5, the mortality curves for BOP as well as impulse shift significantly to the left. This implies that humans can withstand much larger intensity shock waves compared to rats.

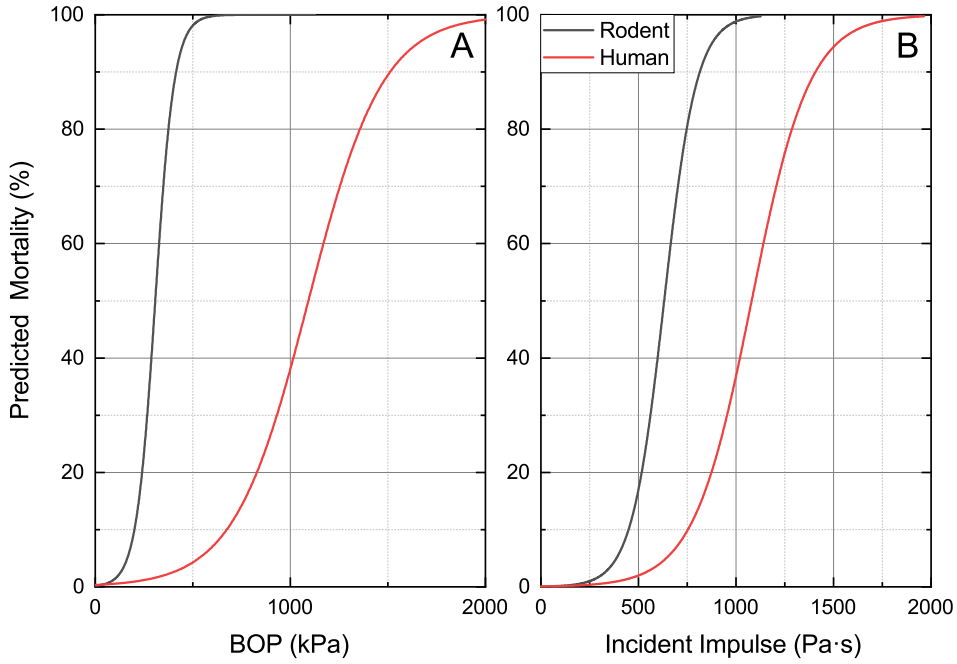

Figure 5.5 Predicted mortality curves for A) BOP and B) Incident impulse.

Mortality may not be the best injury metric to use when trying to compare injuries between species. Mortality, especially for blast, comes with many confounding factors as it is difficult to isolate brain injury from other injuries. Mortality also deviates to much higher overpressures beyond the mild and sub-concussive ranges where most of the interest lies. For this, it is important to examine the differences in the immunohistochemistry and pathophysiology of the brain. For example, Blood Brain Barrier (BBB) breakdown has been investigated and identified as an injury mechanism especially for mild overpressures [26]. Using data from Kuriakose et al. dose-response curves (Figure 5.6) were developed to predict the level extravasation caused by various blast intensities. Extravasation was quantified as the product the area stained and the intensity of the stain. This allows for a more complete quantification of the level of BBB breakdown. Using this metric, we can identify the level of BBB breakdown depending on overpressures within the mild range. As shown in Figure 5.6, again, there is a large shift towards very high incident overpressures. Interestingly, in the frontal cortex where the most injury is taking place, the maximum

injury takes place at around the 200 kPa. This shows that even at relatively low overpressures, humans can experience widespread and diffuse injury throughout the brain.

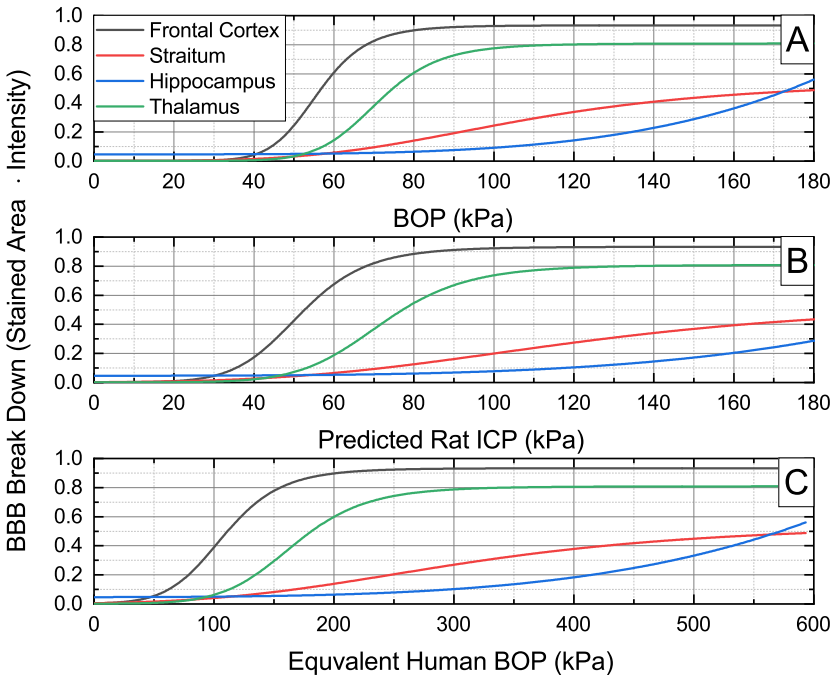

Figure 5.6 A) Dose-response curves examining effect of BOP on the extravasation of Evans Blue across the Blood Brain Barrier at various locations of the rodent brain. B) Based on equations for Rat ICP derived, B) shows dose-response curves adjust for Rat ICP. C)Assuming same tissue level loading, dose-response curves are now adjusted to equivalent BOP necessary to match ICP values in B.

The predictive ability of these transfer functions was additionally tested as described in Section 5.4.2. Equation 5.1 was not able to accurately predict the ICP of porcine specimen in the work described by Shridharani et al. with errors upwards of 30%. This is most likely due to differences in experimental design. The porcine were exposed outside of the shock tube as a side on impact. Exposures outside of shock tubes are shown to have very different loading when compared to the same level blast within the shock tube [18, 52]. This could explain why, as seen in Table 5.1, there seems to be no correlation between the reported BOP and reported ICP in the paper. Furthermore, the range of BOP's tested was well above the mild range

that Equation 5.1 was derived. The work done by Fend et al. was more similar to methods described in Chapter 4. The authors also reported similar waveforms for their ICP profiles to the PMHS data reported in Chapter 4. This work used actual explosives in a head on impact instead of a shock tube. Despite small differences, ICP values were relatively accurate. As expected, accuracy decreases as BOP increases well above the mild range.

In summary, a relationship was developed relating rat ICP and ICI to that of PMHS, which can be the first step towards establishing a transfer function. Currently, there is no such relationship. Using the developed functions, human survival and other pathophysiological outcomes based on rat data can be predicted. The functions also seem to predict loading outside of the species tested with in the mild TBI ranges to some level of success. Additionally, targets that may improve accuracy of future transfer functions have also been identified.

CHAPTER 6

SUMMARY AND FUTURE DIRECTIONS

Blast-induced traumatic brain injury (bTBI) is one of the leading injury modalities in military personnel. It is considered a signature injury in veterans returning from conflicts in the Middle East. Additionally, bTBI affects unsuspecting civilians encountering terrorist threats and law-enforcement officers or military personnel during regular training. One of the main concerns in the study of bTBI is translating preclinical animal experimental results to clinical applications that can be useful to blast victims. Although, there has been promising findings in animal research that mimic behavioral and pathophysiological outcomes to that of humans; animal results have not been translated to humans. This work aims to focus on relating the insults caused by shock waves between animals and humans. With the assumption that on a tissue level similar insults result in similar injuries, it is hypothesized that biomechanical transfer functions can be derived using a comparison of tissue level loading between postmortem rodent and human surrogates, based on consideration of interspecies differences in size, material properties, and skull thickness. To test this, three specific aims were developed: 1) Determine how size, material, and thickness affects pressure loading variation using simple geometry surrogates, 2) Determine how material affects pressure loading variations within brain and brain simulants, 3) Develop a transfer function to relate pressure loading variations between rat and human models of injury.

Beginning with simple 2D geometries, the effects of specimen size and material on surface loading were investigated through reflected pressure profiles. Studies were conducted using plates of various areas and materials to investigate the effects on loading at three discrete incident overpressures, namely 70 kPa, 130 kPa, and 180 kPa. Combined with numerical simulations, results offer insight into how surface loading

(reflected pressure profiles) varies with specimen as well as shock wave parameters. Results demonstrated that the increase in the cross-sectional area of the specimen result in the increase of the dwell time at the center of the plate, due to stagnation of the shock wave flow field. It results in the increased impulse values despite the peak overpressures and durations remaining the same for the equivalent exposure conditions defined by incident shock wave characteristics. The variable duration shock wave shows that from the perspective of a biomechanical loading and injury prediction, a comparison between exposure conditions, with the same peak BOP, is not wholly accurate if the corresponding durations and impulse values are unknown. Furthermore, results demonstrate that for the same peak overpressure the surface loading scales with the duration of the incident shock wave, and it was higher by a factor of 20-30% for the long duration shock waves. The disturbance of the flow field around the specimen also had a pronounced effect on the morphology of the surface ROPs. Similar to the case where larger dimensions of the plate resulted in longer dwell time, the same effects are observed where the plate is placed next to the shock tube wall or in the corner.

With surface level loading characterized, the complexity of surrogates was then increased to 3D specimen to investigate how thickness and material properties affect internal loading. In these studies, boxes were constructed and filled with previously studied brain simulants. Results show the protective effects of thicker materials and point to 20% porcine gelatin as a potential brain simulant due to its similarities to brain biomechanical properties. Based on the average velocities of the waves moving through the materials, the porcine based ballistic gelatins seem to behave the best, with similar acoustic properties to the brain. Interestingly, the peak of the blast seems to remain the same despite the window thickness increases. Despite this, the impulse or energy transmitted significantly decreases. The thinner window allowed

for more of the energy to transmit through to the internal material i.e., the thicker the skull, the less energy transmitted to the brain, but the peak stress is not affected.

Continuing to the second specific aim: to determine the effects of material on the loading of brain and brain simulants; potential brain and skin simulants were accessed by comparing intracranial pressure and skull strain between increasingly complex murine surrogates and live rats. Surrogates were developed to match the geometry of rat models and the effects of material properties on intracranial loading are elucidated. In addition, results help solidify 20% porcine gelatin as an accurate brain simulant for blast testing. As seen in Table 3.1, models with 20% brain simulants typically outperformed other surrogates. With the 20% semi-surrogate performing the best, 20% porcine gelatin seems to be an adequate brain surrogate; matching in most injury metrics independent of BOP or impulse. The synthetic ballistic gel almost completely damped the transmission of the shock wave. The failure of the full surrogate models and relative success of the semi-surrogates shows the importance of flesh materials in dampening the effect of the shock front. Even with minor changes to skin material properties, for example 20% to 25% porcine gelatin, the results showed very different pressure profiles. By increasing material stiffness, results have shown that the shock wave has more difficulty transmitting in terms of impulse to the brain, i.e., the stiffer surrogate materials seem to lessen the amount of energy that is able to transmit into the skull. A thorough investigation of the effect of soft tissue is necessary as it may provide insight into how loading transfers between species. Furthermore, this work validates previous PMHS work that used 20% porcine gelatin. However, the results show that using porcine gelatin will underestimate the loading taking place.

Finally, postmortem surrogates were prepared for murine and human head forms and exposed to three discrete incident overpressures to investigate interspecies loading differences in the mild range of bTBI. The use of similar loading conditions allowed for the one-to-one comparison between the two species. These differences were used

to develop a biomechanical transfer functions for intracranial pressure and impulse targeting specifically the parameters in specific aims 1 and 2. Using multiple linear regression, transfer functions were derived based on specimen skull thickness, as well as, incident shock parameters. Derivation methodologies were then validated with a leave one out cross validation algorithm, in order to test the validity of the functions being derived. Based on these functions, the combination of skull thickness and incident loading parameters significantly predict insult independent of species.

PMHS results showed significantly lower loading compared to the rat data. Interestingly, the intracranial loading with in PMHS subjects, showed a sinusoidal pattern as a function of depth, not seen in the rat. The ICP profiles in rat, as seen in Chapter 3, are very similar to the Friedlander wave seen in incident pressure profiles. This differs significantly in PMHS data; there is not nearly as sharp of a rise nor, a consistent nonlinear decay that is present in rats. PMHS data also showed significantly more between subject variation than the rat data. In order to account for variations, multiple linear regression was performed to identify which physiological parameters ICP and ICI were each more sensitive. As a result, age and BMI were shown to have the ability to significantly account for the variations seen. Due to low n and small range of values, these equations should not be extrapolated to larger populations, but this does show that these are parameters that should be targeted in future works. Results for BMI further validates on results shown in Chapter 3, indicating the importance of soft tissue on loading. In addition, the effects of age shown express the need for more accurate PMHS models. With an average age in the sixties, this does not replicate the average age of soldiers in the field.

With target parameters identified and specimen exposed to a variety of blast intensities, multiple linear regression was used to see which parameters made a significant impact on the equations ability to predict insults. The resulting equations show the combination of skull thickness and incident pressure parameters (BOP and

incident impulse) affect intracranial loading. This combination accounted for 85% and 95% of variation in ICP and ICI, respectively. For mild injuries, this proves to be an important step towards the development of an interspecies transfer function. The functions derived, as of now, are only able to estimate insults between rat and human injury, but with future work on other species, for example porcine models, the development of a true transfer function should be possible. Furthermore, these transfer functions show that widespread injury is present at much lower incident overpressures than are typically tested. By using logistic regression to create dose response curves for BBB breakdown, and then applying the interspecies transfer functions, widespread BBB breakdown is predicted at key locations throughout the brain.

This dissertation is the culmination of the completion of three specific aims: 1) the investigation of size, thickness, and material properties on specimen loading both internal and surface level, 2) the investigation of the response of brain and brain simulants to shock loading, 3) the derivation of interspecies transfer functions for tissue level biomechanical loading based on select interspecies differences. Through these aims, the original hypothesis is partially validated. While size and material properties, were excluded from the final functions, skull thickness showed significant effect on the tissue level loading as predicted.

6.1 Future Directions

This work should serve as tool for future researchers to develop more accurate transfer functions that involve more interspecies differences. More experiments need to be performed in order to investigate the effects of geometry and soft tissue on specimen loading. Soft tissues need to be further investigated to identify potential skin surrogates and elucidate soft tissues effect on shock biostructure interaction. This work also serves as foundation for computational work, to develop more field

accurate models based on materials tested here. While transfer functions established may be effective for the mild range of TBI, further experimentation should be done at higher blast intensities, to gain a more complete picture of blast as a whole. This work also showed the importance of impulse as a factor for biomechanical loading. With this established, future studies relating impulse to variations in pathophysiological changes and downstream behavioral effects need to be elucidated.

APPENDIX A

COMPLETE POSTMORTEM HUMAN SURROGATE DATA SET

Figures A.1-A.12 show pressure profile results for each specimen at 70, 130, and 180 kPa

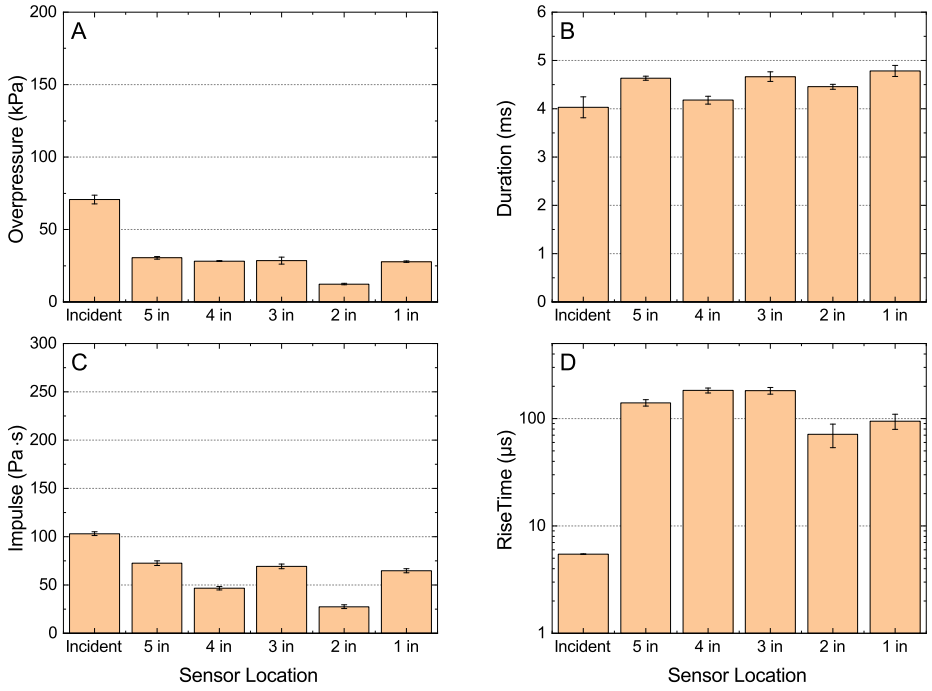

Figure A.1 PMHS specimen 1 exposed to 70 kPa BOP. A) Comparison of peak overpressure. B) Comparison of duration. C) Comparison of impulse. D) Comparison of risetime.

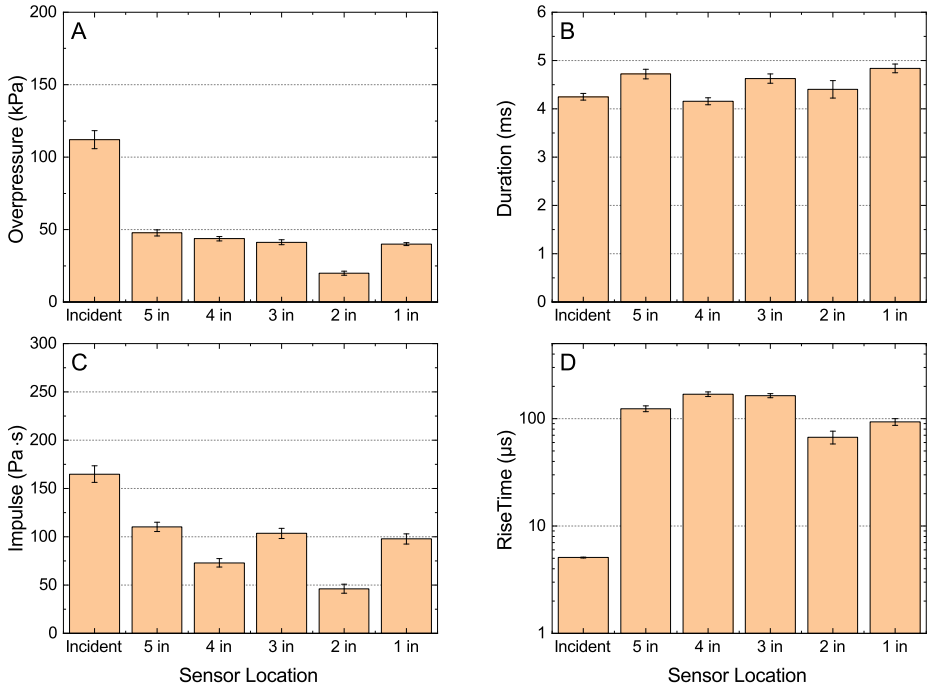

Figure A.2 PMHS specimen 1 exposed to 130 kPa BOP. A) Comparison of peak overpressure. B) Comparison of duration. C) Comparison of impulse. D) Comparison of risetime.

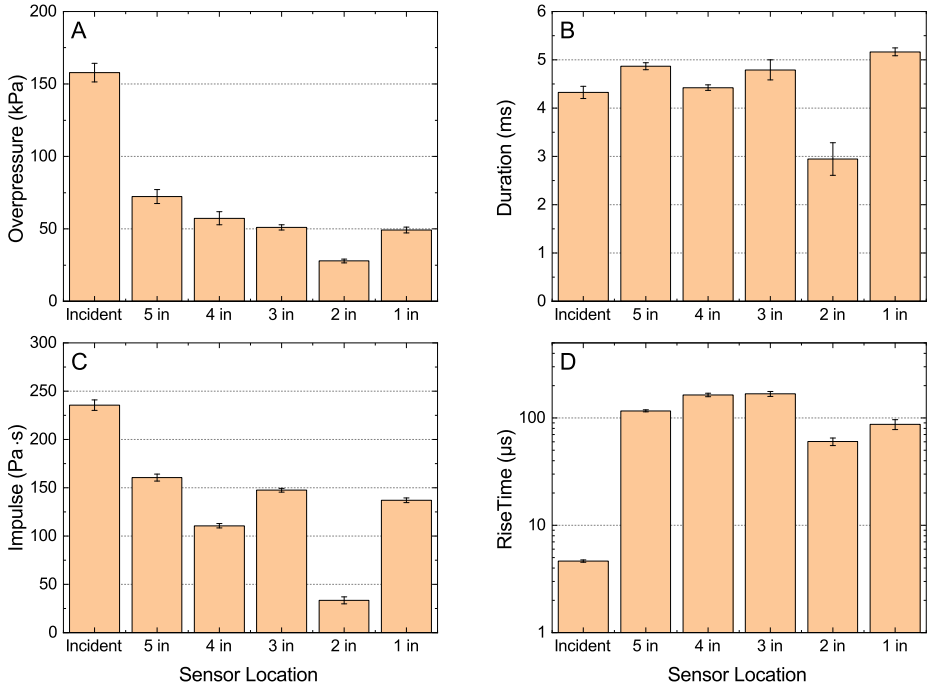

Figure A.3 PMHS specimen 1 exposed to 180 kPa BOP.A) Comparison of peak overpressure. B) Comparison of duration. C) Comparison of impulse. D) Comparison of risetime.

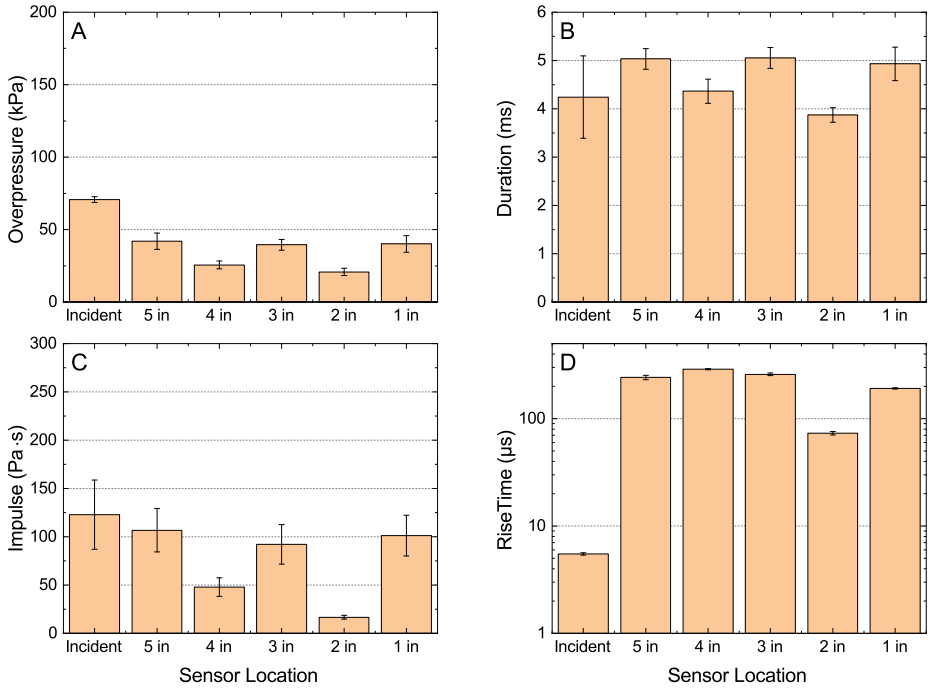

Figure A.4 PMHS specimen 2 exposed to 70 kPa BOP. A) Comparison of peak overpressure. B) Comparison of duration. C) Comparison of impulse. D) Comparison of risetime.

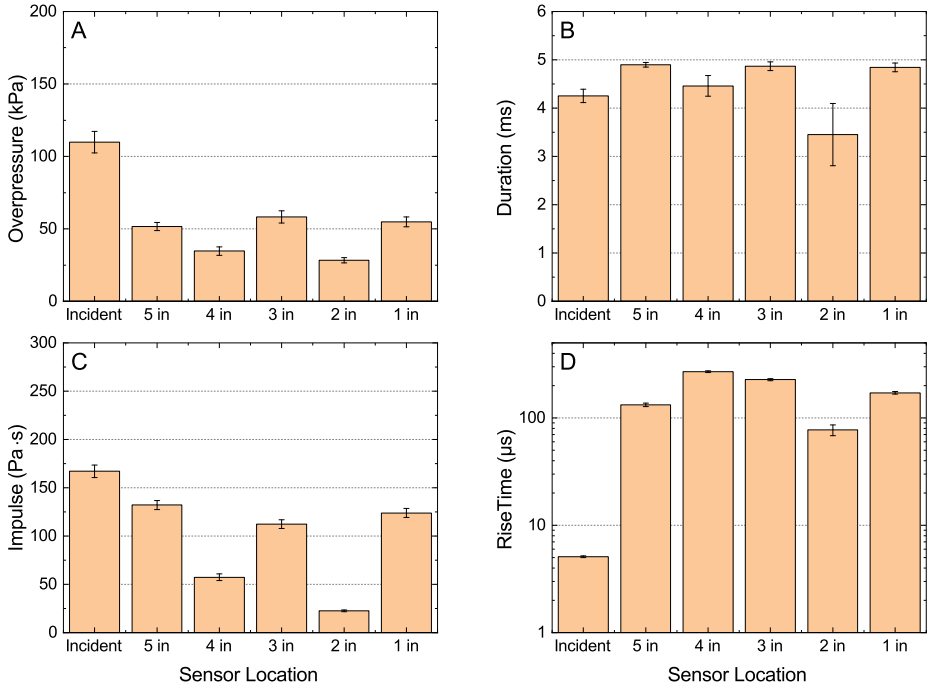

Figure A.5 PMHS specimen 2 exposed to 130 kPa BOP. A) Comparison of peak overpressure. B) Comparison of duration. C) Comparison of impulse. D) Comparison of risetime.

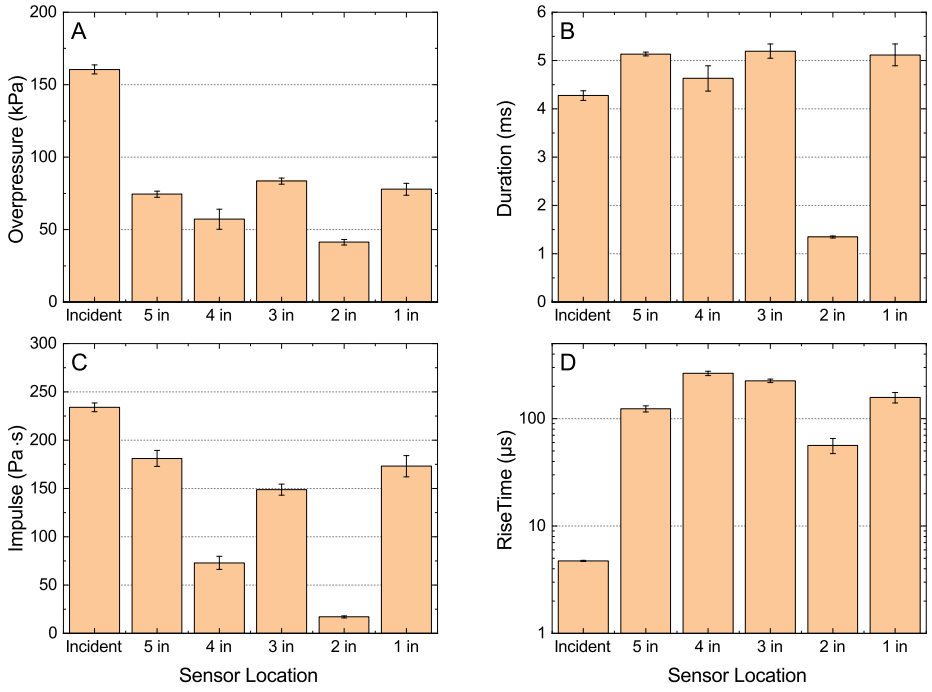

Figure A.6 PMHS specimen 2 exposed to 180 kPa BOP. A) Comparison of peak overpressure. B) Comparison of duration. C) Comparison of impulse. D) Comparison of risetime.

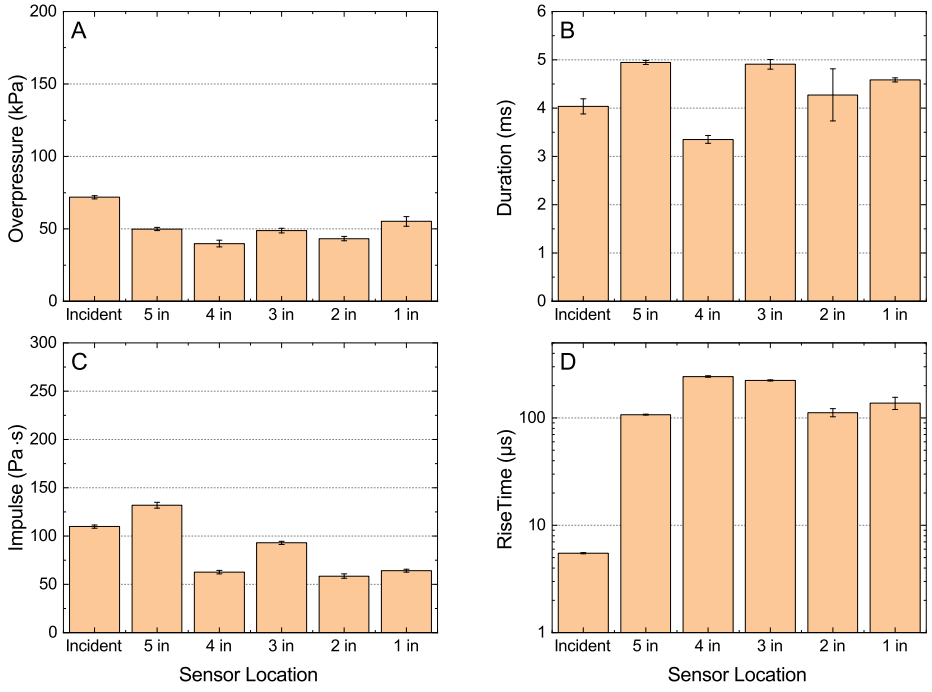

Figure A.7 PMHS specimen 3 exposed to 70 kPa BOP. A) Comparison of peak overpressure. B) Comparison of duration. C) Comparison of impulse. D) Comparison of risetime.

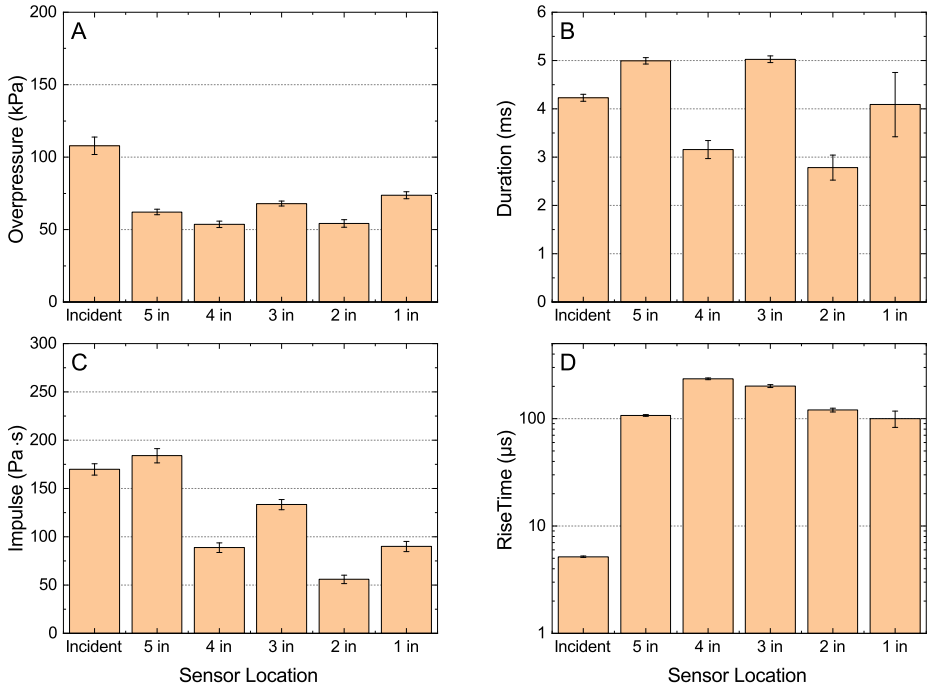

Figure A.8 PMHS specimen 3 exposed to 130 kPa BOP. A) Comparison of peak overpressure. B) Comparison of duration. C) Comparison of impulse. D) Comparison of risetime.

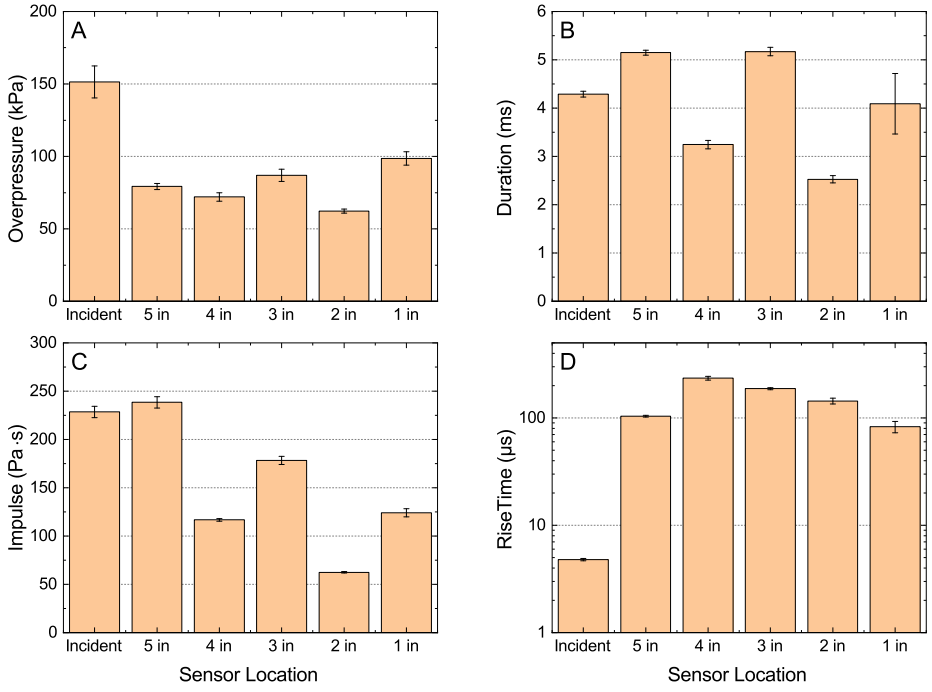

Figure A.9 PMHS specimen 3 exposed to 180 kPa BOP. A) Comparison of peak overpressure. B) Comparison of duration. C) Comparison of impulse. D) Comparison of risetime.

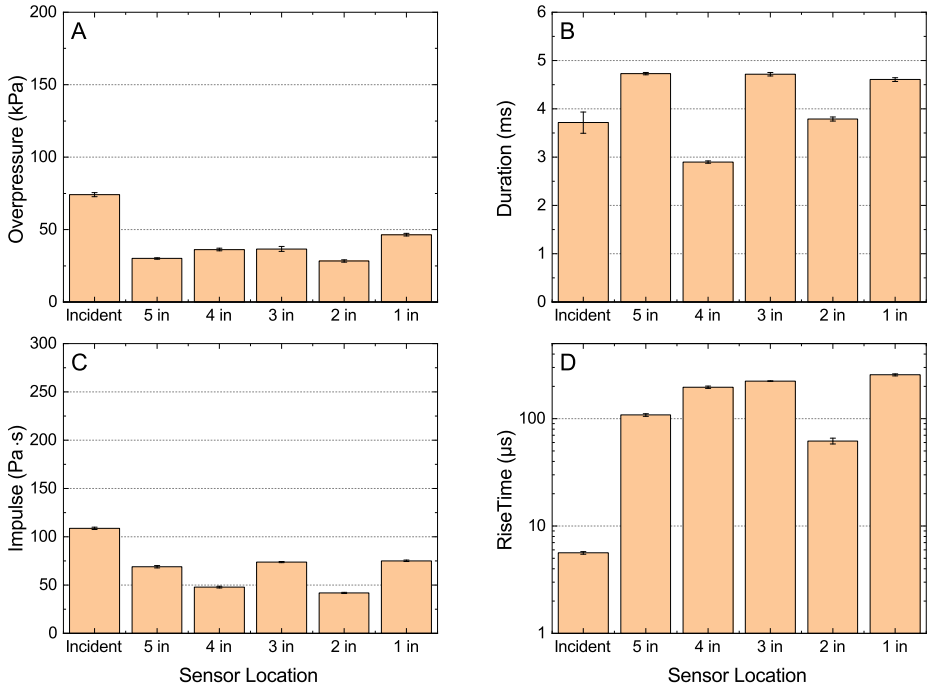

Figure A.10 PMHS specimen 4 exposed to 70 kPa BOP. A) Comparison of peak overpressure. B) Comparison of duration. C) Comparison of impulse. D) Comparison of risetime.

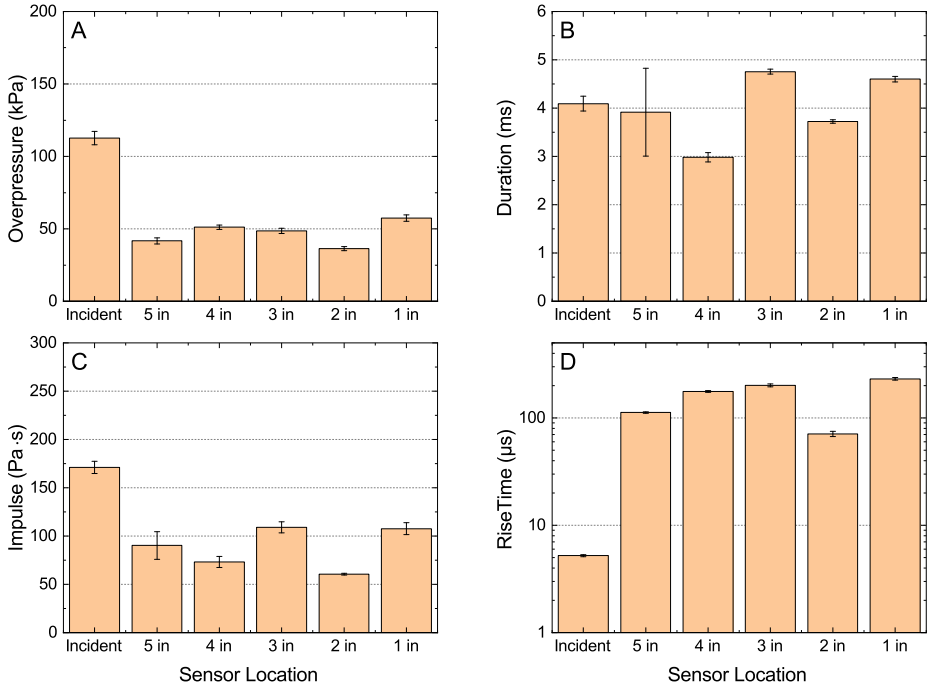

Figure A.11 PMHS specimen 4 exposed to 130 kPa BOP.A) Comparison of peak overpressure. B) Comparison of duration. C) Comparison of impulse. D) Comparison of risetime.

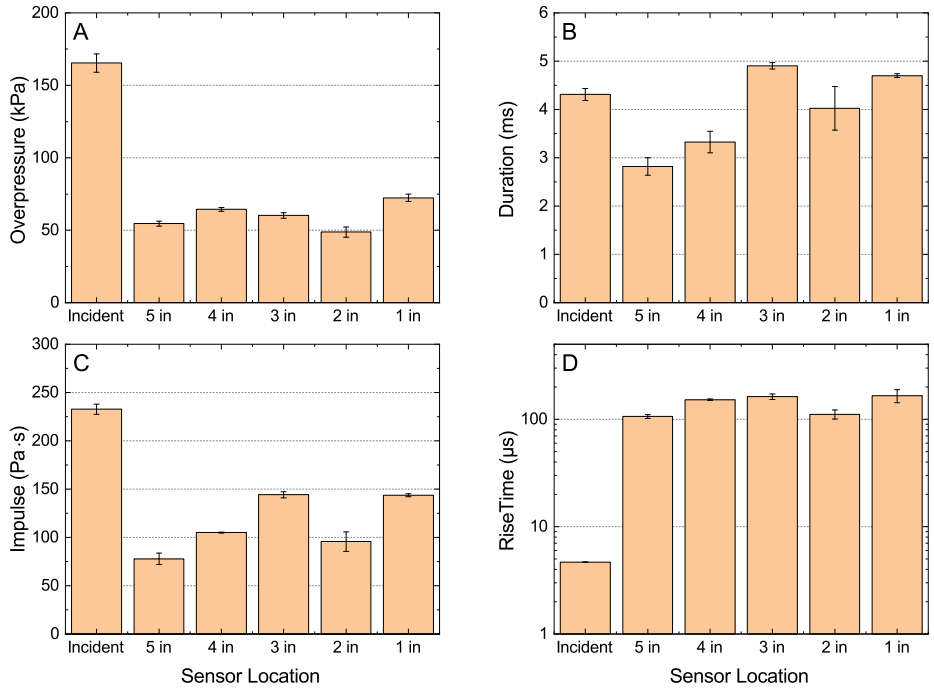

Figure A.12 PMHS specimen 4 exposed to 180 kPa BOP. A) Comparison of peak overpressure. B) Comparison of duration. C) Comparison of impulse. D) Comparison of risetime.

APPENDIX B

MATLAB SCRIPT

MATLAB script written to validate multiple regression technique using LOOCV

```
clc
clear
%% Data Extraction and preparation
data=readtable('Rat_Human.csv', 'Headerlines', 1); % Data Import
y1=data(:,3);% ICP data
x1=data(:,2); %BOP Data
x2=data(:,1); % Thickness

y2=data(:,6); %ICI data
x3=data(:,5); %Incident Impulse
x4=data(:,4); % SKull Thickness

% Sets data as an array
y1=table2array(y1);
x1=table2array(x1);
x2=table2array(x2);

y2=table2array(y2);
x3=table2array(x3);
x4=table2array(x4);

\%Removes Empty cells from data
y1=rmmissing(y1);
y2=rmmissing(y2);
x1=rmmissing(x1);
x2=rmmissing(x2);
x3=rmmissing(x3);
x4=rmmissing(x4);

%% Preparation for Cross validations
IV1 = [ones(size(x1)) x1 x2]; % Prepared predictors for regression
 function with interaction
indices1=zeros(size(y1)); %Preparing index variable for cross validation

IV2 = [ones(size(x3)) x3 x4]; % Prepared predictors for regression
 function with interaction
```

```
indices2=zeros(size(y2)); %Preparing index variable for cross validation

k1=length(y1); % number of folds for ICP (currently set for leave on out)
k2=length(y2); % number of folds for ICI (currently set for leave on out)

\%\% Peak ICP Validation
\% Dividing Data CIP into Random Groups
j=1;
while j<=k1
groupval=randi([1,k1],1);
indtest=find(indices1==groupval); %divides predictors randomly
if length(indtest)>=1 %ensures groups with equal sizes
continue;
else
indices1(j,1)=groupval;
j=j+1;
end
end

error=zeros([1 k1]);
stats_all1=zeros([4 k1]);

for i = 1:k1
test = (indices1 == i);% Creats test index
train = ~test; % creates training index
ytrain=y1(train,:); % Seperates training data
Xtrain=IV1(train,:);
[b,bint,r,rint,stats1] = regress(ytrain,Xtrain); % mutlpile regression
 using training groups
all_b(:,i)=b;
ytest=y1(test,:); %Seperates testing data
Xtest=IV1(test,:);
yp=b(1).*Xtest(:,1)+b(2).*Xtest(:,2)+b(3).*Xtest(:,3);% regression
 equation
error(i)=(ytest-yp).^2; %Squared error
stats_all1(:,i)=stats1; %Reports Stats for each itteration
end
\%\% ICP Results
msetest1=mean(error,'all'); %Mean squared error
rmserror1=sqrt(msetest1);% RMS error

%% Impulse Validation
j=1;
while j<=k2
groupval=randi([1,k2],1);
```

```
indtest=find(indices2==groupval); %divides predictors randomly
if length(indtest)>=1 %ensures groups with equal sizes
continue;
else
indices2(j,1)=groupval;
j=j+1;
end
end

error=zeros([1 k2]);
stats_all2=zeros([4 k1]);

for i = 1:k2
test = (indices2 == i);% Creats test index
train = ~test; % creates training index
ytrain=y2(train,:); % Seperates training data
Xtrain=IV2(train,:);
[b,bint,r,rint,stats2] = regress(ytrain,Xtrain); % mutlpile regression
 using training groups
ytest=y2(test,:); %Seperates testing data
Xtest=IV2(test,:);
yp=b(1).*Xtest(:,1)+b(2).*Xtest(:,2)+b(3).*Xtest(:,3);% regression
 equation
error(i)=(ytest-yp).^2; %Squared error
stats_all2(:,i)=stats2; %Reports Stats for each itteration
end
%% ICI Results
msetest2=mean(error,'all'); %Mean squared error
rmserror2=sqrt(msetest2);% RMS error
```

REFERENCES

[1] C. Taylor, J. Bell, M. Breiding, and L. Xu, "Traumatic brain injury–related emergency department visits, hospitalizations, and deaths — United States, 2007 and 2013," *Morbidity and Mortality Weely Report Surveillance Summary*, vol. 66, no. SS-9, pp. 1–16, 2017.

[2] D. M. Morales, N. Marklund, D. Lebold, H. J. Thompson, A. Pitkanen, W. L. Maxwell, L. Longhi, H. Laurer, M. Maegele, E. Neugebauer, D. I. Graham, N. Stocchetti, and T. K. McIntosh, "Experimental models of traumatic brain injury: Do we really need to build a better mousetrap?," *Neuroscience*, vol. 136, no. 4, pp. 971–989, 2005.

[3] M. C. Morganti-Kossmann, E. Yan, and N. Bye, "Animal models of traumatic brain injury: Is there an optimal model to reproduce human brain injury in the laboratory?," *Injury*, vol. 41, Supplement 1, pp. S10–S13, 2010.

[4] Defense and Veterans Brain Injury Center "DoD worldwide numbers for TBI," Defense and Veterans Brain Injury Center, Silver Spring, Maryland, 2019.

[5] G. W. Hergenroeder, J. B. Redell, A. N. Moore, and P. K. Dash, "Biomarkers in the clinical diagnosis and management of traumatic brain injury," *Molecular Diagnosis & Therapy*, vol. 12, no. 6, pp. 345–358, 2008.

[6] M. B. Panzer, G. W. Wood, and C. R. Bass, "Scaling in neurotrauma: How do we apply animal experiments to people," *Experimental Neurology*, vol. 261, pp. 120–126, 2014.

[7] I. Cernak, "Animal models of head trauma," *NeuroRx*, vol. 2, no. 3, pp. 410–422, 2005.

[8] F. Zhu, C. Wagner, A. D. C. Leonardi, X. Jin, P. VandeVord, C. Chou, K. H. Yang, and A. I. King, "Using a gel/plastic surrogate to study the biomechanical response of the head under air shock loading: a combined experimental and numerical investigation," *Biomechanics and Modeling in Mechanobiology*, vol. 11, no. 3-4, pp. 341–353, 2012.

[9] S. M. Lippa, J. R. Fonda, C. B. Fortier, M. A. Amick, A. Kenna, W. P. Milberg, and R. E. McGlinchey, "Deployment-related psychiatric and behavioral conditions and their association with functional disability in OEF/OIF/OND veterans," *Journal of Traumatic Stress*, vol. 28, no. 1, pp. 25–33, 2015.

[10] J. A. Rowland, J. R. Stapleton-Kotloski, G. E. Alberto, J. A. Rawley, R. J. Kotloski, K. H. Taber, and D. W. Godwin, "Contrasting effects of posttraumatic stress disorder and mild traumatic brain injury on the whole-brain resting-state network: A magnetoencephalography study," *Brain Connectivity*, vol. 7, no. 1, pp. 45–57, 2017.

[11] G. S. Ling, J. Hawley, J. Grimes, C. Macedonia, J. Hancock, M. Jaffee, T. Dombroski, and J. M. Ecklund, "Traumatic brain injury in modern war," in *SPIE Defense, Security, and Sensing*, pp. 87230K–87230K–14, International Society for Optics and Photonics, 2013.

[12] Z. R. Mathews and A. Koyfman, "Blast injuries," *The Journal of Emergency Medicine*, vol. 49, no. 4, pp. 573–587, 2015.

[13] B. Moore, "Blast injuries-a prehospital perspective," *Australasian Journal of Paramedicine*, vol. 4, no. 1, 2015.

[14] S. Ganpule, A. Alai, E. Plougonven, and N. Chandra, "Mechanics of blast loading on the head models in the study of traumatic brain injury using experimental and computational approaches," *Biomechanics and Modeling in Mechanobiology*, vol. 12, no. 3, pp. 511–531, 2013.

[15] R. K. Gupta and A. Przekwas, "Mathematical models of blast-induced tbi: current status, challenges, and prospects," *Frontiers in Neurology*, vol. 4, p. 59, 2013.

[16] M. Skotak, F. Wang, A. Alai, A. Holmberg, S. Harris, R. C. Switzer, and N. Chandra, "Rat injury model under controlled field-relevant primary blast conditions: acute response to a wide range of peak overpressures," *Journal of Neurotrauma*, vol. 30, no. 13, pp. 1147–1160, 2013.

[17] A. Sundaramurthy, A. Alai, S. Ganpule, A. Holmberg, E. Plougonven, and N. Chandra, "Blast-induced biomechanical loading of the rat: an experimental and anatomically accurate computational blast injury model," *Journal of Neurotrauma*, vol. 29, no. 13, pp. 2352–2364, 2012.

[18] E. Alay, M. Skotak, A. Misistia, and N. Chandra, "Dynamic loads on human and animal surrogates at different test locations in compressed-gas-driven shock tubes," *Shock Waves*, vol. 28, no. 1, pp. 51–62, 2018.

[19] A. Rezaei, M. Salimi Jazi, G. Karami, and M. Ziejewski, "A computational study on brain tissue under blast: primary and tertiary blast injuries," *International journal for Numerical Methods in Biomedical Engineering*, vol. 30, no. 8, pp. 781–795, 2014.

[20] D. Singh, D. S. Cronin, and T. N. Haladuick, "Head and brain response to blast using sagittal and transverse finite element models," *International Journal for Numerical Methods in Biomedical Engineering*, vol. 30, no. 4, pp. 470–489, 2014.

[21] L. B. Tan, K. M. Tse, Y. H. Tan, M. A. B. Sapingi, V. B. C. Tan, and H. P. Lee, "Face shield design against blast-induced head injuries," *International journal for Numerical Methods in Biomedical Engineering*, vol. 33, no. 12, p. e2884, 2017.

[22] E. E. Southard, "Shell-shock and neuropsychiatry," *Boston: WW Leonard*, 1919.

[23] G. A. Elder and A. Cristian, "Blast-related mild traumatic brain injury: mechanisms of injury and impact on clinical care," *Mt Sinai Journal of Medicine*, vol. 76, no. 2, pp. 111–8, 2009.

[24] G. A. Elder, J. R. Stone, and S. T. Ahlers, "Effects of low-level blast exposure on the nervous system: Is there really a controversy?," *Frontiers in Neurology*, vol. 5, no. 269, 2014.

[25] P. Abdul-Muneer, H. Schuetz, F. Wang, M. Skotak, J. Jones, S. Gorantla, M. C. Zimmerman, N. Chandra, and J. Haorah, "Induction of oxidative and nitrosative damage leads to cerebrovascular inflammation in an animal model of mild traumatic brain injury induced by primary blast," *Free Radical Biology and Medicine*, vol. 60, pp. 282–291, 2013.

[26] M. Kuriakose, K. V. R. Rao, D. Younger, and N. Chandra, "Temporal and spatial effects of blast overpressure on blood-brain barrier permeability in traumatic brain injury," *Scientific Reports*, vol. 8, no. 1, p. 8681, 2018.

[27] M. Skotak, C. LaValle, A. Misistia, M. J. Egnoto, N. Chandra, and G. Kamimori, "Occupational blast wave exposure during multiday 0.50 caliber rifle course," *Frontiers in Neurology*, vol. 10, no. 797, 2019.

[28] A. Chandra, N; Sundaramurthy, *Acute Pathophysiology of Blast Injury From Biomechanics to Experiments and Computations: Implications on Head and Polytrauma*, book section 18, pp. 195–253. Boca Raton, Florida: CRC Press/Taylor & Francis, 2015.

[29] M. Risling and J. Davidsson, "Experimental animal models for studies on the mechanisms of blast-induced neurotrauma," *Frontiers in Neurology*, vol. 3, no. 30, 2012.

[30] K. E. Gould, "High-explosive field tests, explosion phenomena and environmental impacts," report, Kaman Temo Santa Barbara CA, 1981.

[31] C. E.Needham, D. Ritzel, G. T. Rule, S. Wiri, and L. A. Young, "Blast testing issues andtbi; experimental models that lead to wrong conclusions," *Frontiers in Neurology*, vol. 8, no. 72, 2015.

[32] K. J. G. Gilbert Ford Kinney, *Explosive Shocks in Air*. Heildelberg, New York: Springer Science, Business Media, second ed., 1985.

[33] I. Cernak and L. J. Noble-Haeusslein, "Traumatic brain injury: an overview of pathobiology with emphasis on military populations," *Journal of Cerebral Blood Flow and Metabolism*, vol. 30, no. 2, pp. 255–266, 2010.

[34] M. R. Gill, D. G. Reiley, and S. M. Green, "Interrater reliability of glasgow coma scale scores in the emergency department," *Annals of Emergency Medicine*, vol. 43, no. 2, 2004.

[35] M. D. Budde, A. Shah, M. McCrea, W. E. Cullinan, F. Pintar, and B. D. Stemper, "Primary blast traumatic brain injury in the rat: relating diffusion tensor imaging and behavior," *Frontiers in Neurology*, vol. 4, p. 154, 2013.

[36] S.-K. C. Kwon, E. Kovesdi, A. B. Gyorgy, D. Wingo, A. Kamnaksh, J. Walker, J. B. Long, and D. V. Agoston, "Stress and traumatic brain injury: a behavioral, proteomics, and histological study," *Frontiers in Neurology*, vol. 2, p. 12, 2011.

[37] H. Song, L. M. Konan, J. Cui, C. E. Johnson, M. Langenderfer, D. Grant, T. Ndam, A. Simonyi, T. White, U. Demirci, D. R. Mott, D. Schwer, G. K. Hubler, I. Cernak, R. G. DePalma, and Z. Gu, "Ultrastructural brain abnormalities and associated behavioral changes in mice after low-intensity blast exposure," *Behavioural Brain Research*, vol. 347, pp. 148–157, 2018.

[38] D. Tweedie, L. Rachmany, V. Rubovitch, Y. Zhang, K. G. Becker, E. Perez, B. J. Hoffer, C. G. Pick, and N. H. Greig, "Changes in mouse cognition and hippocampal gene expression observed in a mild physical- and blast-traumatic brain injury," *Neurobiology of Disease*, vol. 54, pp. 1–11, 2013.

[39] I. Humphreys, R. L. Wood, C. J. Phillips, and S. Macey, "The costs of traumatic brain injury: a literature review," *ClinicoEconomics and Outcomes Research : CEOR*, vol. 5, pp. 281–7, 2013.

[40] A. I. R. Maas, B. Roozenbeek, and G. T. Manley, "Clinical trials in traumatic brain injury: Past experience and current developments," *Neurotherapeutics*, vol. 7, no. 1, pp. 115–126, 2010.

[41] D. G. Stein, "Embracing failure: what the phase iii progesterone studies can teach about tbi clinical trials," *Brain Injury*, vol. 29, no. 11, pp. 1259–1272, 2015.

[42] C. R. Bass, M. B. Panzer, K. A. Rafaels, G. Wood, J. Shridharani, and B. Capehart, "Brain injuries from blast," *Annals of Biomedical Engineering*, vol. 40, no. 1, pp. 185–202, 2012.

[43] N. Chandra, A. Sundaramurthy, and R. K. Gupta, "Validation of laboratory animal and surrogate human models in primary blast injury studies," *Military Medicine*, vol. 182, no. S1, pp. 105–113, 2017.

[44] K. Rafaels, C. Bass, M. Panzer, R. Salzar, W. Woods, S. Feldman, T. Walilko, R. Kent, B. Capehart, J. Shridharani, and A. Tolman, "Brain injury from primary blast," *Brain Injury*, vol. 26, no. 4-5, pp. 745–746, 2012.

[45] R. C. Turner, Z. J. Naser, A. F. Logsdon, K. H. DiPasquale, G. J. Jackson, M. J. Robson, R. T. T. Gettens, R. R. Matsumoto, J. D. Huber, and C. L. Rosen, "Modeling clinically relevant blast parameters based on scaling principles produces functional & histological deficits in rats," *Experimental Neurology*, vol. 248, pp. 520–529, 2013.

[46] A. C. Courtney and M. W. Courtney, "A thoracic mechanism of mild traumatic brain injury due to blast pressure waves," *Medical Hypotheses*, vol. 72, no. 1, pp. 76–83, 2009.

[47] S. Yeoh, E. D. Bell, and K. L. Monson, "Distribution of blood–brain barrier disruption in primary blast injury," *Annals of Biomedical Engineering*, vol. 41, no. 10, pp. 2206–2214, 2013.

[48] K. Feng, L. Zhang, X. Jin, C. Chen, S. Kallakuri, T. Saif, J. Cavanaugh, and A. King, "Biomechanical responses of the brain in swine subject to free-field blasts," *Frontiers in Neurology*, vol. 7, no. 179, 2016.

[49] N. A. Fomin, "110 years of experiments on shock tubes," *Journal of Engineering Physics and Thermophysics*, vol. 83, no. 6, pp. 1118–1135, 2010.

[50] P. Vieille, "Sur les discontinuités produites par la détente brusque de gaz comprimés," *Comptes Rendus*, vol. 129, no. 1228, p. 68, 1899.

[51] G. W. Wood, M. B. Panzer, C. A. Cox, and C. R. Bass, "Interspecies scaling in blast pulmonary trauma," *Human Factors and Mechanical Engineering for Defense and Safety*, vol. 2, no. 1, p. 3, 2018.

[52] S. Kahali, M. Townsend, M. Mendez Nguyen, J. Kim, E. Alay, M. Skotak, and N. Chandra, "The evolution of secondary flow phenomena and their effect on primary shock conditions in shock tubes: Experimentation and numerical model," *PLOS One*, vol. 15, no. 1, p. e0227125, 2020.

[53] Y. Chen and S. Constantini, "Caveats for using shock tube in blast-induced traumatic brain injury research," *Frontiers in Neurology*, vol. 4, no. 117, 2013.

[54] M. Kuriakose, M. Skotak, A. Misistia, S. Kahali, A. Sundaramurthy, and N. Chandra, "Tailoring the blast exposure conditions in the shock tube for generating pure, primary shock waves: The end plate facilitates elimination of secondary loading of the specimen," *PLOS One*, vol. 11, no. 9, p. e0161597, 2016.

[55] I. Bowen, E. Fletcher, and D. Richmond, "Estimate of mans's tolerance to the direct effects of air blast," Report DA-49-146-XZ-372, Lovelace Foundation for Medical Education and Research, Albuquerque, New Mexico, 87108, 1968.

[56] I. Bowen, E. Fletcher, D. Richmond, E. Hirsch, and C. White, "Biophysical mechanisms and scaling procedures applicable in assessing responses of the thorax energized by air blast overpressures or by non-penetrating missiles," report, Lovelace Foundation for medical eduacation and research, Albuquerque, New Mexico, 1966.

[57] A. Jean, M. K. Nyein, J. Q. Zheng, D. F. Moore, J. D. Joannopoulos, and R. Radovitzky, "An animal-to-human scaling law for blast-induced traumatic brain injury risk assessment," *Proceedings of the National Academy of Sciences of the United States of America*, vol. 111, no. 43, 2014.

[58] R. N. Saunders, X. G. Tan, S. M. Qidwai, and A. Bagchi, "Towards identification of correspondence rules to relate traumatic brain injury in different species," *Annals of Biomedical Engineering*, 2018.

[59] H. Kinder, E. Baker, and F. West, "The pig as a preclinical traumatic brain injury model: current models, functional outcome measures, and translational detection strategies," *Neural Regeneration Research*, vol. 14, no. 3, pp. 413–424, 2019.

[60] A. K. Ommaya, A. E. Hirsch, P. Yarnell, and E. H. Harris, "Scaling of experimental data on cerebral concussion in sub-human primates to concussion threshold for man," David W Taylor Naval Ship Research and Development Center, Bethesda, MD 1967.

[61] M. B. Panzer and C. R. D. Bass, "Human results from animal models: Scaling laws for blast neurotrauma," *Journal of Neurotrauma*, vol. 29, no. 10, pp. A151–A151, 2012.

[62] G. Wood, M. Panzer, A. Yu, K. A. Rafaels, K. A. Matthews, and C. R. Bass, *Scaling in Blast Neurotrauma*. 2013.

[63] K. Rafaels, C. Bass, R. Salzar, M. Panzer, W. Woods, S. Feldman, T. Cummings, and B. Capehart, "Survival risk assessment for primary blast exposures to the head," *Journal of Neurotrauma*, vol. 28, 2011.

[64] M. T. Townsend, E. Alay, M. Skotak, and N. Chandra, "Effect of tissue material properties in blast loading: coupled experimentation and finite element simulation," *Annals of Biomedical Engineering*, vol. 47, no. 9, 2019.

[65] F. Zhu, C. C. Chou, K. H. Yang, and A. I. King, "Some considerations on the threshold and inter-species scaling law for primary blast-induced traumatic brain injury: A semi-analytical approach," *Journal of Mechanics in Medicine & Biology*, vol. 13, no. 4, pp. –1, 2013.

[66] M. Skotak, E. Alay, and N. Chandra, "On the accurate determination of shock wave time-pressure profile in the experimental models of blast-induced neurotrauma," *Frontiers in Neurology*, vol. 9, no. 52, 2018.

[67] C. R. Bass, K. A. Rafaels, and R. S. Salzar, "Pulmonary injury risk assessment for short-duration blasts," *The Journal of Trauma and Acute Care Surgery*, vol. 65, no. 3, pp. 604–15, 2008.

[68] A. Wermer, J. Kerwin, K. Welsh, R. Mejia-Alvarez, M. Tartis, and A. Willis, "Materials characterization of cranial simulants for blast-induced traumatic brain injury," *Military Medicine*, vol. 185, no. Supplement_1, pp. 205–213, 2020.

[69] S. Schraml and D. Hisley, "Euler and Navier-Stokes simulations of shock wave interaction with a generic block target (Final Report, Jan. - Nov. 1992)," technical report, Army Research Lab Aberdeen Proving Ground, Maryland, 1995.

[70] N. Chandra, S. Ganpule, N. N. Kleinschmit, R. Feng, A. D. Holmberg, A. Sundaramurthy, V. Selvan, and A. Alai, "Evolution of blast wave profiles in simulated air blasts: experiment and computational modeling," *Shock Waves*, vol. 22, no. 5, pp. 403–415, 2012.

[71] A. Marty, E. Daniel, J. Massoni, L. Biamino, L. Houas, D. Leriche, and G. Jourdan, "Experimental and numerical investigations of shock wave propagation through a bifurcation," *Shock Waves*, 2018.

[72] A. Sundaramurthy and N. Chandra, "A parametric approach to shape field-relevant blast wave profiles in compressed-gas-driven shock tube," *Frontiers in Neurology*, vol. 5, no. 253, 2014.

[73] N. Chandra, S. Ganpule, R. Salzar, and B. Perry, "Role of helmets in blast mitigation: insights from experiments on PMHS surrogate" *International Journal of Experimental and Computational Biomechanics*, vol. 4, no. 1, pp. 13–31, 2016.

[74] G. Appleby-Thomas, P. Hazell, R. Sheldon, C. Stennett, A. Hameed, and J. Wilgeroth, "The high strain-rate behaviour of selected tissue analogues," *Journal of the Mechanical Behavior of Biomedical Materials*, vol. 33, pp. 124–135, 2014.

[75] N. Awad, W. W. El-Dakhakhni, and A. A. Gilani, "A physical head and neck surrogate model to investigate blast-induced mild traumatic brain injury," *Arabian Journal for Science and Engineering*, vol. 40, no. 3, pp. 945–958, 2015.

[76] B. Fontenier, A. Hault-Dubrulle, P. Drazetic, C. Fontaine, and H. Naceur, "On the mechanical characterization and modeling of polymer gel brain substitute under dynamic rotational loading," *Journal of the Mechanical Behavior of Biomedical Materials*, vol. 63, pp. 44–55, 2016.

[77] J. Goeller, A. Wardlaw, D. Treichler, J. O'Bruba, and G. Weiss, "Investigation of cavitation as a possible damage mechanism in blast-induced traumatic brain injury," *Journal of Neurotrauma*, vol. 29, no. 10, pp. 1970–1981, 2012.

[78] D. Singh, S. Boakye-Yiadom, and D. Cronin, "Comparison of porcine brain mechanical properties to potential tissue simulant materials in quasi-static and sinusoidal compression," *Journal of Biomechanics*, 2019.

[79] J. Zhang, F. A. Pintar, N. Yoganandan, T. A. Gennarelli, and S. F. Son, "Experimental study of blast-induced traumatic brain injury using a physical head model," report, Society of Automotive Engineering Technical Paper, 2009.

[80] J. Zhang, B. Song, F. A. Pintar, N. Yoganandan, W. Chen, and T. A. Gennarelli, "How to test brain and brain simulant at ballistic and blast strain rates," *Biomedical Sciences Instrumentation*, vol. 44, pp. 129–134, 2008.

[81] J. Zhang, N. Yoganandan, F. A. Pintar, Y. Guan, and T. A. Gennarelli, "Experimental model for civilian ballistic brain injury biomechanics quantification," *Journal of Biomechanics*, vol. 40, no. 10, pp. 2341–2346, 2007.

[82] L. Zhang, W. J. Jackson, and S. A. Bentil, "The mechanical behavior of brain surrogates manufactured from silicone elastomers," *Journal of the Mechanical Behavior of Biomedical Materials*, vol. 95, pp. 180–190, 2019.

[83] R. S. Salzar, D. Treichler, A. Wardlaw, G. Weiss, and J. Goeller, "Experimental investigation of cavitation as a possible damage mechanism in blast-induced traumatic brain injury in post-mortem human subject heads," *Journal of Neurotrauma*, vol. 34, no. 8, pp. 1589–1602, 2017.

[84] L. Falland-Cheung, M. Scholze, N. Hammer, J. N. Waddell, D. C. Tong, and P. A. Brunton, "Elastic behavior of brain simulants in comparison to porcine brain at different loading velocities," *Journal of the Mechanical Behavior of Biomedical Materials*, vol. 77, pp. 609–615, 2018.

[85] L. Falland-Cheung, J. N. Waddell, M. S. Lazarjan, M. C. Jermy, T. Winter, D. Tong, and P. A. Brunton, "Use of agar/glycerol and agar/glycerol/water as a translucent brain simulant for ballistic testing," *Journal of the Mechanical Behavior of Biomedical Materials*, vol. 65, pp. 665–671, 2017.

[86] L. Falland-Cheung, N. Piccione, T. Zhao, M. S. Lazarjan, S. Hanlin, M. Jermy, and J. N. Waddell, "Investigation of dental alginate and agar impression materials as a brain simulant for ballistic testing," *Forensic Science International*, vol. 263, pp. 169–175, 2016.

[87] S. Ouellet, C. Bir, and A. Bouamoul, "Direct comparison of the primary blast response of a physical head model with post-mortem human subjects," report, Defence Research and Development Canada-Valcartier Research Center Quebec ..., 2014.

[88] F. Faul, E. Erdfelder, A.-G. Lang, and A. Buchner, "A flexible statistical power analysis program for the social, behavioral, and biomedical sciences," *Behavior Research Methods*, vol. 39, pp. 175–191, 2007.

[89] J. Fox, "The r commander: A basic statistics graphical user interface to r.," *Journal of Statistical Software*, vol. 14, no. 9, pp. 1–42, 2005.

[90] J. Fox, *Using the R Commander: A Point-and-Click Interface of R.* Boca Raton FL: Chapman and Hall/CRC Press, 2017.

[91] J. Fox and M. Bouchet-Valat, "Rcmdr: R commander," (Version R package version 2.4-4), 2018.

[92] IT'IS Foundation, "Tissue properties database v4.0," IT'IS Foundation, 2018.

[93] T. L. Poepping, H. N. Nikolov, M. L. Thorne, and D. W. Holdsworth, "A thin-walled carotid vessel phantom for doppler ultrasound flow studies," *Ultrasound in medicine & biology*, vol. 30, no. 8, pp. 1067–1078, 2004.

[94] F. R. Pereira, J. C. Machado, and W. C. Pereira, "Ultrasonic wave speed measurement using the time-delay profile of rf-backscattered signals: Simulation and experimental results," *The Journal of the Acoustical Society of America*, vol. 111, no. 3, pp. 1445–1453, 2002.

[95] M. O. Culjat, D. Goldenberg, P. Tewari, and R. S. Singh, "A review of tissue substitutes for ultrasound imaging," *Ultrasound in Medicine & Biology*, vol. 36, no. 6, pp. 861–873, 2010.

[96] B. Meirza, Development of vessel phantoms for ultrasound methods, Thesis, Lund Univeristy, 2018.

[97] A. I. Farrer, H. Odéen, J. de Bever, B. Coats, D. L. Parker, A. Payne, and D. A. Christensen, "Characterization and evaluation of tissue-mimicking gelatin phantoms for use with mrgfus," *Journal of Therapeutic Ultrasound*, vol. 3, no. 1, p. 9, 2015.

[98] F. W. Kremkau, R. W. Barnes, and C. P. McGraw, "Ultrasonic attenuation and propagation speed in normal human brain," *The Journal of the Acoustical Society of America*, vol. 70, no. 1, pp. 29–38, 1981.

[99] C. N. Kingery and G. A. Coulter, "Reflected overpressure impulse on a finite structure," technical report, Army Ballistic Research Lab, Aberdeen Proving Ground, Maryland, 1983.

[100] R. E. Lottero, J. D. Wortman, B. P. Bertrand, and C. W. Kitchens Jr, "Three-dimensional oblique shock diffraction over a rectangular parallelepiped: Computational/experimental comparison," techical report, Army Ballistic Research Lab, Aberdeen Proving Ground, Maryland, 1982.

[101] S. Ganpule, R. Salzar, B. Perry, and N. Chandra, "Role of helmets in blast mitigation: insights from experiments on pmhs surrogate," *International Journal of Experimental and Computational Biomechanics*, vol. 4, no. 1, pp. 13–31, 2016.

[102] A. S. Iwaskiw, K. A. Ott, R. S. Armiger, A. C. Wickwire, V. D. Alphonse, L. M. Voo, C. M. Carneal, and A. C. Merkle, "The measurement of intracranial pressure and brain displacement due to short-duration dynamic overpressure loading," *Shock Waves*, 2017.

[103] A. Merkle, R. Armiger, K. Ott, A. Wickwire, A. Iwaskiw, L. Voo, and C. Carneal, "Characterizing brain mechanics during a two-phase response to dynamic overpressure loading," *Injury Biomechanics Research, Proceedings of the Fortieth International Workshop*, pp. 1–13, 2012.

[104] R. Banton, T. Piehler, N. Zander, R. Benjamin, and J. Duckworth, Comparison of Numerical Simulations with Experiments of Blast-Induced Pressure Wave Impact on a Surrogate Head Model, *Dynamic Behavior of Materials, Volume 1*, pp. 181–187, Springer International Publishing, 2018.

[105] F. Zhu, C. Wagner, A. Dal Cengio Leonardi, X. Jin, P. VandeVord, C. Chou, K. H. Yang, and A. I. King, "Using a gel/plastic surrogate to study the biomechanical response of the head under air shock loading: a combined experimental and numerical investigation," *Biomechanics and Modeling in Mechanobiology*, vol. 11, no. 3, pp. 341–353, 2012.

[106] N. H. Ethridge, R. E. Lottero, J. D. Wortman, and B. P. Bertrand, "Computational and experimental studies of blockage effects in a blast simulator," report, Army Ballistic Research Lab, Aberdeen Proving Ground, Maryland, 1984.

[107] J. D. Wortman and R. E. Lottero, "Comparison of hull hydrocode computations of shock tube blockage effects on target loading for step shocks and rapidly-decaying shocks," technical report, Army Ballistic Research Lab, Aberdeen Proving Ground, Maryland, 1982.

[108] X. Tan, A. J. Przekwas, and J. B. Long, "Validations of virtual animal model for investigation of shock/blast wave TBI," in *ASME 2013 International Mechanical Engineering Congress and Exposition*, American Society of Mechanical Engineers, 2013.

[109] M. Chavko, T. Watanabe, S. Adeeb, J. Lankasky, S. T. Ahlers, and R. M. McCarron, "Relationship between orientation to a blast and pressure wave propagation inside the rat brain," *J Neuroscience Methods*, vol. 195, no. 1, pp. 61–6, 2011.

[110] D. R. Richmond, E. G. Damon, E. R. Fletcher, I. G. Bowen, and C. S. White, "The relationship between selected blast-wave parameters and the response of mammals exposed to air blast," *Annals of the New York Academy of Sciences*, vol. 152, no. 1, pp. 103–121, 1968.

[111] A. Saljo, M. Mayorga, H. Bolouri, B. Svensson, and A. Hamberger, "Mechanisms and pathophysiology of the low-level blast brain injury in animal models," *Neuroimage*, vol. 54 Suppl 1, pp. S83–8, 2011.

[112] M. A. G. Sosa, R. De Gasperi, G. S. P. Garcia, G. M. Perez, C. Searcy, D. Vargas, A. Spencer, P. L. Janssen, A. E. Tschiffely, R. M. McCarron, B. Ache, R. Manoharan, W. G. Janssen, S. J. Tappan, R. W. Hanson, S. Gandy, P. R. Hof, S. T. Ahlers, and G. A. Elder, "Low-level blast exposure disrupts gliovascular and neurovascular connections and induces a chronic vascular pathology in rat brain," *Acta Neuropathologica Communications*, vol. 7, p. 20, 2019.

[113] X. Jin, F. Zhu, H. Mao, M. Shen, and K. H. Yang, "A comprehensive experimental study on material properties of human brain tissue," *Journal of Biomechanics*, vol. 46, no. 16, pp. 2795–2801, 2013.

[114] F. Pervin and W. W. Chen, *Mechanically similar gel simulants for brain tissues*, pp. 9–13. Springer, 2011.

[115] J. Zhang, N. Yoganandan, F. A. Pintar, and T. A. Gennarelli, "Temporal cavity and pressure distribution in a brain simulant following ballistic penetration," *Journal of neurotrauma*, vol. 22, no. 11, pp. 1335–1347, 2005.

[116] K. Zell, J. I. Sperl, M. W. Vogel, R. Niessner, and C. Haisch, "Acoustical properties of selected tissue phantom materials for ultrasound imaging," *Physics in Medicine & Biology*, vol. 52, no. 20, p. N475, 2007.

[117] C. Bir, "Measuring blast-related intracranial pressure within the human head," report, Wayne State University Detroit, Michigan, 2011.

[118] M. S. Chafi, G. Karami, and M. Ziejewski, "Biomechanical assessment of brain dynamic responses due to blast pressure waves," *Annals of Biomedical Engineering*, vol. 38, no. 2, pp. 490–504, 2010.

[119] V. Mishra, M. Skotak, H. Schuetz, A. Heller, J. Haorah, and N. Chandra, "Primary blast causes mild, moderate, severe and lethal tbi with increasing blast overpressures: Experimental rat injury model," *Scientific Reports*, vol. 6, p. 26992, 2016.

[120] X. Chen and N. Chandra, "The effect of heterogeneity on plane wave propagation through layered composites," *Composites Science and Technology*, vol. 64, no. 10, pp. 1477–1493, 2004.

[121] C. E. Clauser, J. T. McConville, and J. W. Young, "Weight, volume, and center of mass of segments of the human body," report, Antioch Coll Yellow Springs OH, 1969.

[122] R. Drillis, R. Contini, and M. Bluestein, "Body segment parameters," *Artificial Limbs*, vol. 8, no. 1, pp. 44–66, 1964.

[123] A. Kalra, F. Zhu, K. Feng, T. Saif, S. Kallakuri, X. Jin, K. Yang, and A. King, "Development and validation of a numerical model of the swine head subjected to open-field blasts," *Shock Waves*, vol. 27, no. 6, pp. 947–964, 2017.

[124] K. L. Thibault and S. S. Margulies, "Age-dependent material properties of the porcine cerebrum: effect on pediatric inertial head injury criteria," *Journal of Biomechanics*, vol. 31, no. 12, pp. 1119–1126, 1998.

[125] F. Zhu, P. Skelton, C. C. Chou, H. Mao, K. H. Yang, and A. I. King, "Biomechanical responses of a pig head under blast loading: a computational simulation," *International Journal of Numerical Methods in Biomedical Engineering*, vol. 29, no. 3, pp. 392–407, 2013.

[126] J. K. Shridharani, G. W. Wood, M. B. Panzer, B. P. Capehart, M. K. Nyein, R. A. Radovitzky, and C. R. d. Bass, "Porcine head response to blast," *Frontiers in Neurology*, vol. 3, p. 70, 2012.